AD-A086 567 NAVAL POSTGRADUATE SCHOOL MONTEREY CA F/G 9/4
MODELING OF PULSES HAVING ARBITRARY AMPLITUDE AND FREQUENCY MOD--ETC(U)
MAR 80 F M LUNNEY

UNCLASSIFIED NL

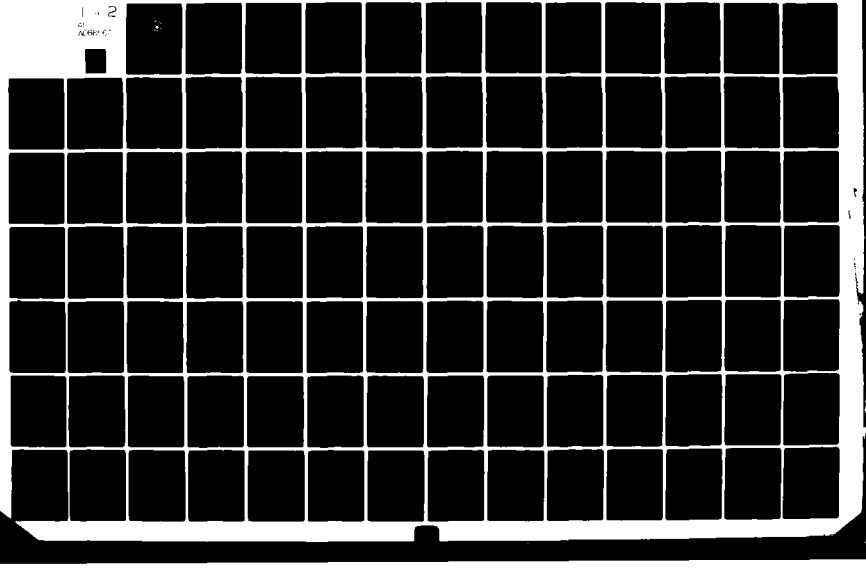

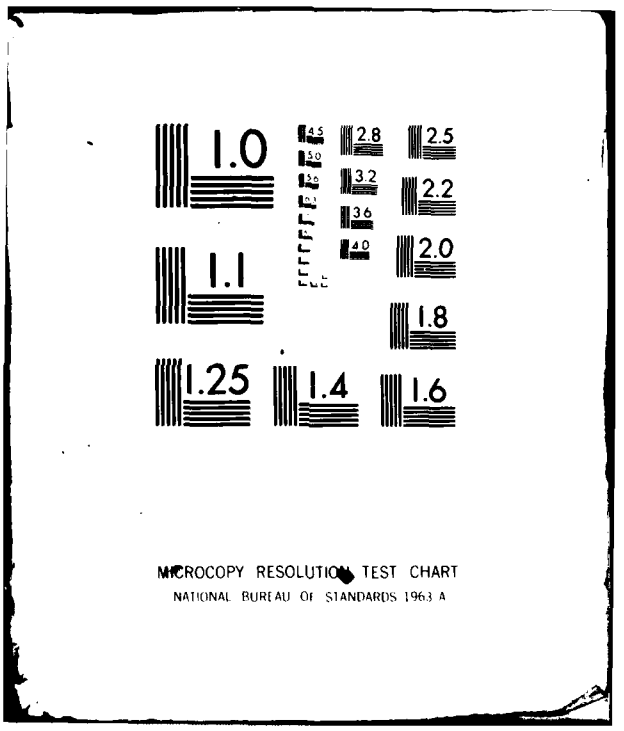
1.0
1.1
1.25
1.4
1.6
1.8
2.0
2.2
2.5
2.8
3.2
3.6
4.0
4.5
5.0
MICROCOPY RESOLUTION TEST CHART
NATIONAL BUREAU OF STANDARDS 1963 A

NAVAL POSTGRADUATE SCHOOL

Monterey, California

(9) Doctoral

THESIS,

(6) MODELING OF PULSES HAVING ARBITRARY AMPLITUDE AND FREQUENCY MODULATION.

by

(10) Francis Martin/Lunney

(11) March 1980

(12) 154

Dissertation Advisor: S. Jauregui

Approved for public release; distribution unlimited

UNCLASSIFIED

SECURITY CLASSIFICATION OF THIS PAGE (When Data Entered)

REPORT DOCUMENTATION PAGE	READ INSTRUCTIONS BEFORE COMPLETING FORM
1. REPORT NUMBER	2. GOVT ACCESSION NO. AD-A086 567 / 3. RECIPIENT'S CATALOG NUMBER
4. TITLE (and Subtitle) Modeling of Pulses Having Arbitrary Amplitude and Frequency Modulation	5. TYPE OF REPORT & PERIOD COVERED Doctoral Dissertation (March 1980) / 6. PERFORMING ORG. REPORT NUMBER
7. AUTHOR(s) Francis Martin Lunney	8. CONTRACT OR GRANT NUMBER(s)
9. PERFORMING ORGANIZATION NAME AND ADDRESS Naval Postgraduate School Monterey, CA 93940	10. PROGRAM ELEMENT, PROJECT, TASK AREA & WORK UNIT NUMBERS
11. CONTROLLING OFFICE NAME AND ADDRESS Naval Postgraduate School Monterey, CA 93940	12. REPORT DATE March 1980 / 13. NUMBER OF PAGES 149
14. MONITORING AGENCY NAME & ADDRESS(if different from Controlling Office) Naval Postgraduate School Monterey, CA 93940	15. SECURITY CLASS. (of this report) Unclassified / 15a. DECLASSIFICATION/DOWNGRADING SCHEDULE
16. DISTRIBUTION STATEMENT (of this Report) Approved for public release; distribution unlimited	
17. DISTRIBUTION STATEMENT (of the abstract entered in Block 20, if different from Report)	
18. SUPPLEMENTARY NOTES	
19. KEY WORDS (Continue on reverse side if necessary and identify by block number) Spectrum modeling Spectrum analysis Signal classification	

20. ABSTRACT (Continue on reverse side if necessary and identify by block number)

A model is developed which provides for the generation of the approximate spectra of pulsed signals with arbitrary amplitude and frequency modulation. Error bounds associated with the model are developed providing an insight into performance accuracy. The concept of using two approximate spectra to generate a more exact spectrum by means of computationally trivial calculations is addressed. The model is used to validate the feasibility of using frequency domain discriminants in the signal classification process.

DD FORM 1 JAN 73 1473 (Page 1)

EDITION OF 1 NOV 65 IS OBSOLETE

S/N 0102-014-6601

UNCLASSIFIED

SECURITY CLASSIFICATION OF THIS PAGE (When Data Entered)

Approved for Public Release
Distribution Unlimited

Modeling of Pulses Having Arbitrary Amplitude and Frequency Modulation

by

Francis Martin Lunney
Lieutenant Commander, United States Navy
B.S., Saint Joseph's University 1968

Submitted in partial fulfillment of the
requirements for the degree of

DOCTOR OF ENGINEERING

from the
NAVAL POSTGRADUATE SCHOOL
March 1980

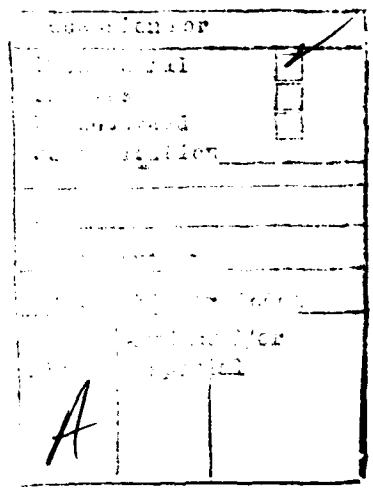

Author _____

Approved by:

G. A. Myers Associate Professor of Electrical Engineering	A. L. Schoenstadt Associate Professor of Mathematics
J. B. Knorr Associate Professor of Electrical Engineering	R. R. Washburn Associate Professor of Operations Research
S. Jauregui Associate Professor of Electrical Engineering Dissertation Supervisor	B. O. Shubert Associate Professor of Operations Research

Approved by _____
Chairman, Department of Electrical Engineering

Approved by _____
Academic Dean

ABSTRACT

A model is developed which provides for the generation of the approximate spectra of pulsed signals with arbitrary amplitude and frequency modulation. Error bounds associated with the model are developed providing an insight into performance accuracy. The concept of using two approximate spectra to generate a more exact spectrum by means of computationally trivial calculations is addressed. The model is used to validate the feasibility of using frequency domain discriminants in the signal classification process.

TABLE OF CONTENTS

INDEX OF TABLES

INDEX OF FIGURES

ACKNOWLEDGEMENT

I wish to express my appreciation to Henry Adaniya, Naval Weapons Center, China Lake, and to Professor Schoenstadt, Naval Postgraduate School, Monterey, for interest shown in and assistance provided during the development of this work. I am also grateful to Professor Jauregui for guidance provided. Most especially, I must thank June, Beth and Kevin.

I. INTRODUCTION

The classical radar pulse consists of a rectangular pulse modulating a constant carrier frequency. This gives rise to the characteristic [sin(x)]/x spectrum centered about the carrier frequency.

In practice, this idealized pulse is not realized since pulse envelopes tend to be more trapezoidal than rectangular and since carrier frequencies are not, de facto, constant. Frequency modulation (FM), intentional or unintentional, may be a property of all radars. As an example of this, oscillators may experience finite turn-on and shut-down periods during which a transient frequency modulation can be introduced onto the carrier. Figure 1 illustrates what a typical instantaneous frequency of a "constant" carrier radar pulse might look like.

The question of how modulation affects the frequency spectrum is one of interest in pulse analysis. Thus it is desirable to model the amplitude spectrum of a pulse with arbitrary amplitude and frequency modulation to provide a vehicle to study the effects of modulation on the amplitude spectrum.

One approach to this general modeling problem is to generate a digital representation of the pulse waveform and apply a Discrete Fourier Transform (DFT) algorithm to the data to generate the frequency domain representation. This approach for the general case can be cumbersome in generating the digital signal, satisfying the Nyquist criteria, and trading-off between frequency resolution and transform size.

An approach to addressing the amplitude spectrum of frequency modulation waveforms is to view the problem in terms of the quasi-stationary

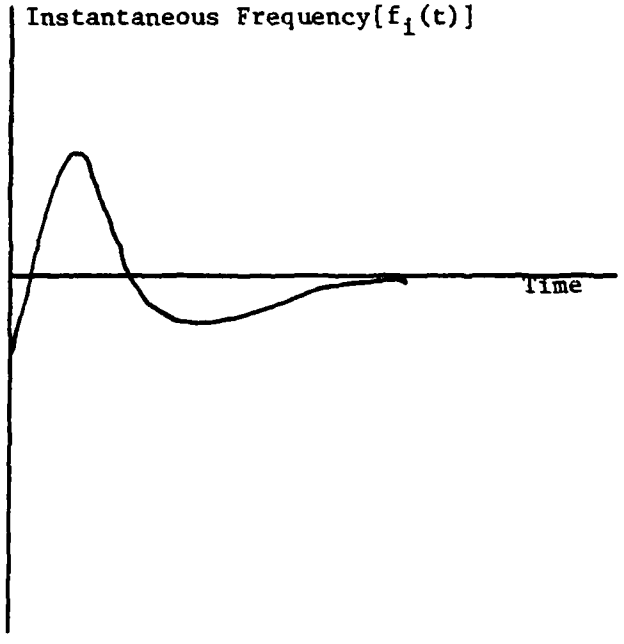

Figure 1 - Instantaneous Frequency Function Associated with a Pulsed Signal

principle. The fraction of time that the instantaneous frequency for the waveform spends in a particular frequency interval is the fraction of power that belongs to the corresponding Fourier frequency interval. This principle, however, is only validly applicable asymptotically for large modulation indices. [1].

Holway and Mullen [1] have addressed a special case of FM spectra generation. Using a Fourier Series approach and with the aid of Fresnel integrals, a closed form expression has been developed for the line spectrum for periodic frequency modulated signals in those cases when the modulating function is trapezoidal. This model is flexible in that the form of the trapezoidal modulation can be varied from square-wave modulation at one extreme to saw-tooth modulation at the other.

As with the work of Holway and Mullen, the model developed in this paper uses the Fresnel integral as one of its keystones, but addresses a broader scope of modulated signals. The Elemental Cell Model which is to be addressed is designed to generate the approximate spectrum of pulsed signals with arbitrary amplitude and frequency modulation. The approach is to partition the amplitude envelope and instantaneous frequency function associated with a signal into an arbitrary number of "elemental cells" of arbitrary length. Across each elemental cell the amplitude and frequency is linearly approximated so that the original envelope and instantaneous frequency function have both been formed into piecewise linear continuous functions. Each elemental cell has associated with it a characteristic frequency spectrum which can be represented in closed form. With phase continuity maintained between contiguous cells, the individual elemental cell spectra can be summed to provide the approximated spectrum of the original signal. This model provides a

flexible, easy to use tool for spectrum analysis.

II. ELEMENTAL CELL MODEL

A. DEVELOPMENT OF THE ELEMENTAL CELL MODEL FOR THE UNIT PULSE

In this section, the elemental cell model is developed for the unit amplitude pulse waveform. The model provides a flexible, easily applied method of generating approximated spectra for pulsed signals with arbitrary frequency modulation. The approach of the model is to decompose pulse waveforms into sequences of elemental (waveforms) cells, each of which has a characteristic spectrum in closed analytic form.

Consider a unit pulse with an arbitrary frequency modulation as shown in figure 2. The pulse waveform, p(t), can be expressed analytically as:

$$p(t) = \cos\left\{2\pi f_c t + \phi(T_{po}) + 2\pi k_f \int_{T_{po}}^{t} m(x)\,dx\right\} \qquad \text{(II-1)}$$

for $T_{po} < t < T_{po} + \tau_p$ where:

T_{po} = pulse starting time

f_c = pulse carrier frequency

$\phi(T_{po})$ = initial pulse carrier phase

k_f = constant of proportionality

$m(x)$ = frequency modulating function

τ_p = pulse width

The instantaneous frequency function, $f_i(t)$, associated with this pulse is:

$$f_i(t) = f_c + k_f m(t) \qquad T_{po} < t < T_{po} + \tau_p \qquad \text{(II-2)}$$

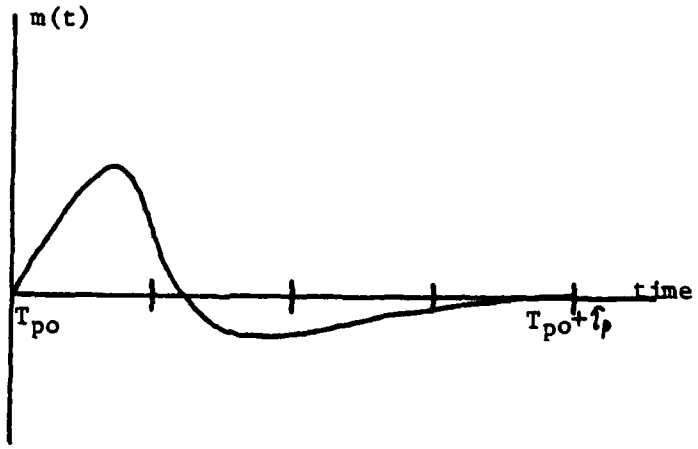

Figure 2 - Arbitrary Frequency Modulation Function, m(t)

The spectrum of the pulse waveform can then be expressed as the Fourier Transform of p(t) in equation (II-1):

$$P(f) = \int_{-\infty}^{\infty} p(t) e^{-j\omega t} dt \qquad \text{(II-3)}$$

But since p(t) is nonzero only during the pulse duration:

$$P(f) = \int_{T_{po}}^{T_{po}+\tau_p} p(t) e^{-j\omega t} dt \qquad \text{(II-4)}$$

The difficulty in evaluating this expression lies in the fact that p(t) is a function of m(t). Since m(t), in general, is not representable in analytic form, its integral and ultimate application to equation (II-4) is mathematically untractable. An exact spectrum for a pulse with arbitrary frequency modulation can be generated using equations (II-1) and (II-4) for only certain m(t). However, the concept of approximating m(t) across the pulse holds promise for generating approximate spectra.

Since integration is a linear operation, the integral in equation (II-4) can be partitioned and rewritten as the sum of n integrals. This is, in essense, the decomposition of the waveform, p(t), into n contiguous cells. The linear additivity property of the Fourier transform then allows equation (II-4) to be written as:

$$P(f) = \sum_{i=0}^{n-1} \int_{t_i}^{t_{i+1}} p(t) e^{-j\omega t} dt \qquad \text{(II-5)}$$

where in the case at hand $t_o = T_{po}$ and $t_n = T_{po} + \tau_p$

The spectrum, then, of the pulse waveform with arbitrary frequency

modulation, p(t), can be thought of as being composed of the sum of the spectra of elemental cells. If each elemental cell has a characteristic spectrum associated with it, then P(f), the total pulse spectrum, can be generated quite easily. However, the problem of dealing with the untractable form of m(t) across the pulse and elemental cells still persists. There are cases, however, in which the approximation of m(t) across an elemental cell results in that cell having a spectrum that is representable in closed analytic form. For example, consider the case where m(t) is approximated by a constant value across an elemental cell. Let the left end point of the cell be T_0, the cell width be τ, the initial phase of the cell be $\phi(T_0)$ and the radian center frequency of the cell be ω_c. The characteristic spectrum of this constant frequency unit cell, Z(f), is of the form sin(x)/x and is written as:

$$(II\text{-}6) \quad Z(f) = j\frac{e^{-j\omega T_0}}{2}\left\{\frac{e^{j\phi(T_0)}}{\omega_c-\omega}\left[1-e^{j(\omega_c-\omega)\tau}\right]-\frac{e^{-j\phi(T_0)}}{\omega_c+\omega}\left[1-e^{-j(\omega_c+\omega)\tau}\right]\right\}$$

Thus the elemental cell's spectrum can be generated for any frequency component as long as the four cell parameters (T_0, τ, ω_c and $\phi(T_0)$) are known.

A similar type of characteristic spectrum results if m(t) is linearly approximated across an elemental cell. Consider the instantaneous frequency function shown in figure 3. Let a unit cell be selected as shown extending from T_0 to $T_0+\tau$. Then the Fourier Transform, Z(f), of this elemental cell is:

$$(II\text{-}7) \quad Z(f) = \int_{T_0}^{T_0+\tau} p_e(t)e^{-j\omega t}\,dt$$

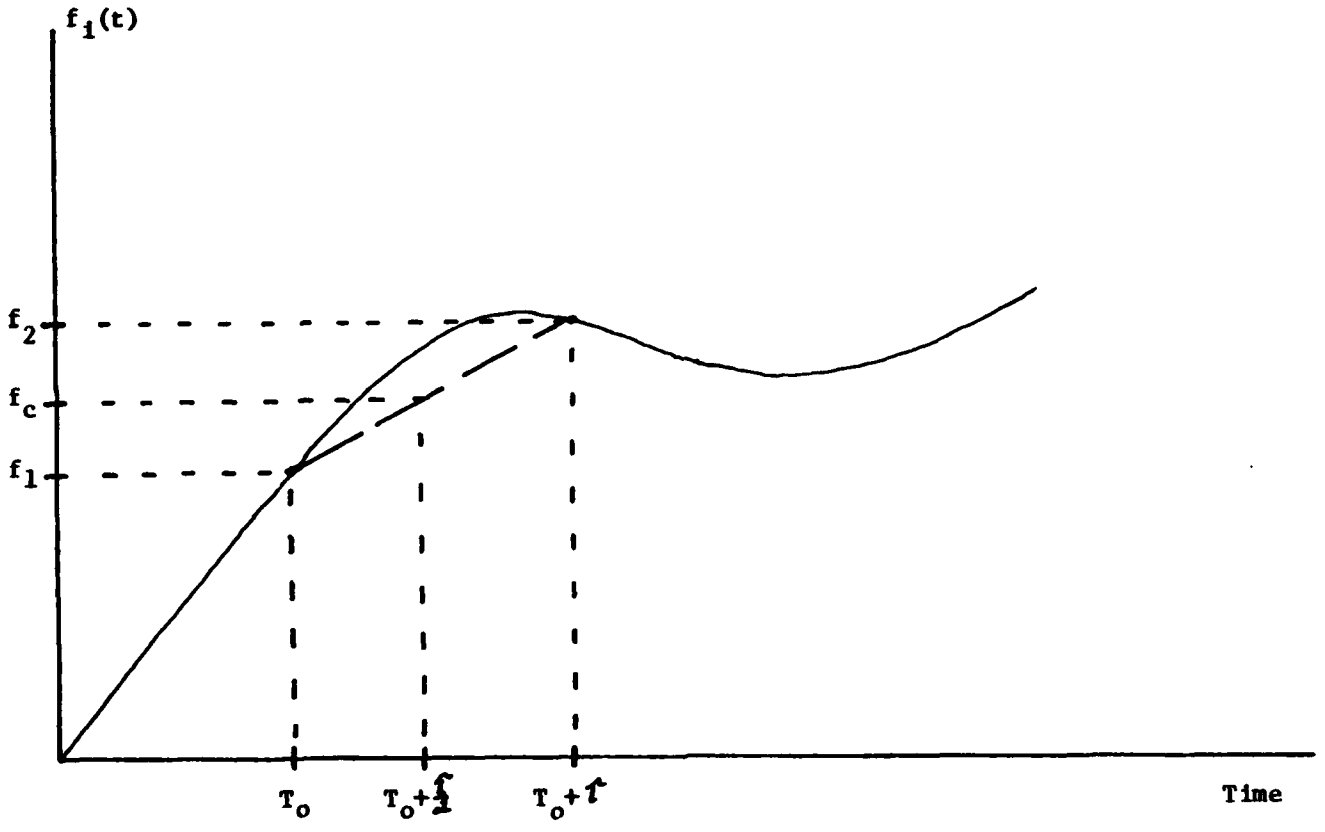

Figure 3 - Generation of the Linearized Instantaneous Frequency Function for Use in the Elemental Cell Model

where $p_e(t)$ is that segment of p(t) (equation II-1) contained within the elemental cell under consideration. The instantaneous frequency of this cell is:

$$f_i(t) = f_c + k_f m(t) \qquad T_o < t < T_o + \tau \tag{II-8}$$

Let the instantaneous frequency ($f_i(t)$) be linearly approximated ($\hat{f}_i(t)$) as shown in figure 3, then:

$$\hat{f}_i(t) = f_1 + \rho(t - T_o) \qquad T_o < t < T_o + \tau \tag{II-9}$$

where ρ is the frequency sweep rate, $\rho = (f_2 - f_1)/\tau$. Such linear FM is called "chirp" modulation. Using equation (II-9), the approximated instantaneous phase can be expressed as:

$$\hat{\phi}(t) = \phi(T_o) + 2\pi \int_{T_o}^{t} [f_1 + \rho(x - T_o)]\, dx \qquad T_o < t < T_o + \tau \tag{II-10a}$$

$$\hat{\phi}(t) = \phi(T_o) + 2\pi f_1 (t - T_o) + \pi\rho(t - T_o)^2 \qquad T_o < t < T_o + \tau \tag{II-10b}$$

This gives rise to the approximate form of the Fourier Transform of the elemental cell.

$$Z(f) = \int_{T_o}^{T_o + \tau} \cos\left[\phi(T_o) + 2\pi f_1 (t - T_o) + \pi\rho(t - T_o)^2\right] e^{-j\omega t}\, dt \tag{II-11}$$

By expressing the cosine as a sum of exponentials, completing the square of the exponential arguments and letting

(II-12a) $$z_1 = \sqrt{2\rho}\left[(t-\tau_0) + \frac{(f_1-f)}{\rho}\right]$$

(II-12b) $$z_2 = \sqrt{2\rho}\left[(t-\tau_0) + \frac{(f_1+f)}{\rho}\right]$$

equation (II-11) reduces to:

(II-13) $$Z(f) = \frac{e^{j\beta_1}}{2\sqrt{2\rho}}\int_{z_{1L}}^{z_{1H}} e^{j\left(\frac{\pi z_1}{2}\right)^2} dz_1 + \frac{e^{-j\beta_2}}{2\sqrt{2\rho}}\int_{z_{2L}}^{z_{2H}} e^{-j\left(\frac{\pi z_2}{2}\right)^2} dz_2$$

where:

(II-14a) $$\beta_1 = \phi(\tau_0) - 2\pi f \tau_0 - \frac{\pi}{\rho}(f_1-f)^2$$

(II-14b) $$\beta_2 = \phi(\tau_0) + 2\pi f \tau_0 - \frac{\pi}{\rho}(f_1+f)^2$$

(II-15a) $$z_{1L} = \sqrt{\frac{2}{\rho}}(f_1-f)$$

(II-15b) $$z_{1H} = \sqrt{2\rho}\left[\tau + \frac{(f_1-f)}{\rho}\right]$$

(II-15c) $$z_{2L} = \sqrt{\frac{2}{\rho}}(f_1+f)$$

(II-15d) $$z_{2H} = \sqrt{2\rho}\left[\tau + \frac{(f_1+f)}{\rho}\right]$$

The integrals in equation (II-13) are the Fresnel integrals. They can be evaluated with the use of tables, the Cornu spiral or the τ-method of Lanczos(2). Equation (II-13) can be written more compactly as:

(II-16) $$Z(f) = \frac{1}{\sqrt{8\rho}}\left\{e^{j\beta_1}\left[C(z_{1H}) - C(z_{1L}) + j\left(S(z_{1H}) - S(z_{1L})\right)\right] + e^{-j\beta_2}\left[C(z_{2H}) - C(z_{2L}) + j\left(S(z_{2L}) - S(z_{2H})\right)\right]\right\}$$

where the Fresnel integrals are given by:

(II-17a) $$S(x) = \int_0^x \sin\left(\frac{\pi v^2}{2}\right) dv$$

(II-17b) $$C(x) = \int_0^x \cos\left(\frac{\pi v^2}{2}\right) dv$$

Thus the Fourier Transform of the elemental cell with a linear frequency sweep can be obtained in a straight-forward manner by evaluating the Fresnel integrals. The derivation provided assumes that the frequency sweep within the elemental cell is positive. It can be shown that if the sweep rate is negative the governing equation is similar to equation (II-16),

(II-18) $$Z(f) = \frac{1}{\sqrt{8\rho}} \left\{ e^{j\beta_1'} \left[C(z_{1H}') - C(z_{1L}') - j\left(S(z_{1H}') - S(z_{1L}')\right) \right] + e^{-j\beta_2'} \left[C(z_{2H}') - C(z_{2L}') - j\left(S(z_{2L}') - S(z_{2H}')\right) \right] \right\}$$

where the primed variables are now defined as:

(II-19a) $$\beta_1' = \Phi(T_0) - 2\pi f T_0 + \frac{\pi}{\beta}(f_1 - f)^2$$

(II-19b) $$\beta_2' = \Phi(T_0) + 2\pi f T_0 + \frac{\pi}{\beta}(f_1 + f)^2$$

(II-20a) $$z_{1L}' = -\sqrt{\frac{2}{\rho}}\left[f_1 - f\right]$$

(II-20b) $$z_{1H}' = \sqrt{2\rho}\left[\tau - \frac{(f_1 - f)}{\rho}\right]$$

(II-20c) $$z_{2L}' = -\sqrt{\frac{2}{\rho}}\left[f_1 + f\right]$$

(II-20d) $$2\lambda H' = \sqrt{2\rho}\left[\hat{\tau} - \frac{(f_1 + f)}{\rho}\right]$$

Thus as with the case of a constant frequency elemental cell, the spectrum of a cell with a linear frequency sweep can be generated for any frequency component given the cell parameters: $\hat{\tau}, T_o, \phi(T_o), f_1$, and ρ .

In summary, an approach has been developed using an approximation to arbitrary FM to generate an approximation to the pulse spectrum. The instantaneous frequency, $f_i(t)$, is linearly approximated over an arbitrary number of elemental cells of arbitrary duration. The Fourier transforms of these elemental cells (of the constant frequency or chirp form) are then coherently summed to produce an approximation to the original pulse spectrum. Appendix A is a program listing for implementation of the elemental cell model. Nomenclature and notation in the listing parallels that of the development above. The program in the appendix treats the unit pulse problem as a special case of the more general model developed in section IV.

B. ILLUSTRATION OF THE ELEMENTAL CELL MODEL FOR THE UNIT PULSE.

It is desirable to model an FM pulse for which an exact spectrum can be generated so that some insight into and assessment of the model performance can be made. It is equally desirable to model a pulse in which the instantaneous frequency profile is dynamic; i.e., constantly changing across the pulse. Both of these objectives are achieved by selecting a pulse which is subject to sinusoidal frequency modulation. Appendix B addresses the generation of spectra for pulses with sinusoidal FM.

Consider the case of a 5 microsecond pulse, which has an instantaneous frequency function, $f_i(t)$, given by:

$$f_i(t) = f_c + k_f f_m \cos[\omega_m t] \tag{II-21}$$

where

f_c = carrier frequency = 30 MHz

k_f = modulation index = 1.0

f_m = modulating frequency = 200 kHz

This instantaneous frequency function is illustrated in figure 4. The figure demonstrates, using two examples, the linearization and elemental cell formation process. In case I, two element cells are used to generate the spectrum while in Case II, six cells are used. Assume that the desired frequency resolution is 25 kHz and that the primary interest rests in the first three upper and lower spectral sidelobes. In generating the spectrum then, 80 frequency components are required at 25 kHz intervals starting at 29 MHz. It is worth noting that in the elemental cell model, there is no requirement that the frequency or time intervals be of equal size. Since the spectral components are generated by evaluating analytic expressions for specific frequencies, the spectral values for any combination of frequencies can be produced.

Figure 5 displays the model-generated amplitude spectra for the cases developed in figure 4. The solid curve represents the exact amplitude spectrum developed according to Appendix B. It is not at all unexpected that the 6 cell model provides a more accurate solution than the 2 cell model. It is of interest, however, that the two cell model in itself provides a good approximation to the exact spectrum. The question that

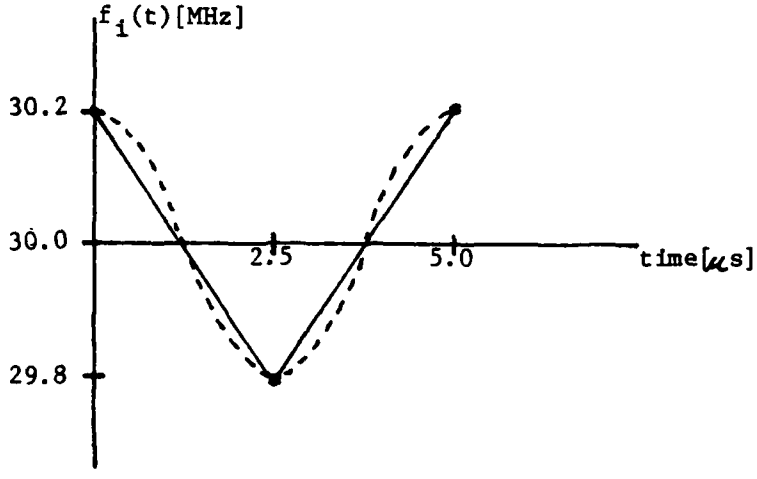

(a)

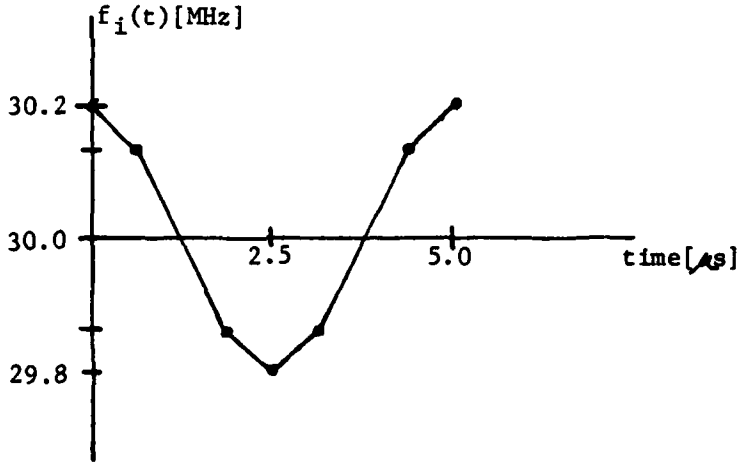

(b)

Figure 4 - Elemental Cell Generation Using (a) Two and (b) Six Cells to Model Sinusoidal Frequency Modulation

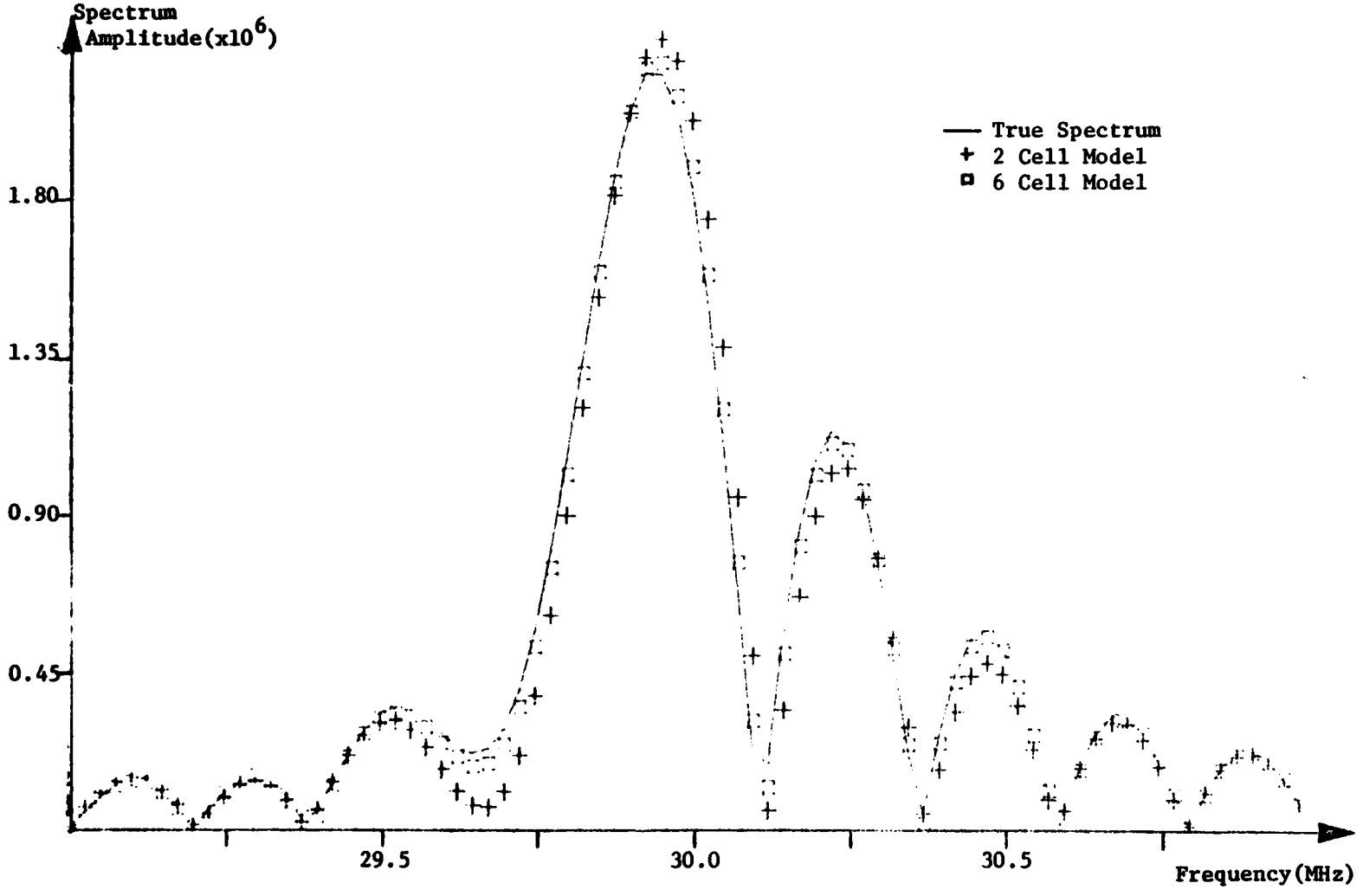

Figure 5 - Spectrum of a Sinusoidally Modulated Unit Pulse

naturally arises is how well do the results of the model approximate those of the actual spectrum?

III. ERROR ANALYSIS APPLIED TO THE ELEMENTAL CELL MODEL FOR THE UNIT PULSE

A. ERROR BOUND

How accurate is the elemental cell model? How many cells are required to achieve a given accuracy? More basically, how does the model accuracy change as the number of elemental cells is increased or decreased?

This section assesses the elemental cell model performance in terms of error bounds. The establishment of these bounds is based on an approach used by Gerald(3) and is developed in conjunction with Schoenstadt(4).

In analyzing the errors associated with the elemental cell model essentially two pulses are being compared:

(1) the actual pulse, p(t)

(III-1) $$p(t) = \cos[\phi(t)] \qquad T_{p_0} < t < T_{p_0} + \tau_p$$

(2) the approximated pulse, $\hat{p}(t)$

(III-2) $$\hat{p}(t) = \cos[\hat{\phi}(t)] \qquad T_{p_0} < t < T_{p_0} + \tau_p$$

where:

T_{po} = pulse start time

τ_p = pulse duration

$\phi(t)$ = pulse instantaneous phase

$\hat{\phi}(t)$ = pulse approximated instantaneous phase based on the linearized instantaneous frequency function

In analyzing the spectral error, the instantaneous frequency error is first addressed. This forms the foundation for the phase error analysis and ultimately the pulse and spectral error analysis.

Consider the instantaneous frequency function, $f_i(t)$, shown in figure 6. For simplicity, n elemental cells of equal length, h, can be used to generate the piecewise linear approximation, $\hat{f}_i(t)$, such that:

$$\hat{f}_i(t) = \sum_{\kappa=1}^{n} \hat{f}_{i\kappa}(t)\left[\mu(t-t_{\kappa-1}) - \mu(t-t_{\kappa})\right] \tag{III-3}$$

where: $\hat{f}_{i\kappa}(t)$ = linear approximation of the instantaneous frequency function across the k^{th} cell.

$\mu(x)$ = unit step function

If it is assumed that $f_i(t)$ is at least twice differentiable, Gerald(3) shows that the error introduced by the linear approximation in the k^{th} cell, $e_k(t)$, can be expressed as:

$$e_\kappa(t) = f_i(t) - \hat{f}_{i\kappa}(t) = \frac{1}{2}(t-t_{\kappa-1})(t-t_\kappa) f''_{i\kappa}(\eta) \tag{III-4}$$

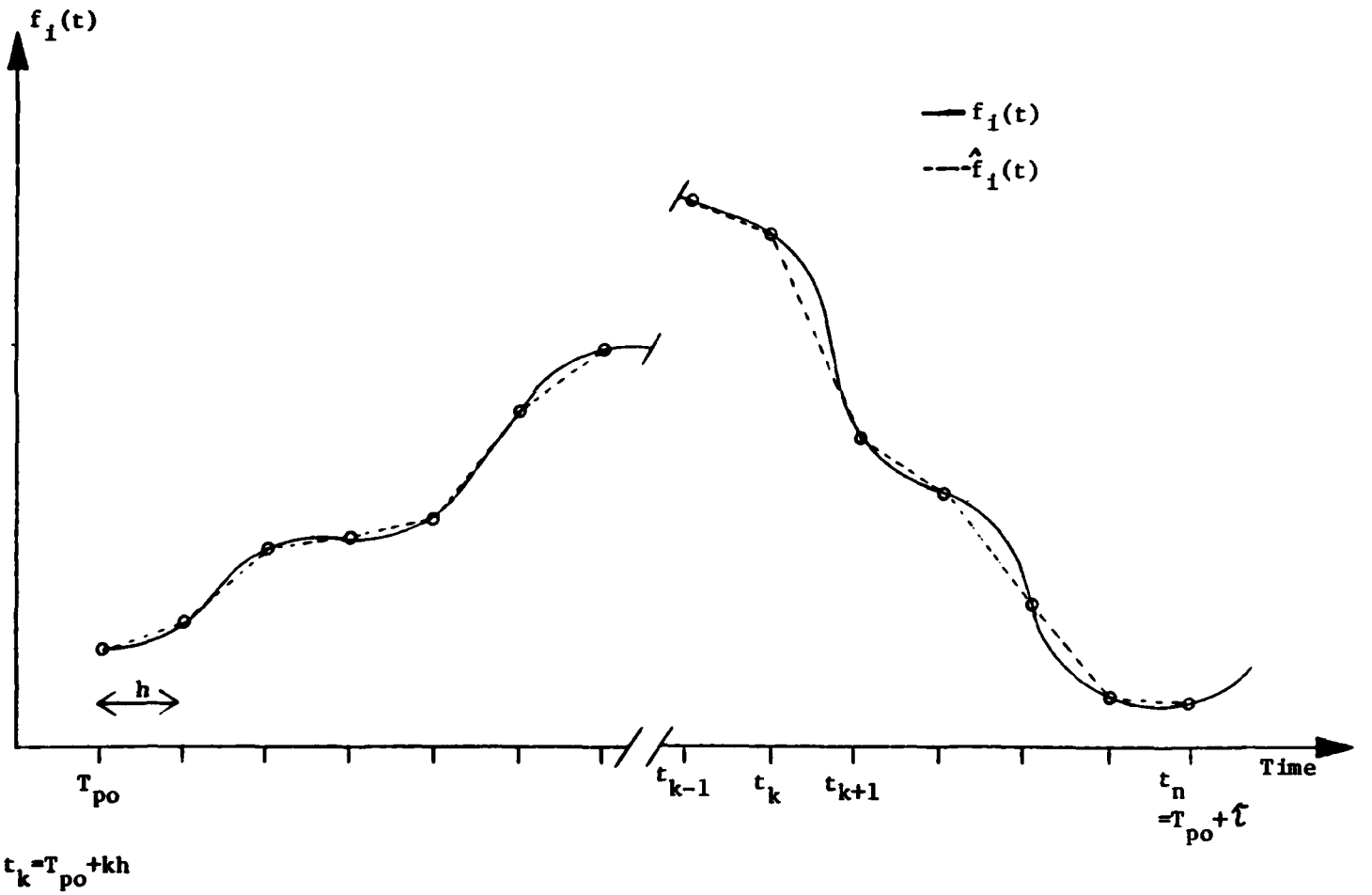

Figure 6 - Generation of $\hat{f}_i(t)$ from $f_i(t)$ Using Cells of Equal Length

where $t_{k-1} < t < t_k$ and $t_{k-1} < \eta < t_k$.

In the actual pulse equation, however, the instantaneous frequency error is reflected as an error in the instantaneous phase; namely,

$$\text{(III-5)} \qquad \phi(t) - \hat{\phi}(t) = \phi(T_{po}) - \hat{\phi}(T_{po}) + 2\pi \int_{T_{po}}^{t} \left[f_i(s) - \hat{f}_i(s) \right] ds$$

Assume that $\phi(T_{po})$, the initial phase, is known. Since $\hat{\phi}(T_{po})$ can be set arbitrarily, allow $\hat{\phi}(T_{po})$ to be equal to $\phi(T_{po})$ causing the first two terms on the right to vanish. Over the interval T_{po} to $T_{po} + \tau_p$, for any t there exists a $t_k = T_{po} + kh$ such that $t \leq t_k$. Selecting k to be the smallest integer such that $t \leq t_k$, the phase error then at any time, t, can be bounded from above in the following manner:

$$\text{(III-6)} \qquad \left| \phi(t) - \hat{\phi}(t) \right| \leq 2\pi \int_{T_{po}}^{t_k} \left| f_i(s) - \hat{f}_i(s) \right| ds$$

This integral can be written as the sum of integrals over the k individual cells:

$$\text{(III-7)} \qquad \left| \phi(t) - \hat{\phi}(t) \right| \leq 2\pi \sum_{j=1}^{k} \int_{t_{j-1}}^{t_j} \left| f_{ij}(s) - \hat{f}_{ij}(s) \right| ds$$

where $t_j = T_{po} + jh$. By construction, the limits of integration are such that the integrand in each term of the summation is given by equation (III-4). Thus,

$$\text{(III-8)} \qquad \left| \phi(t) - \hat{\phi}(t) \right| \leq \pi \sum_{j=1}^{k} \int_{t_{j-1}}^{t_j} \left| (s - t_{j-1})(s - t_j) f_{ij}''(\eta) \right| ds$$

for $t_{j-1} < \eta < t_j$. By a change of variable, let $hw = s - t_{j-1}$ so that

$$|\phi(t) - \hat{\phi}(t)| \leq \pi h^3 \sum_{j=1}^{K} \int_0^1 |w(w-1)||f_{ij}''(\eta)|\,dw \tag{III-9}$$

for $0 \leq \eta \leq 1$. The theorem of the mean for integrals states that

$$\int f(x)g(x)dx = f(\eta)\int g(x)dx \tag{III-10}$$

provided that g(x) does not change sign on the interval of integration and that η is found in the interval of integration. By virtue of this theorem, equation (III-9) can be written:

$$|\phi(t) - \hat{\phi}(t)| \leq \pi h^3 \sum_{j=1}^{K} |f_{ij}''(\eta_j)| \int_0^1 |w(w-1)|dw \tag{III-11}$$

for $0 \leq \eta_j \leq 1$. Equation (III-11) essentially expresses the bound on the instantaneous phase error as the accumulation of errors over k individual elemental cells. An upper bound can be set on the second derivative of the instantaneous frequency in each cell such that for the j^{th} cell the bound is $M_j = \max\{f_{ij}''(\eta_j)\}$ for $t_{j-1} < \eta_j < t_j$. Making use of this bound and integrating equation (III-11) yields:

$$|\phi(t) - \hat{\phi}(t)| \leq \frac{\pi h^3}{6} \sum_{j=1}^{K} M_j \tag{III-12}$$

More generally the second derivative can be bounded over the entire pulse such that $M = \max M_j$ for $j = 1,2,3,.....,k$. It follows then that

equation (III-12) becomes:

$$|\phi(t) - \hat{\phi}(t)| \leq \frac{\pi h^3 k M}{6} \qquad \text{(III-13)}$$

The original selection of k, however, required that $T_{po}+h(k-1) \leq t \leq T_{po}+hk$. In other words, $kh \leq t - T_{po} + h$. Making use of this and the fact that $hn = \tau_p$, equation (III-13) can be written:

$$|\phi(t) - \hat{\phi}(t)| \leq \frac{\pi M \tau_p^2}{6n^2}\left[t - T_{po} + \frac{\tau_p}{n}\right] \qquad \text{(III-14)}$$

Thus an upper bound on the absolute phase error has been obtained as a function of time. It now remains to relate this error to the actual pulse error.

The absolute pulse error can be formed using equations (III-1) and (III-2) as:

$$|p(t) - \hat{p}(t)| = |\cos[\phi(t)] - \cos[\hat{\phi}(t)]| \qquad \text{(III-15)}$$

$$|p(t) - \hat{p}(t)| = \left|-2 \sin\left[\frac{\phi(t)+\hat{\phi}(t)}{2}\right] \sin\left[\frac{\phi(t)-\hat{\phi}(t)}{2}\right]\right| \qquad \text{(III-16)}$$

Since the sin(x) is less than or equal to one,

$$|p(t) - \hat{p}(t)| \leq \left|2 \sin\left[\frac{\phi(t)-\hat{\phi}(t)}{2}\right]\right| \qquad \text{(III-17)}$$

By making use of the fact that $|\sin(x)| \leq |x|$, the pulse error bound reduces to:

$$|p(t) - \hat{p}(t)| \leq |\phi(t) - \hat{\phi}(t)| \tag{III-18}$$

$$|p(t) - \hat{p}(t)| \leq \frac{\pi M \tau_p^2}{6n^2}\left(t - T_{po} + \frac{\tau_p}{n}\right) \tag{III-19}$$

With this knowledge of the pulse error, the bound on the spectral error can be addressed. Writing the spectral error in terms of the pulse error,

$$P(f) - \hat{P}(f) = \int_{T_{po}}^{T_{po}+\tau_p} [p(t) - \hat{p}(t)] e^{-j\omega t} dt \tag{III-20}$$

where P(f) and $\hat{P}(f)$ are the exact and approximated spectra respectively. The absolute error can be written:

$$|P(f) - \hat{P}(f)| \leq \int_{T_{po}}^{T_{po}+\tau_p} |p(t) - \hat{p}(t)| dt \leq \int_{T_{po}}^{T_{po}+\tau_p} |\phi(t) - \hat{\phi}(t)| dt \tag{III-21}$$

Using the derived expression for the absolute phase error (equation III-14),

$$|P(f) - \hat{P}(f)| \leq \int_{T_{po}}^{T_{po}+\tau_p} \left(\frac{\pi M \tau_p^2}{6n^2}\right)\left(t - T_{po} + \frac{\tau_p}{n}\right) dt \tag{III-22}$$

$$|P(f) - \hat{P}(f)| \leq \frac{\pi M \tau_p^4}{12n^2}\left(1 + \frac{2}{n}\right) \tag{III-23}$$

Additionally, since the absolute value of a difference is greater than or equal to the absolute value of the difference of the absolute values, the

bound on the spectrum error using the cell model can be expressed as:

$$\left| |P(f)| - |\hat{P}(f)| \right| \leq \frac{\pi M \tau_p^4}{12 n^2}\left(1 + \frac{1}{n}\right) \qquad \text{(III-24)}$$

In general then, the accuracy of the elemental cell model depends on the maximum value of the second derivative of the instantaneous frequency function (a measure of how nonlinear the modulation is), the pulse width and the number of elemental cells which subdivide the pulse. It is significant to note that the model converges to the actual spectrum inversely as the square of the number of cells.

While the error bound developed above assumed elemental cells of equal length and bounded the second derivative of the instantaneous frequency function across the entire pulse, a tighter bound, and one which is more generally applicable to elemental cells of unequal length, can be obtained by bounding the error contribution from each individual cell and then summing these contributions over the total number of elemental cells. The total spectrum error is given by

$$P(f) - \hat{P}(f) = \left[P_1(f) - \hat{P}_1(f)\right] + \left[P_2(f) - \hat{P}_2(f)\right] + \ldots . \qquad \text{(III-25)}$$

where $P_i(f)$ and $\hat{P}_i(f)$ are the true and approximated spectra respectively of the i^{th} elemental cell. So that the absolute spectrum error can be bounded from above by summing over the absolute error associated with each elemental cell.

$$\left| P(f) - \hat{P}(f) \right| \leq \sum_{i=1}^{n} \left| P_i(f) - \hat{P}_i(f) \right| \qquad \text{(III-26)}$$

The absolute spectrum error associated with each elemental cell, $|P_i(f) - \hat{P}_i(f)|$, remains to be developed. Consider the k^{th} elemental cell as depicted in figure 7. An expression analogous to equation (III-5) can be developed to describe the absolute instantaneous phase error at some time, t, associated with the k^{th} elemental cell,

$$|\phi(t) - \hat{\phi}(t)| \leq |\phi(T_{ok}) - \hat{\phi}(T_{ok})| + 2\pi \int_{T_{ok}}^{t} |f_i(s) - \hat{f}_i(s)| ds \qquad \text{(III-27)}$$

where $T_{ok} \leq t \leq T_{ok} + \tau_k = T_{o(k+1)}$. In addressing the analogous equation (III-5), the phase error at the beginning of the pulse was set equal to zero since $\hat{\phi}(T_o)$ was arbitrarily set equal to $\phi(T_o)$. In the general case, in which successive elemental cells are being considered, $\hat{\phi}(T_{ok})$ is not arbitrary. The phase difference at T_{ok} must be viewed as a cummulative error resulting from the approximations made in the successive elemental cells occurring before T_{ok}. To develop this point, assume as before that at the beginning of the pulse (that is the first elemental cell) that $\phi(T_o) = \phi(T_{o1}) = \hat{\phi}(T_{o1}) = \hat{\phi}(T_o)$. Using the above equations, the phase error at the end of the first cell or, equivalently, at the beginning of the second cell is:

$$|\phi(T_{o2}) - \hat{\phi}(T_{o2})| \leq 2\pi \int_{T_{o1}}^{T_{o1}+\tau_1} |f_i(s) - \hat{f}_i(s)| ds \qquad \text{(III-28)}$$

Using the expression for the elemental cell instantaneous frequency error developed in equation (III-4),

$$|\phi(T_{o2}) - \hat{\phi}(T_{o2})| \leq \pi \int_{T_{o1}}^{T_{o1}+\tau_1} |(t - T_{o1})(t - T_{o1} - \tau_1)| |f''_{i1}(\nu)| dt \qquad \text{(III-29)}$$

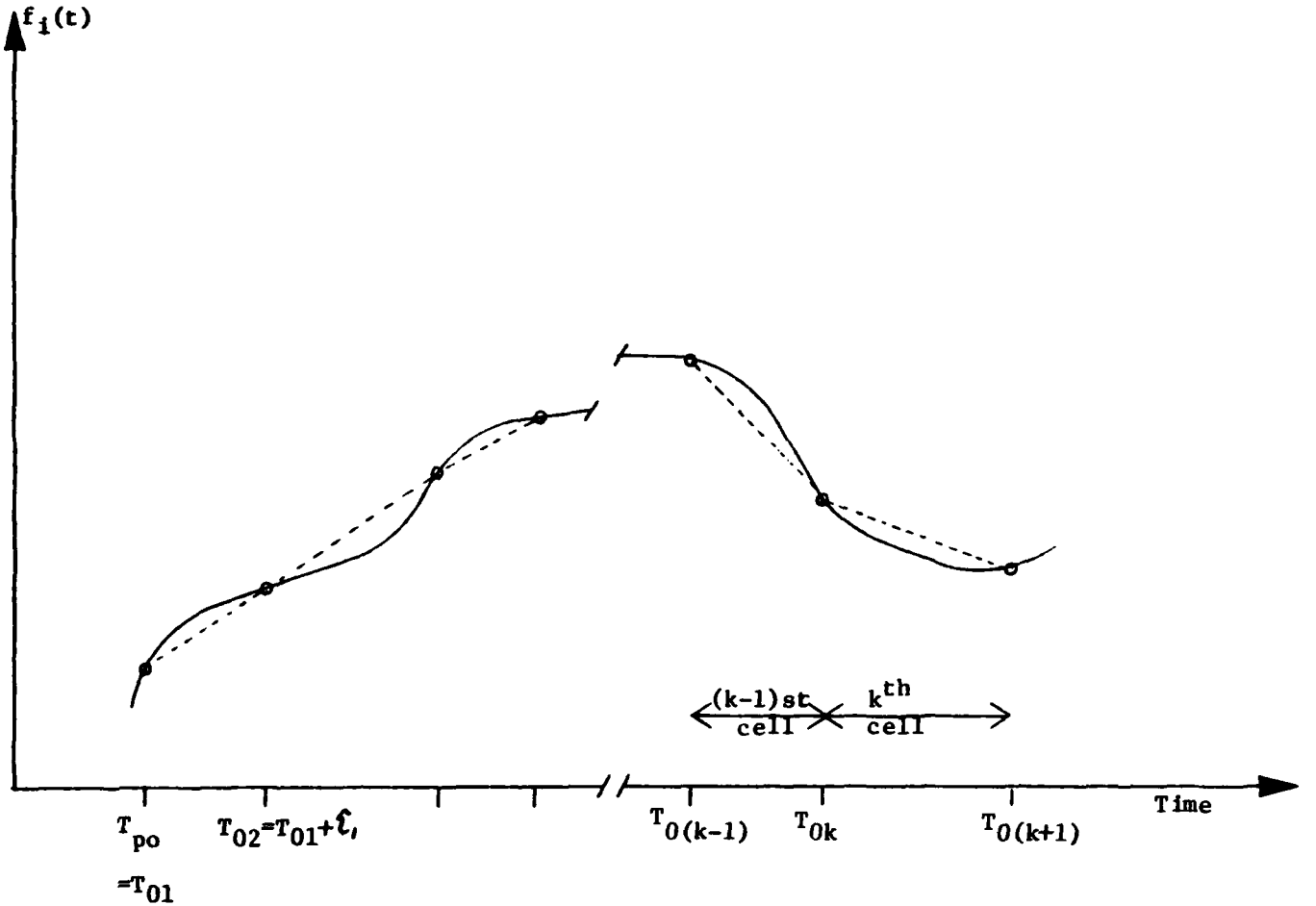

Figure 7 - Generation of $\hat{f}_i(t)$ from $f_i(t)$ Using Cells of Unequal Length

for $T_{01} \leq \eta \leq T_{01} + \tau_1$. Applying the mean value theorem of integrals, bounding the second derivative of the instantaneous frequency across the cell by its maximum value, M_1, and integrating yields:

$$\text{(III-30)} \qquad \left|\phi(T_{02}) - \hat{\phi}(T_{02})\right| \leq \frac{\pi M_1 \tau_1^3}{6}$$

Thus the phase error at the beginning of the second cell is a function of the quality of the approximation made in the first cell. A similar development can be applied to generate the phase error at the end of the second cell (beginning of the third cell); the absolute phase error at the beginning of the third cell being:

$$\text{(III-31)} \qquad \left|\phi(T_{03}) - \hat{\phi}(T_{03})\right| \leq \left|\phi(T_{02}) - \hat{\phi}(T_{02})\right| + \pi \int_{T_{02}}^{T_{02}+\tau_2} \left|(t - T_{02})(t - T_{02} - \tau_2)\right| \left|f_{i2}''(\omega)\right| dt$$

The first term on the right is given by equation (III-30) and the integral can be evaluated as above to yield:

$$\text{(III-32)} \qquad \left|\phi(T_{03}) - \hat{\phi}(T_{03})\right| \leq \frac{\pi}{6}\left(M_1 \tau_1^3 + M_2 \tau_2^3\right)$$

Extending this result, the absolute phase error at the beginning of the k^{th} cell can be expressed as:

$$\text{(III-33)} \qquad \left|\phi(T_{0k}) - \hat{\phi}(T_{0k})\right| \leq \frac{\pi}{6} \sum_{j=1}^{k-1} M_j \tau_j^3$$

This result can be applied to equation (III-27) along with the expression for the instantaneous frequency error in equation (III-4) to develop an

expression for the absolute phase error associated with the k^{th} cell as a function of time:

$$(III\text{-}34) \qquad |\phi(t) - \hat{\phi}(t)| \le \frac{\pi}{6} \sum_{j=1}^{K-1} M_j \tau_j^3 + \frac{\pi M_K}{6} \left\{ \left| 2(t - T_{0K})^3 - 3\tau_K (t - T_{0K})^2 \right| \right\}$$

for $T_{0k} \le t \le T_{0k} + \tau_K$. This expression for the phase error can be used in combination with equation (III-21) to form the upper bound on the spectral error associated with the k^{th} elemental cell.

$$(III\text{-}35) \qquad |P_K(f) - \hat{P}_K(f)| \le \frac{\pi}{6} \int_{T_{0K}}^{T_{0K} + \tau_K} \left\{ \left(\sum_{j=1}^{K-1} M_j \tau_j^3 \right) + M_K \left| 2(t - T_{0K})^3 - 3\tau_K (t - T_{0K})^2 \right| \right\} dt$$

$$(III\text{-}36) \qquad |P_K(f) - \hat{P}_K(f)| \le \frac{\pi \tau_K}{6} \sum_{j=1}^{K-1} M_j \tau_j^3 + \frac{\pi M_K \tau_K^4}{12}$$

This represents then a bound on the local spectrum error associated with the k^{th} elemental cell. To obtain a bound on the global error across the pulse, the local error of each cell can be summed over all of the elemental cells, as in equation (III-26), so that

$$(III\text{-}37) \qquad \left| |P(f)| - |\hat{P}(f)| \right| \le \sum_{K=1}^{n} \left(\frac{\pi \tau_K}{6} \sum_{j=1}^{K-1} M_j \tau_j^3 \right) + \frac{\pi M_K \tau_K^4}{12}$$

While this expression for the error bound is more unwieldy than that developed in equation (III-24), it has provisions for addressing elemental cells of non-uniform length. It also bounds the second derivative of the instantaneous frequency function on a cell by cell basis, yielding a tighter spectral error bound. This tighter bound is, of course, at the

expense of complexity of evaluation. The determination of the bound on the second derivative of the instantaneous frequency function, M, for equation (III-24) may be difficult enough. To further determine the bounds M_j for all elemental cells for application to equation (III-37) may be unacceptably tedious. A trade-off can be made to loosen the error bound of equation (III-37) while preserving the provision for addressing non-uniform elemental cell lengths by bounding the second derivative of the instantaneous frequency function across the pulse (i.e., $M = \max \{M_j\}$, $j = 1,2,.....n$)

$$\text{(III-38)} \qquad \left\| |P(f)| - |\hat{P}(f)| \right\| \leq \sum_{K=1}^{n} \left\{ \frac{\pi M \tau_K}{6} \sum_{j=1}^{K-1} \tau_j + \frac{\pi M \tau_K}{12} \right\}$$

Thus various approaches of different degrees of compexity can be used to develop theoretical maximum error bounds on the spectrum error associated with the elemental cell model. The choice of approach must be based on problem complexity and a priori knowledge of the pulse structure. The most important insight, however, that the maximum error bound provides is that in applying the elemental cell model, this error tends toward zero inversely as the square of the number (n) of cells.

B. EMPIRICAL ASSESSMENT

The objective of this section is to assess the actual elemental cell model performance in the light of the error bounds developed in section III-A. To achieve this a unit pulse with sinusoidal FM is examined (as in Section II-B). The pulse is such that the carrier

frequency, f_c, is 30 MHz; the modulating frequency, f_m, is 200 kHz; the modulation index, k_f, is one; and the pulse duration, ℓ_p, is five microseconds. The exact spectrum of this pulse can be determined (see Appendix B). Using the elemental cell model (Section II-B), approximate spectra can be generated for cases where the number of elemental cells, n, is 1,2,3,..... Each of these approximated spectra can then be compared to the exact spectrum to determine the maximum spectrum error calculated for n=1,2,3..... (For the purpose of this analysis, frequency components between 29 MHz and 31 MHz are examined at 20 kHz intervals.)

Since the unit pulse under consideration has an instantaneous frequency function, $f_i(t)$, given by

$$f_i(t) = f_c + k_f f_m \cos[\omega_m t] \tag{III-39}$$

the maximum bound on the second derivative of the instantaneous frequency function can be determined analytically. Since this is the "M" of equation (III-24), that equation can be evaluated to yield the maximum theoretical spectrum error bound as a function of n, the number of elemental cells used to approximate the pulse.

It is also possible to generate a tighter theoretical bound on the spectrum error by using equation (III-37) and determining from equation (III-39) the bound on the second derivative of the instantaneous frequency function across each individual cell.

Thus a set of three curves can be generated:

(1) The maximum theoretical spectrum error bound with

$f_i''(t)$ bounded across the pulse (equation III-24) as a function of n, the number of elemental cells;

(2) The maximum theoretical spectrum error bound with $f_i''(t)$ bounded across each elemental cell (equation III-37) as a function of n;

(3) The maximum calculated spectrum error as a function of n.

Figure 8 presents this set of curves for the pulse with sinusoidal FM discussed above. The first theoretical bound (equation III-24) is represented by the solid line; the second (equation III-37), by the dashed line; and the calculated error, by the dotted line. The tightening of the maximum theoretical error by bounding the second derivative of the instantaneous frequency function across each elemental cell vice across the pulse can be observed quantitatively by comparing the solid and dashed curves. The maximum calculated error (dotted curve) is well within the bounds set by equations (III-24) and (III-37). In fact, the calculated error is generally an order of magnitude smaller than the maximum error bound set by equation (III-24). Inspection of Figure 8 indicates that all three curves generally follow the characteristic convergence, which goes inversely as the square of the number (n) of elemental cells.

An important consideration in applying the elemental cell model is the determination of the number of elemental cells to be used. Obviously, the greater the number of cells, the closer the approximated spectrum is to the exact spectrum, but at the cost of complexity and processing time. The establishment of the inverse squared relationship between the number of cells and the theoretical maximum error bound allows the determination

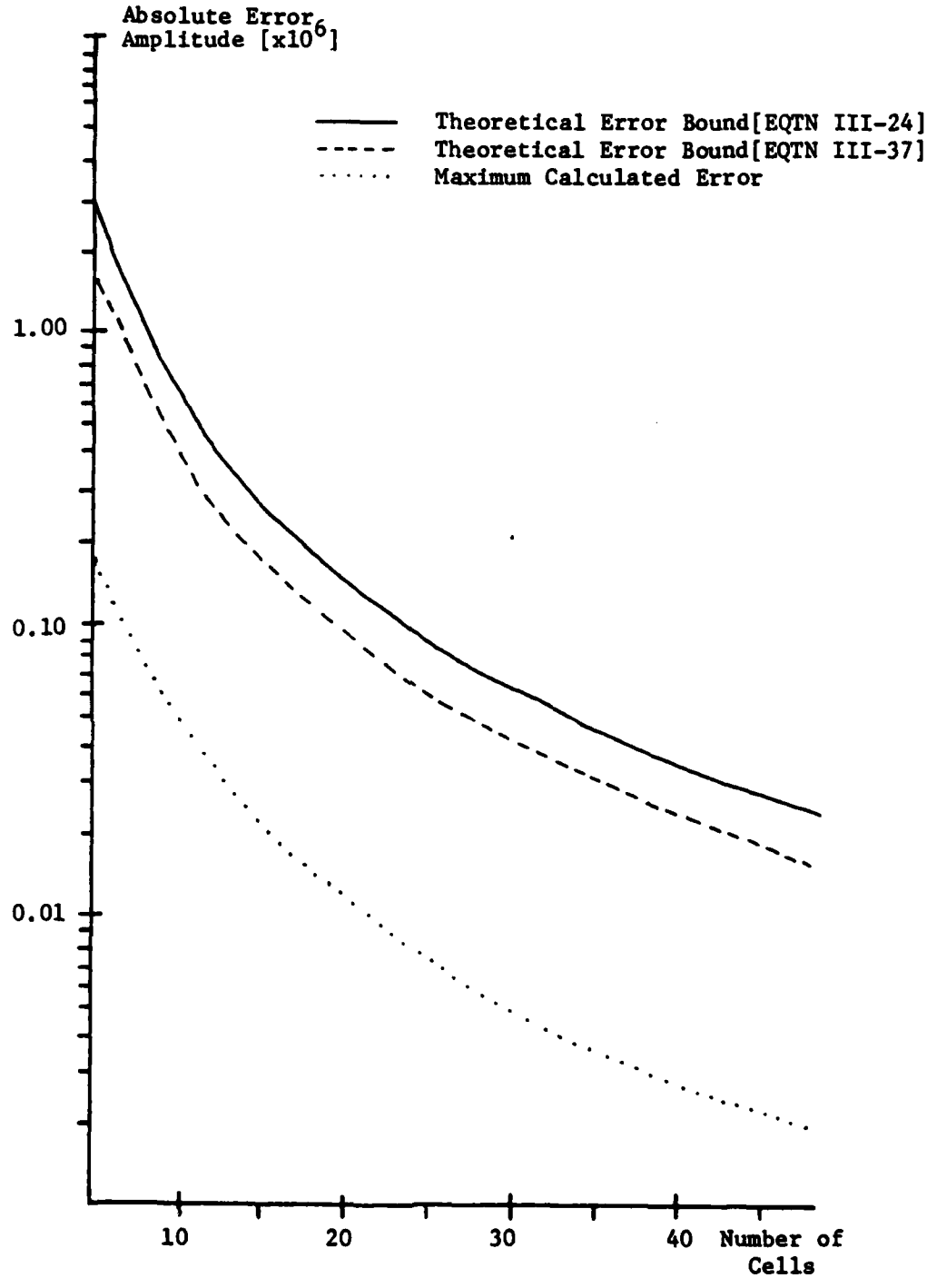

Figure 8 - Theoretical Error Bound and Maximum Calculated Error as a Function of the Number of Elemental Cells Used in the Model Process

of the minimum number of cells required as a function of the maximum tolerable error. Let $\mathcal{E}$ be the maximum tolerable error, then equation (III-24) can be written as:

$$\frac{\pi M \tau_p^4}{12 n^2}\left(1+\frac{2}{n}\right) < \mathcal{E} \qquad \text{(III-40)}$$

so that

$$\frac{n^3}{n+2} > \frac{\pi M \tau_p^4}{12 \mathcal{E}} \qquad \text{(III-41)}$$

or for the case when the number of cells in large:

$$n > \frac{\tau_p^2}{2}\sqrt{\frac{M}{\mathcal{E}}} \qquad \text{(III-42)}$$

For example, in the case of the unit pulse with a 200 kHz sinusoidal FM discussed above, the spectrum has a peak value on the order of $(\tau_p/2)\ 2.5\times10^{-6}$. If the interest is primarily in the mainlobe, the maximum tolerable error may be an order of magnitude less than the peak value, so that $\mathcal{E} = 2.5\times10^{-7}$. Then, knowing the value of M and τ_p, equation (III-42) can be evaluated (or, equivalently Figure 8 could be consulted) to determine that 15 cells (n = 14.3) are required to assure that the maximum tolerable error is not exceeded. In this example, n=15 provides considerably more accuracy than is required, but does also provide the guarantee that the error will not be greater than the accepted limit.

In practice, the second derivative, used freely above, may seldom be available in analytic form. In those cases, a sizing of the problem can

be made using the central difference approximation to the second derivative (3). Specifically, given a function g(t), as in figure 9, the approximation to the second derivative at T_o is:

(III-43) $$g_o'' = \frac{g_{-1} - 2g_o + g_{+1}}{h^2}$$

In the case of the test signal discussed above, the maximum of the second derivative of the instantaneous frequency function across the pulse is given by: $M = 3.1583 \times 10^{17}$. If the central difference approximation of equation (III-43) is applied to the test pulse at T_o = 2.5 microseconds for various values of h and the resulting approximated derivatives applied to equation (III-42), the following estimates of the numbers of cells required to produce an error no worse than 2.5×10^{-7} are obtained:

for h = 1.2500 μs; $\hat{f}_i''(T_o) = 2.56 \times 10^{17}$; n = 12.6

for h = 0.6250 μs; $\hat{f}_i''(T_o) = 3.00 \times 10^{17}$; n = 13.7

for h = 0.3125 μs; $\hat{f}_i''(T_o) = 3.12 \times 10^{17}$; n = 13.9

Thus this approximate approach to sizing the modeling problem is in close agreement with the exact solution of n = 14.3.

The maximum error bounds developed in Section (III-A) provide a valuable insight into the nature of the convergence of the elemental cell model and a useful tool in determining the number of elemental cells required to model a specific pulse.

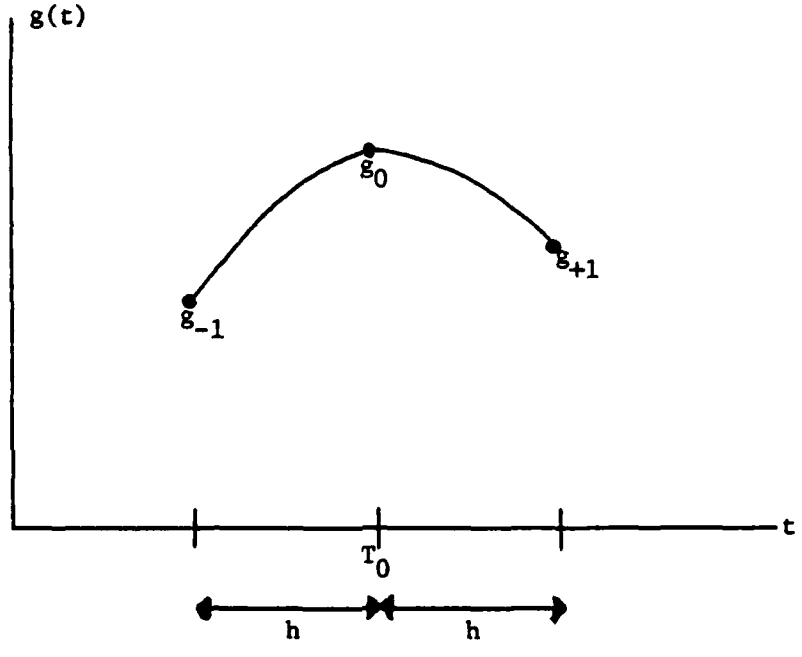

$$g_0'' = (g_{-1} - 2g_0 + g_{+1})/h^2$$

Figure 9 - Central Difference Approximation to the Second Derivative

C. ASSESSMENT OF ERRORS ACROSS THE SPECTRUM

To this point, the error analysis has addressed the worst case, maximum error bound, aspects of the elemental cell model and has emphasized the $1/n^2$ convergence. But this maximum error is simply a bound and does not address the error associated with individual frequency components across the spectrum.

Consider the difference, E_t, between the exact and the approximated pulses in the time domain,

$$E_t(t) = \cos[\phi(t)] - \cos[\hat{\phi}(t)] \tag{III-44}$$

where $\phi(t)$ is derived from the instantaneous frequency function, $f_i(t)$, equation (II-2) and $\hat{\phi}(t)$ is similarly derived from the linearly approximated instantaneous frequency function, $\hat{f}_i(t)$. Then $\phi(t)$ and $\hat{\phi}(t)$ are related by:

$$\phi(t) = \hat{\phi}(t) + \epsilon(t) \tag{III-45}$$

where $\epsilon(t)$ is the phase error as a function of time such that

$$\epsilon(t) = \phi(t) - \hat{\phi}(t) = 2\pi \int_0^t [f_i(x) - \hat{f}_i(x)]dx \tag{III-46}$$

$$\epsilon(t) = 2\pi \int_0^t e(x)dx \tag{III-47}$$

where e(t) is the instantaneous frequency error as a function of time.

Substituting equation (III-45) into (III-44) yields:

(III-48) $$E_t(t) = \cos[\hat{\phi}(t) + \epsilon(t)] - \cos[\hat{\phi}(t)]$$

(III-49) $$E_t(t) = 2\sin\left(\hat{\phi}(t) + \frac{\epsilon(t)}{2}\right)\sin\left(\frac{\epsilon(t)}{2}\right)$$

If $\epsilon(t)$ is small, that is, for example, if $\epsilon(t) \leq 0.5$ (arbitrarily), then

(III-50) $$E_t(t) \approx \epsilon(t)\sin\left(\hat{\phi}(t) + \frac{\epsilon(t)}{2}\right)$$

Additionally, if $\hat{\phi}(t) \gg \frac{\epsilon(t)}{2}$, then

(III-51) $$E_t(t) \approx \epsilon(t)\sin[\hat{\phi}(t)]$$

If $\epsilon(t)$ has a Fourier Transform, $\epsilon(f)$, and $\sin\hat{\phi}(t)$ has a Fourier Transform, $\hat{P}(f)$; then the error associated with $E_t(t)$ in the frequency domain, $E_f(f)$, is given by the convolution of $\epsilon(f)$ and $\hat{P}(f)$.

(III-52) $$E_t(t) = \epsilon(t)\sin[\hat{\phi}(t)] \iff \epsilon(f) \circledast \hat{P}(f) = E_f(f)$$

While this expression is far from simple, it may provide an insight into the behavior of errors across the spectrum as the number of elemental cells is varied.

Consider, again, the test pulse of unit amplitude with sinusoidal FM. If this pulse is modeled, using four elemental cells, the instantaneous frequency error, e(t), and the instantaneous phase error, $\epsilon(t)$, can be

generated as in figure 10. Before applying the instantaneous phase error function to equation (III-52), let us first examine the applicability of the equation to the case at hand.

In arriving at equation (III-51) and, ultimately, (III-52), two assumptions were made: (1) that the instantaneous phase error, $\epsilon(t)$, was small (that is that $\epsilon(t) \approx \sin(\epsilon(t))$ and (2) that $\epsilon(t) \ll \hat{\phi}(t)$. Figure 10 illustrates that assumption one is satisfied; i.e. $\epsilon(t) < 0.5$. As for assumption (2), generally, $\hat{\phi}(t)$ behaves as $\phi(t)$, so that

(III-53) $$\hat{\phi}(t) \approx 60\pi T - \sin(0.4\pi T)$$

for T in microseconds. Realizing that this function is based on modulo two pi, there will be a few cases where $\epsilon(t) \approx \phi(t)$, but in general over the pulse $\hat{\phi}(t) \gg \epsilon(t)$. (See Figure 11).

Consider now the instantaneous phase error, $\epsilon(t)$, in figure 10, in the light of equation (III-52). The Fourier transform of $\epsilon(t)$ is essentially a sin(x)/x function centered about the carrier frequency, in this case 200 kHz. In actuality, the spectrum is not quite this straightforward, because of the relative proximity of carrier frequency to the origin (f=0). The spectrum, as shown in figure 12, is, in general, characterized by two main lobes of 400 kHz, sidelobes of 200 kHz, and a spacing between the mainlobes on the order of 440 kHz.

The basic form of the spectrum, $\hat{P}(f)$, generated by the instantaneous frequency function, $f_i(t)$, is of the form shown in figure 13. $E_f(f)$, can be considered generally based on figures 12 and 13. It is expected that $E_f(f)$ would have a basic sin(x)/x form with two mainlobes being about 400 kHz wide and symmetrically spaced 220 kHz above and below the

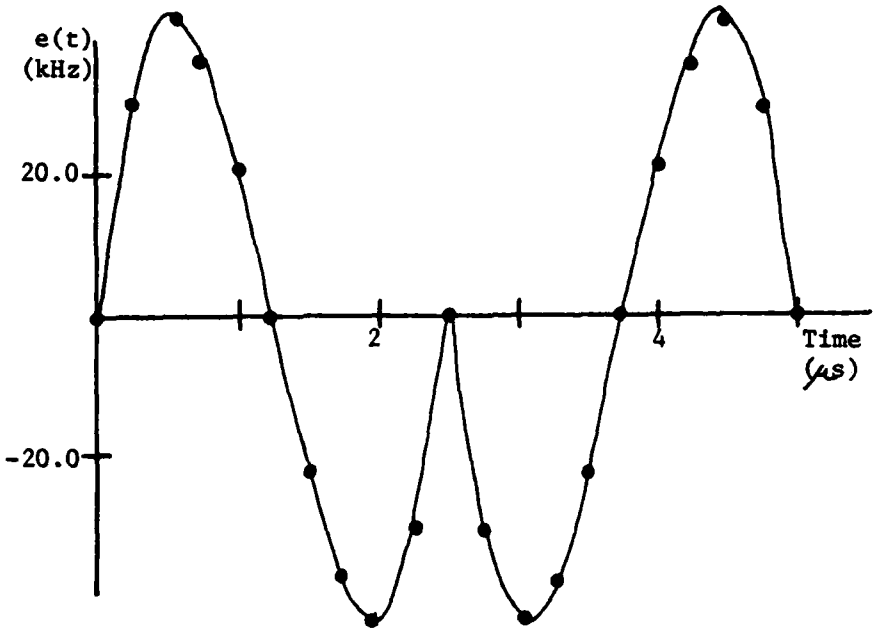

(a) Instantaneous Frequency Error vs. Time

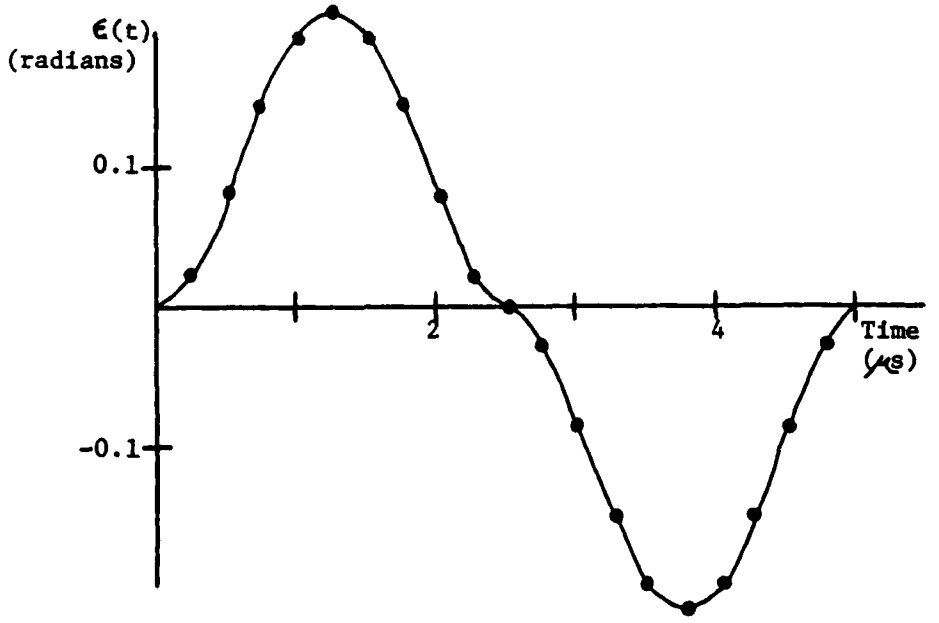

(b) Instantaneous Phase Error vs. Time

Figure 10 - Time Domain Error Functions for a Four Cell Model of a Pulse with Sinusoidal FM

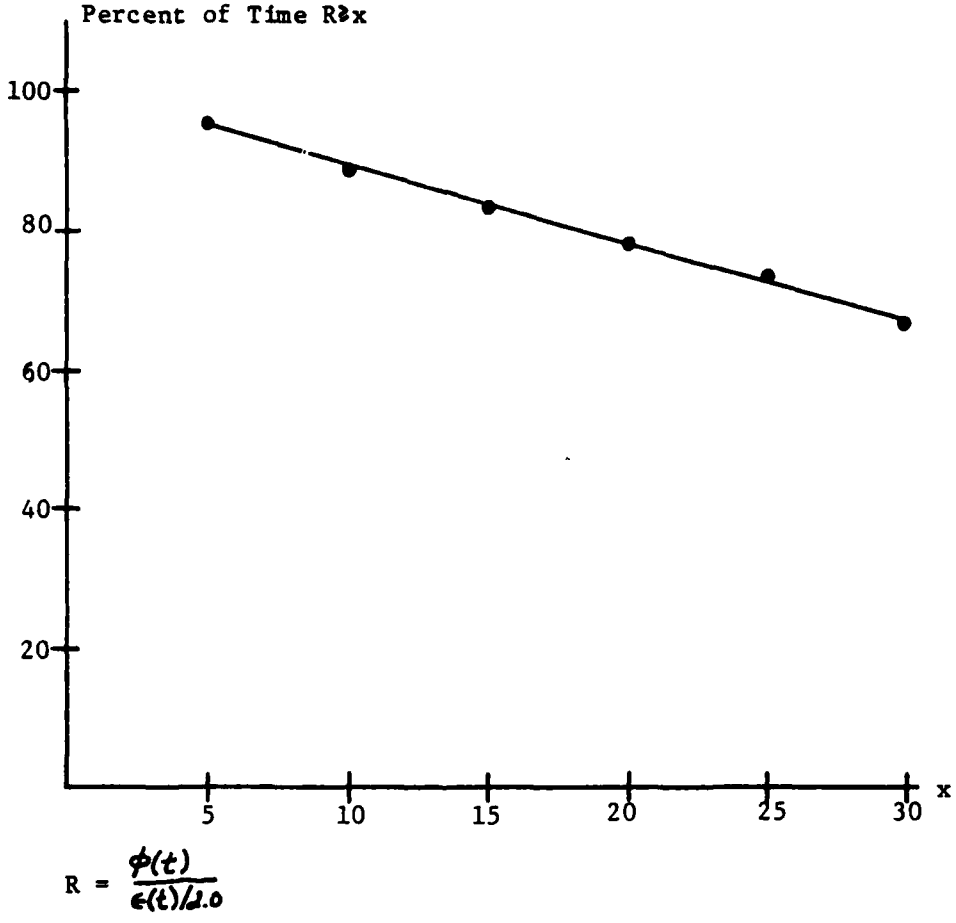

Figure 11 - Comparison of Phase and Phase Error across a Sinusoidally Modulated Unit Pulse Using a Four Elemental Cell Model; Percent of Time that the Ratio, R, is Greater Than a Given Threshold Value, x, as a Function of the Threshold Value

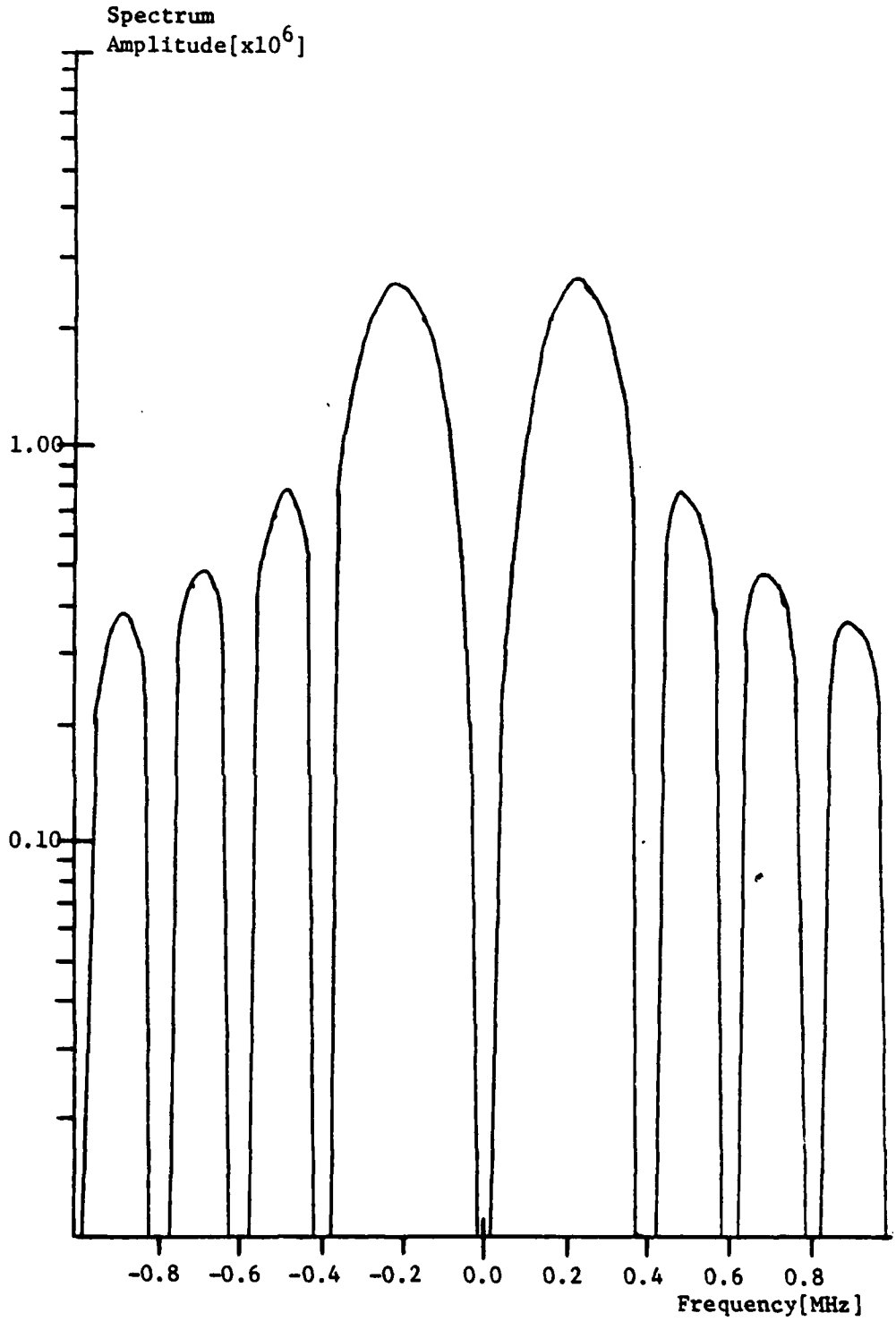

Figure 12 - Amplitude Spectrum of a 5.0μs Pulse with a 200 kHz Carrier

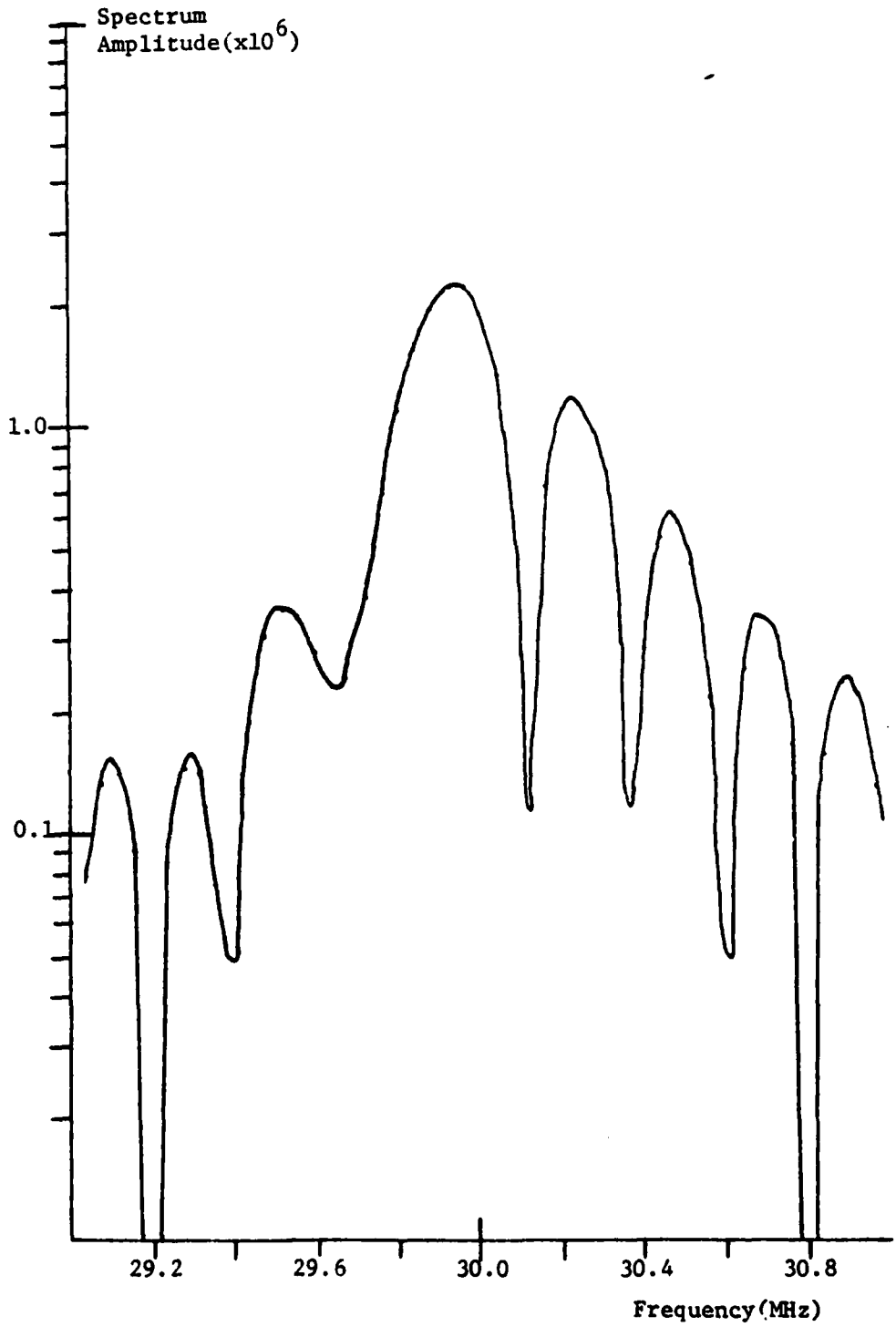

Figure 13 - Exact Amplitude Spectrum of a 5μs Pulse with 200 kHz Sinusoidal FM (Modulation Index = 1.0)

peak frequency component of $\hat{P}(f)$. Further, it would be expected that a negligible error would be associated with the peak value of $\hat{P}(f)$ and that the upper and lower sidelobes of $E_f(f)$ would be about 200 kHz wide. Figure 14 is helpful in addressing this qualitative analysis of $E_f(f)$. The solid line in the figure represents the exact spectrum of a unit pulse with a 200 kHz sinusoidal frequency modulation imposed upon it. (i.e. The test signal discussed above). The additional projections (x's, circles and triangles) represent the spectrum error, $E_f(f)$, associated with the modeling of the test signal using four, eight and sixteen elemental cells, respectively. For the moment, the case of four elemental cells will be addressed. Note that the mainlobes of $E_f(f)$ are on the order of 400 kHz wide and that these lobes are centered fairly symmetrically about the peak value of P(f), being offset by 200 to 250 kHz. As predicted, the upper sidelobes tend to decrease in width to the order of 200 kHz. Thus, while equation (III-52) is fairly unwieldy, a basic insight into the behavior of $E_f(f)$ can be obtained.

Consider now the two additional cases presented in figure 14 for the cases when eight and sixteen cells are used. The instantaneous frequency and phase error for an eight cell and a sixteen cell simulation are shown as functions of time in figures 15 and 16, respectively. It can be seen that in both cases the instantaneous phase error departs slightly from that examined under the case n=4, but that the general form of $\epsilon(t)$ persists. In the frequency domain, this is reflected in the similar forms of $E_f(f)$ for n=4,8,16. Of particular interest is the scaling associated with each of the three phase error functions. All three instantaneous phase error functions are forms of a perturbed

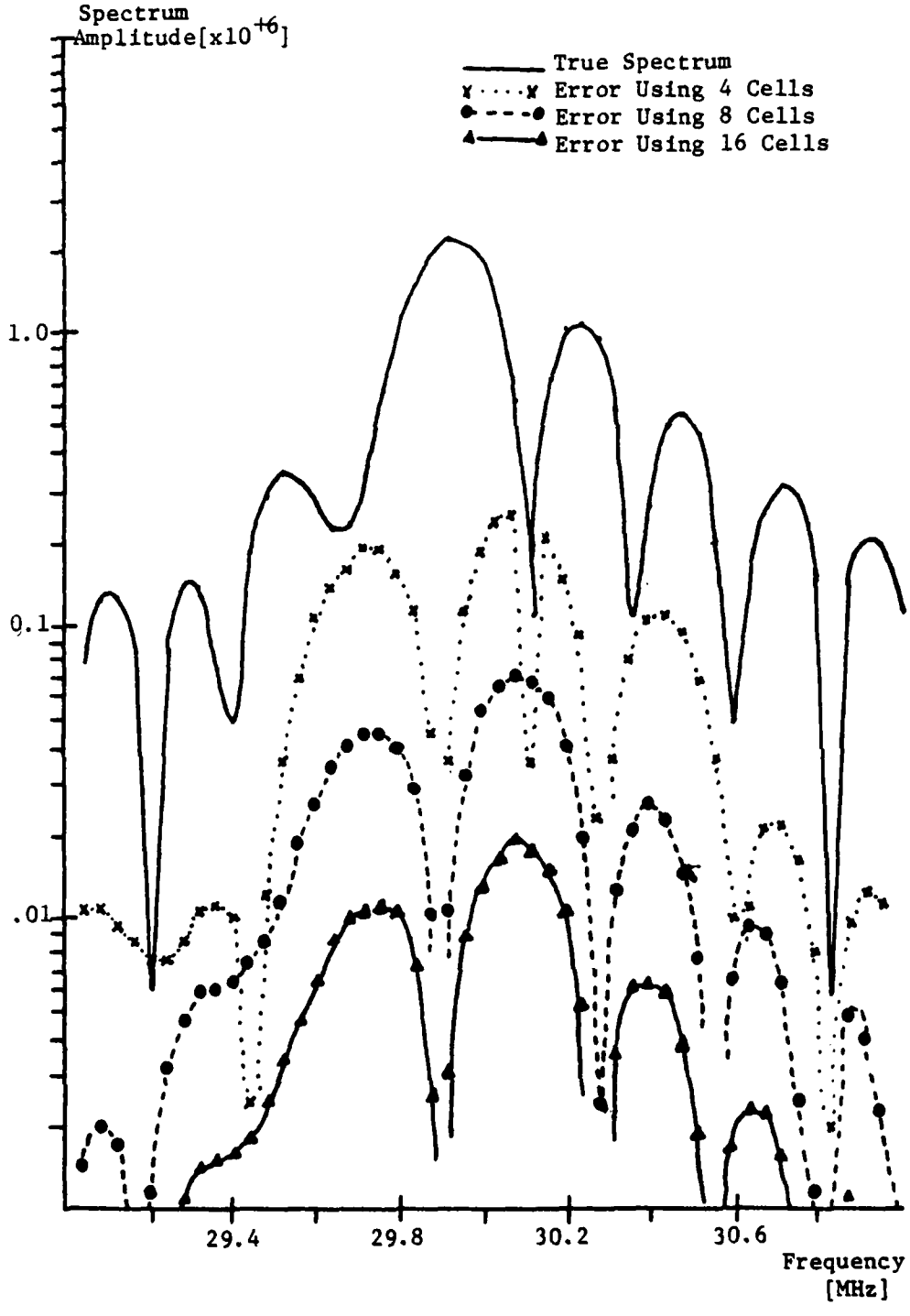

Figure 14 - Amplitude Spectrum Error for a Unit Pulse with Sinusoidal Frequency Modulation for Elemental Cell Modeling Using 4, 8, and 16 Cells

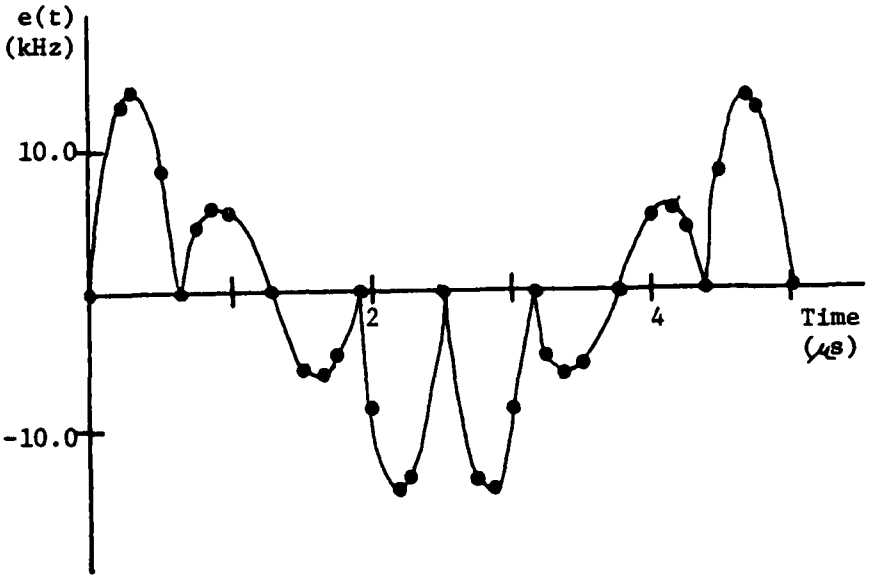

(a) Instantaneous Frequency Error vs. Time

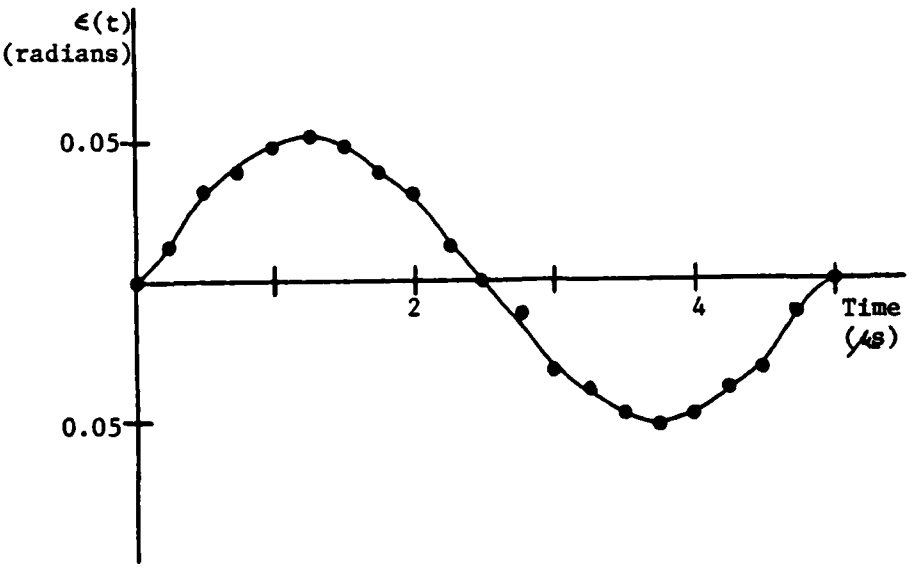

(b) Instantaneous Phase Error vs. Time

Figure 15 - Time Domain Error Functions for an Eight Cell Model of a Pulse with Sinusoidal FM

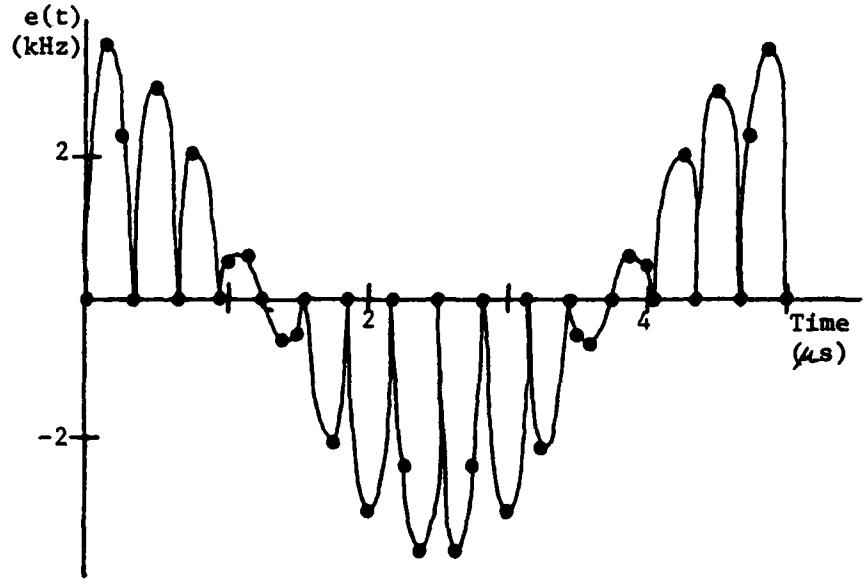

(a) Instantaneous Frequency Error vs. Time

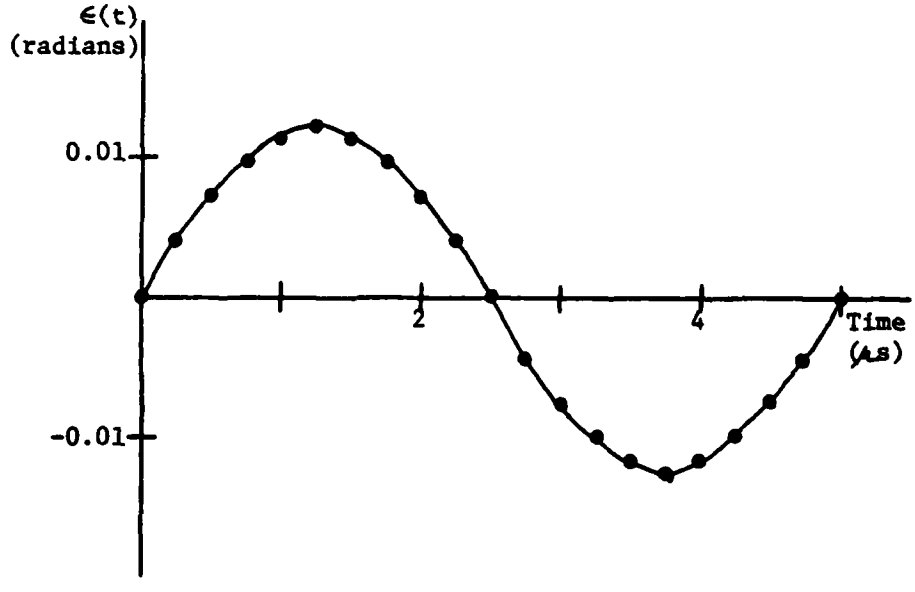

(b) Instantaneous Phase Error vs Time

Figure 16 - Time Domain Error Functions for a Sixteen Cell Model of a Pulse with Sinusoidal FM

200 kHz waveform with varying amplitudes:

for four cells, the amplitude is .214 radians
for eight cells, the amplitude is .051 radians
for sixteen cells, the amplitude is .012 radians.

So that in increasing the number of cells from four to eight, the peak phase error is reduced by a factor of 0.24. An increase in the number of cells from eight to sixteen reduces the peak phase error by a factor of 0.24. Considering then the convolution of equation (III-52) and assuming that P(f) is essentially constant for n=4,8,16, it would be expected that $E_f(f)$ would be improved by about a factor of 0.24 for increases in the number of elemental cells from four to eight and from eight to sixteen. This is, in fact, the case generally portrayed in figure 14. Typically, the improvement experienced in going from four to eight cells and from eight to sixteen cells is on the order of a 0.20 to 0.25 reduction in the spectrum error. Again, this reduction in spectrum error by a factor of 4 when the number of elemental cells are doubled is characteristic of the $1/n^2$ convergence discussed in section III-A. While some abberations occur in the convergence to the exact spectrum (e.g. between 29.0 and 29.4 MHz), it is significant that the convergence across the spectrum is generally uniform. Even in cases of anomalies (29.0 to 29.4 MHz), the convergence tends to be uniform as n increases.

In summary, by examining the phase error, it is possible to project the basic form of the spectrum error, $E_f(f)$ and, perhaps of more significance, to examine the behavior of the spectrum error as the number of

cells is varied. This provides an important insight into $E_f(f)$ and the convergence of $\hat{P}(f)$ to $P(f)$.

IV. GENERALIZED ELEMENTAL CELL MODEL

A. DEVELOPMENT OF THE GENERALIZED ELEMENTAL CELL MODEL

The elemental cell model developed in Section II accommodates a unit pulse with arbitrary frequency modulation. That model can be generalized to accommodate arbitrary amplitude modulation. The modeling approach is the same, i.e., the pulse is decomposed into elemental cells and across each elemental cell the frequency and amplitude modulation are linearly approximated. Thus, in the generalized model, both the instantaneous frequency function and the pulse envelope are represented by linear piecewise continuous functions.

Consider a pulse, s(t), with arbitrary amplitude modulation, v(t), and arbitrary frequency modulation, m(t), then:

$$s(t) = v(t)\cos[\phi(t)] \qquad T_{po} < t < T_{po} + \tau_p \tag{IV-1}$$

where, as in Section II,

$$\phi(t) = \phi(T_{po}) + 2\pi \int_{T_{po}}^{t} f_i(x)\,dx \tag{IV-2a}$$

and

$$f_i(t) = f_c + k_f m(t) \tag{IV-2b}$$

If V(f) is the Fourier transform of v(t), the amplitude spectrum S(f)

of the pulse s(t) in equation (IV-1) is given by the convolution of V(f) and the Fourier transform of $\cos\Phi(t)$:

$$S(f) = V(f) \circledast \mathcal{F}[\cos\Phi(t)] = V(f) \circledast P(f) \tag{IV-3}$$

where P(f) is given by equation (II-3). Using the approach of equation (II-5), the spectrum, S(f), can be represented by the sum of the spectra of elemental cells:

$$S(f) = \sum_{i=0}^{n-1} \int_{t_i}^{t_{i+1}} s(t) e^{-j\omega t} dt \tag{IV-4}$$

where $t_o = T_{po}$ and $t_n = T_{po} + \tau_p$. The spectrum, $Z(f)$, of any individual element cell is given by

$$Z(f) = \int_{T_o}^{T_o + \tau} s(t) e^{-j\omega t} dt \tag{IV-5}$$

where T_o is the start time of the elemental cell and τ is the pulse duration of the elemental cell. Section II treated the special case of equation (IV-5) when v(t) is equal to one across the elemental cell and developed equations (II-6 and II-13) for the characteristic elemental cell spectra for constant and chirp frequency cells. If the pulse envelope, v(t), is not equal to one, but rather some constant across the elemental cell, then equations (II-6 and II-13) still apply and need only be modified by a scale factor. If, on the other hand, v(t) is not constant across the cell, equations (II-6 and II-13) must be modified to account for this non-constant behavior.

Consider the instantaneous frequency function, $f_i(t)$, and amplitude

modulation, v(t), depicted in Figure 17. In the figure, an elemental cell extending from T_o to $T_o + \tau$ is generated by linearly approximating $f_i(t)$ and v(t) across the elemental cell. The linearized instantaneous frequency function, $\hat{f}_i(t)$, has been discussed in great detail in Section II. The linearized amplitude modulation, $\hat{v}(t)$, is given by:

$$\hat{v}(t) = A + h(t - T_o) \qquad T_o < t < T_o + \tau \tag{IV-6}$$

where "A" is the initial cell amplitude and "h" is the slope of the linearized envelope. This allows the element cell spectrum, $Z(f)$, of equation (IV-5) to be approximated by:

$$Z(f) = A\int_{T_o}^{T_o+\tau} \cos[\hat{\Phi}(t)]e^{-j\omega t}dt + h\int_{T_o}^{T_o+\tau} (t - T_o)\cos[\hat{\Phi}(t)]e^{-j\omega t}dt \tag{IV-7}$$

The first integral is simply the problem addressed in Section II modified by a multiplicative constant. The second integral adds a degree of generality to the elemental cell model by accounting for the fact that the amplitude modulation is not constant. In consonance with the model development of Section II, there are two special cases of equation (IV-7) that merit attention:

(1) $h \neq o$ and the instantaneous frequency function is constant across the cell; and

(2) $h \neq o$ and the instantaneous frequency function is linear across the cell.

In the first case, the approximated instantaneous phase function, $\hat{\Phi}(t)$

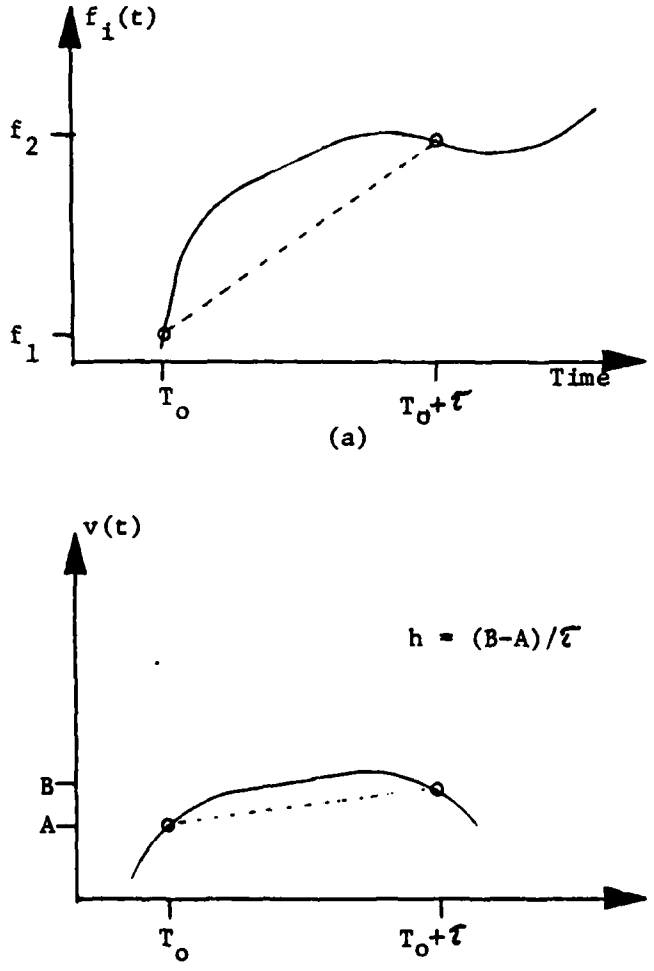

Figure 17 - Generation of a Generalized Elemental Cell with (a) Frequency Modulation and (b) Amplitude Modulation

is:

$$\text{(IV-8)} \qquad \hat{\phi}(t) = \phi(T_0) + 2\pi f_c t$$

for $T_0 \le t \le T_0 + \tau$. By applying this function to equation (IV-7), straightforward integration yields the following expression for the characteristic spectrum of an elemental cell with linear amplitude modulation and a constant carrier frequency:

$$\text{(IV-9)} \qquad Z(f) = \frac{e^{j[\phi(T_0) - \omega T_0]}}{2}\left\{\frac{jA}{\omega_c - \omega}\left[1 - e^{j(\omega_c - \omega)\tau}\right] - \frac{h}{(\omega_c - \omega)^2}\left[1 - \left(1 - j(\omega_c - \omega)\tau\right)e^{+j(\omega_c - \omega)\tau}\right]\right\}$$
$$- \frac{e^{-j[\phi(T_0) + \omega T_0]}}{2}\left\{\frac{jA}{\omega_c + \omega}\left[1 - e^{j(\omega_c + \omega)\tau}\right] + \frac{h}{(\omega_c + \omega)^2}\left[1 - \left(1 + j(\omega_c + \omega)\tau\right)e^{-j(\omega_c + \omega)\tau}\right]\right\}$$

In the generalized elemental cell model, this expression is the analog of equation (II-6).

In addressing the special case of equation (IV-7) in which both the elemental cell amplitude and frequency are linearly swept, an expression analogous to equation (II-13) will be developed. In this case, the approximated instantaneous phase function, $\hat{\phi}(t)$, is given by equation (II-10b). The first integral of equation (IV-7) is simply a constant, A, times an integral evaluated in Section (II-A); namely, equation (II-13). Using Euler's equations, the second integral of equation (IV-7) can be arranged as the sum of two integrals; the first

is a function of (f_1-f) while the second is a function of (f_1+f). Designating the first of these integrals by $I_1(f)$ and the second by $I_2(f)$, $I_1(f)$ can be written:

$$\text{(IV-10)} \qquad I_1(f) = \frac{h}{2} e^{j[\Phi(T_0) - \omega T_0]} \int_{T_0}^{T_0+\tau} (t-T_0) e^{j[\gamma\rho(t-T_0) + 2\pi(f_1-f)(t-T_0)]} dt$$

By completing the square of the integrand's exponential argument, and defining z_1 as in equation (II-12); β_1, as in equation (II-14); and Z1L and Z1H as in equation (II-15), $I_1(f)$ can be written:

$$\text{(IV-11)} \qquad I_1(f) = \frac{h e^{j\beta_1}}{\sqrt{8\rho}} \left\{ \frac{1}{\sqrt{2\rho}} \int_{Z1L}^{Z1H} z_1 e^{j\left(\frac{\pi z_1^2}{2}\right)} dz_1 - \frac{(f_1-f)}{\rho} \int_{Z1L}^{Z1H} e^{j\left(\frac{\pi z_2^2}{2}\right)} dz_2 \right\}$$

The first integral is directly integrable. The second is of the Fresnel form. Defining the Fresnel integrals, C(x) and S(x), as in equation (II-17), $I_1(f)$ can be written as:

$$\text{(IV-12)} \qquad I_1(f) = \frac{jh e^{j\beta_1}}{2\sqrt{\pi\rho}} \left\{ e^{j\frac{\pi}{2}(Z1L)^2} - e^{j\frac{\pi}{2}(Z1H)^2} - \frac{\pi}{2}(Z1L)\left[C(Z1H) - C(Z1L) + j\left(S(Z1H) - S(Z1L)\right)\right] \right\}$$

A similiar analysis can be applied to the integral $I_2(f)$.

For simplicity, define the evaluated Fresnel integrals as:

$$\text{(IV-13a)} \qquad F_1 = C(Z1H) - C(Z1L) + j\left[S(Z1H) - S(Z1L)\right]$$

(IV-13b) $$F_2 = C(Z_2H) - C(Z_2L) + j\left[S(Z_2L) - S(Z_2H)\right]$$

With this definition and letting the limits of integration be defined as in equation (II-15) and letting β_1 and β_2 be defined as in equation (II-14), equation (IV-7) can be written in integrated form as:

(IV-14) $$Z(f) = \frac{e^{j\beta_1}}{\sqrt{8\rho}}\left\{AF_1 + \sqrt{\frac{2}{\rho}}\left(\frac{h}{\pi}\right)\left[\frac{1}{2}j\left(e^{j\frac{\pi}{2}(Z_1L)^2} - e^{j\frac{\pi}{2}(Z_1H)^2}\right) - \frac{\pi}{2}(Z_1L)F_1\right]\right\}$$

$$+ \frac{e^{-j\beta_2}}{\sqrt{8\rho}}\left\{AF_2 + \sqrt{\frac{2}{\rho}}\left(\frac{h}{\pi}\right)\left[\frac{1}{2}j\left(e^{-j\frac{\pi}{2}(Z_2H)^2} - e^{-j\frac{\pi}{2}(Z_2L)^2}\right) - \frac{\pi}{2}(Z_2L)F_2\right]\right\}$$

This expression is the analog of equation (II-13) for the case where arbitrary amplitude modulation is considered. This is apparent in the terms that have been added that are a function of the envelope's slope.

Thus any pulse with an arbitrary amplitude and frequency modulation can be modeled by expressing the pulse envelope and the instantaneous frequency as linear piecewise continuous functions. These linearized function are then segmented into a series of successive elemental cells such that each cell can be classified as one of the following:

(1) linear frequency sweep; linear envelope

(2) linear frequency sweep; constant envelope

(3) constant frequency sweep; linear envelope

(4) constant frequency sweep; constant envelope

Associated with each of the four classes of elemental cells is a characteristic spectrum, so that once the elemental cell's class has

been determined, its spectrum can be generated directly from cell parameters. Finally, the total pulse spectrum is obtained by summing over the spectra of all elemental cells.

The generalized elemental cell model is flexible and easy to use. There is no requirement that the elemental cells be of uniform length. In fact, judicious construction of the element cells allows for the possibility of dynamic sampling. That is smaller elemental cells (higher sampling rates) may be used during transient portions of the pulse while larger cells (lower sampling rates) may be used during more static portions of the pulse. Additionally frequency resolution is not a function of the sampling rate and the number of samples used. Arbitrary frequency resolution can be achieved since the model uses an analytic approach to spectrum generation. For the same reason, an arbitrary number of spectrum frequency component can be generated.

A program listing which implements the generalized elemental cell model is provided in Appendix A.

B. ILLUSTRATION OF THE GENERALIZED ELEMENTAL CELL MODEL

To illustrate the application of the generalized model, consider as in Section (II-B) the sinusoidally frequency modulated pulse but allow the pulse envelope to also be sinusoidally shaped as shown in Figure 18. The spectrum of this pulse is discussed in Appendix B. Let the pulse be such that the carrier frequency, f_c is 30 MHz; the frequency modulating frequency, f_m, is 200 kHz; the frequency modulation index, k_f, is one; the amplitude modulating frequency is 100 kHz; and the pulse duration

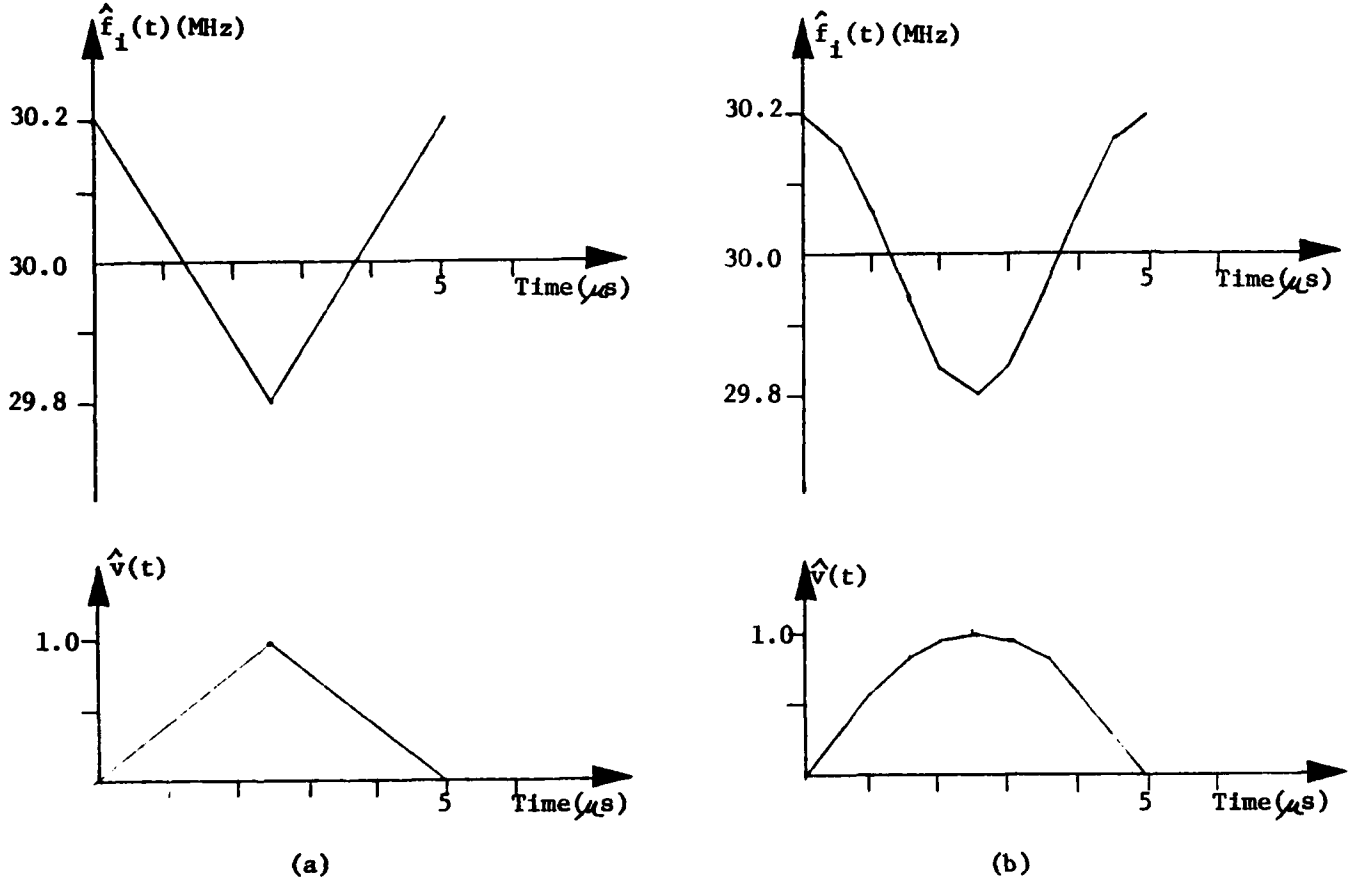

Figure 18 - Elemental Cell Generation for a Sinusoidally Frequency and Amplitude Modulated Pulse Using (a) Two Cells and (b) Eight Cells

is five microseconds. (Assume, again, that a 25 kHz resolution is desired and that the primary interest is in the first three upper and lower spectral sidelobes.)

Figure 18 demonstrates the generation of elemental cells for this pulse. Two cases are considered. In case I, two cells are used to generate the spectrum; while, in case II, eight cells are used. Figure 19 displays the amplitude spectra generated by these two cases. The solid line represents the exact spectrum, the development of which is addressed in Appendix B. The general results are not unlike those obtained for the unit pulse in Section (II-B). In the following section it will be shown that the convergence of the generalized model parallels that of the unit pulse model being inversely related to the square of the number of elemental cells used in generating the spectrum.

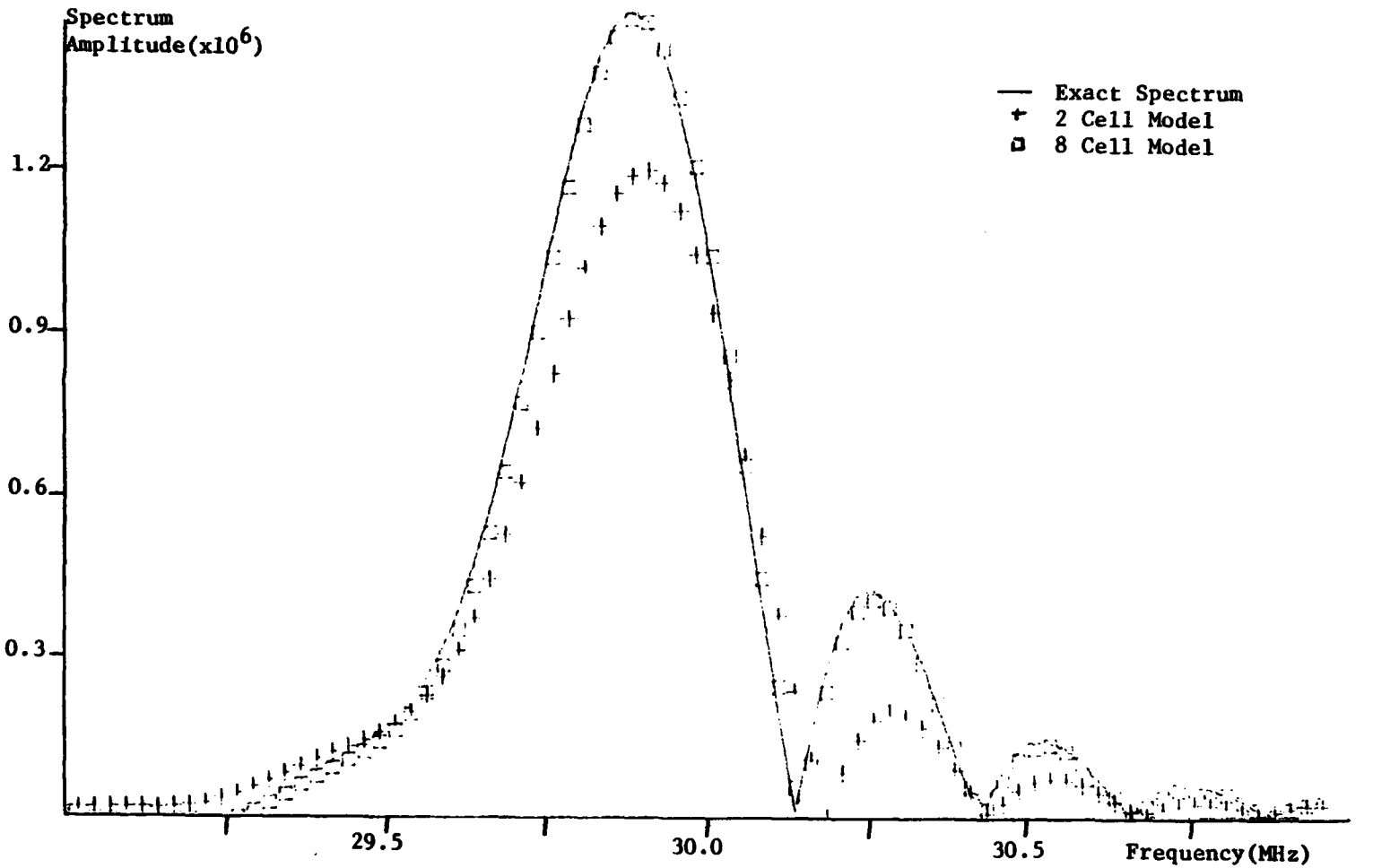

Figure 19 - Amplitude Spectrum of a 5.0 μs Pulse with Sinusoidal Amplitude and Frequency Modulation

V. ERROR ANALYSIS (GENERALIZED MODEL)

A. ERROR BOUND

The methodology used in this error analysis parallels that used in the development of equation (III-37) in Section III. The local error bound associated with the k^{th} elemental cell is generated and then applied across the pulse to develop a maximum error bound on a global basis.

For a pulse with arbitrary amplitude and frequency modulation, the difference between the actual pulse waveform, $s(t)$, and its approximated form, $\hat{s}(t)$ is given by:

$$s(t) - \hat{s}(t) = v(t)\cos[\phi(t)] - \hat{v}(t)\cos[\hat{\phi}(t)] \tag{V-1}$$

where $\phi(t)$ and $\hat{\phi}(t)$ represent the exact and approximated instantaneous phase functions respectively and $v(t)$ and $\hat{v}(t)$ represent the exact and approximated pulse envelopes respectively. The pulse envelope expressions are related by:

$$v(t) = \hat{v}(t) + v_e(t) \tag{V-2}$$

where $v_e(t)$ is the error that results from linearly approximating the amplitude modulation. Making use of this relationship, the absolute

pulse error in the time domain can be bounded from above such that:

$$(V\text{-}3) \quad |s(t) - \hat{s}(t)| \leq |\hat{v}(t)||\cos[\phi(t)] - \cos[\hat{\phi}(t)]| + |v_e(t)||\cos[\phi(t)]|$$

In the first term, the results of Section (III-A) can be used to bound the absolute difference of cosines by the absolute difference of their arguments. Equations (III-15) thru (III-18) are germane. In the second term, use can be made of the fact that $|\cos(x)| \leq 1$, so that:

$$(V\text{-}4) \quad |s(t) - \hat{s}(t)| \leq |\hat{v}(t)||\phi(t) - \hat{\phi}(t)| + |v_e(t)|$$

Since the intent is to extrapolate a local error to a global error, consider the k^{th} elemental cell starting at T_{ok} and of duration, $\hat{\tau}_k$. If $|\phi(t) - \hat{\phi}(t)|_k$ is the instantaneous absolute phase error associated with the k^{th} cell and $v_{ek}(t)$ is the error associated with the amplitude modulation in the k^{th} cell, the absolute pulse error associated with the k^{th} cell, $|s(t)-\hat{s}(t)|_k$, can be written using equation (IV-6)

$$(V\text{-}5) \quad |s(t) - \hat{s}(t)|_k \leq |A_k + h_k(t - T_{ok})||\phi(t) - \hat{\phi}(t)|_k + |v_{ek}(t)|$$

where A_k is the initial pulse envelope amplitude at T_{ok} and h_k is the slope of the pulse envelope across the cell. In a manner analogous to equation (III-21), the local spectrum error associated with the k^{th} cell can be bound as follows:

$$(V\text{-}6) \quad |S(f) - \hat{S}(f)|_k \leq \int_{T_{ok}}^{T_{ok}+\hat{\tau}} \{|A_k + h_k(t - \tau_o)||\phi(t) - \phi(t)|_k + |v_{ek}(t)|\} dt$$

If it is assumed that the amplitude modulation function, v(t),

is at least twice differentiable, then in the k^{th} elemental cell, the linear approximation, $\hat{v}(t)$, results in error, $v_{ek}(t)$, given by:

$$v_{ek}(t) = \frac{1}{2}(t - T_{ok})(t - T_{ok} - \hat{\tau}_k)v''(\eta) \qquad \text{(V-7)}$$

where $T_{ok} \leq \eta \leq T_{ok} + \hat{\tau}_k$ and $T_{ok} \leq t \leq T_{ok} + \hat{\tau}_k$. By bounding the second derivative of the modulation function over the k^{th} elemental cell,

$$\left| v_{ek}(t) \right| \leq \frac{N_k}{2}(t - T_{ok})(t - T_{ok} - \hat{\tau}_k) \qquad \text{(V-8)}$$

where $N_k = \max \left\{ v''(\eta) \right\}$, $T_{ok} \leq \eta \leq T_{ok} + \hat{\tau}_k$. Applying this bound to equation (V-6), using the expression for the absolute instantaneous phase error developed in equation (III-34), and replacing the variable $t - T_{ok}$ by w the spectrum error associated with the k^{th} elemental cell can be bounded by:

$$\left| S(f) - \hat{S}(f) \right|_k \leq \frac{\pi}{6} \int_0^{\hat{\tau}_k} \left| A_k + h_k w \right| \left\{ \sum_{j=1}^{k-1} M_j \hat{\tau}_j^3 + M_k \left| 2w^3 - 3\hat{\tau}_k w^2 \right| \right\} dw + \frac{N_k}{2} \int_0^{\hat{\tau}_k} \left| w(w - \hat{\tau}_k) \right| dw \qquad \text{(V-9)}$$

This expression can be integrated to yield the local bound on the spectrum error of the k^{th} cell,

$$\left| S(f) - \hat{S}(f) \right|_k \leq \frac{\pi \hat{\tau}_k}{6} \left(\sum_{j=1}^{k-1} M_j \hat{\tau}_j^3 \right) \left(A_k + \frac{h_k \hat{\tau}_k}{2} \right) + \frac{\pi M_k \hat{\tau}_k^4}{12} \left(A_k + 0.7 h_k \hat{\tau}_k \right) + \frac{N_k \hat{\tau}_k^3}{12} \qquad \text{(V-10)}$$

Summing the local error bounds over all cells provides the global spectrum error bound:

$$(V\text{-}11)\qquad \left|S(f)-\hat{S}(f)\right| \le \sum_{k=1}^{n}\left\{\frac{\pi\hat{\tau}_k}{6}\left(A_k+\frac{h_k\hat{\tau}_k}{2}\right)\sum_{j=1}^{k-1}M_j\hat{\tau}_j^3 + \frac{\pi M_k\hat{\tau}_k^4}{12}\left(A_k+0.7h_k\hat{\tau}_k\right)+\frac{N_k\hat{\tau}_k^3}{12}\right\}$$

This is a very general bound on the spectrum error, applicable to elemental cells of uniform and nonuniform length, and, as such, is unwieldy. To identify the characteristics of the convergence process, some simplifications can be made resulting in increased clarity at the cost of broadening the bound. The expression $(A_K + (h_k\hat{\tau}_k/2))$ is the pulse amplitude at the midpoint of the k^{th} cell. The expression $(A_k+0.7h_k)$ is the pulse amplitude at a point seven tenths the width of the k^{th} cell. Both of these expressions can be upper bounded by the maximum pulse amplitude, V. Additionally, the second derivatives of the modulating functions can be bounded by their maximum value over the entire pulse, such that:

$$(V\text{-}12a)\qquad M = \max\{M_j\} \qquad j = 1,2,3,\cdots,n$$

$$(V\text{-}12b)\qquad N = \max\{N_j\} \qquad j = 1,2,3,\cdots,n$$

As a final simplification, let the elemental cells be of equal length, $\hat{\tau}$, where the total pulse width is $\tau_p = n\hat{\tau}$. With these considerations,

equation (V-11) reduces to:

$$(V\text{-}13) \qquad \left|S(f)-\hat{S}(f)\right| \leq \frac{\pi M \tau_p^4 V}{12n^2}\left\{2\sum_{k=1}^{n}\frac{(k-1)}{n^2}+\frac{1}{n}\right\}+\frac{N\tau_p^3}{12n^2}$$

Realizing that $2\sum_{k=1}^{n}(k-1) = n^2-n$, the spectral error bound becomes:

$$(V\text{-}14) \qquad \left|S(f)-\hat{S}(f)\right| \leq \frac{\pi M \tau_p^4 V}{12n^2}+\frac{N\tau_p^3}{12n^2}$$

Thus the generalized elemental cell model converges inversely as the square of the number of cells used.

B. EMPIRICAL ASSESSMENT

In order to assess the performance of the generalized element cell model in the light of the theoretical error bounds developed, consider a pulse with sinusoidal amplitude and frequency modulation as in Section (IV-B). The exact spectrum of this pulse is known (Appendix B). Using the techniques of Section IV, the pulse can be modeled using n elemental cells where n = 1,2,3,.... to produce approximate spectra. For each choice of n, the approximate and exact spectrum can be compared to determine the maximum calculated spectrum error experienced using the elemental cell model.

Since the instantaneous frequency function, $f_i(t)$ and the amplitude modulation function, v(t), are known analytically (Appendix B), equations (V-11) and (V-14) can be evaluated to generate maximum theoretical error

bounds as a function of the number of elemental cells, n, used in the modeling process. Thus a set of three curves can be generated:

(1) The maximum theoretical spectrum error bound as a function of the number of elemental cells with modulation variables bounded across the pulse (equation V-14)

(2) The maximum theoretical spectrum error bound as a function of the number of elemental cells with modulation variables bounded across elemental cells (equation V-11)

(3) The maximum calculated spectrum error as a function of the number of elemental cells.

The three curves are presented in Figure 20. The solid curve (equation V-14) and the dashed curve (equation V-11) display the quantitative tightening of the error bound achieve through the increased complexity of equation (V-11). The dotted curve represents the calculated maximum error and is well within the established theoretical bounds. In general, all curves follow the characteristic one over n-squared convergence.

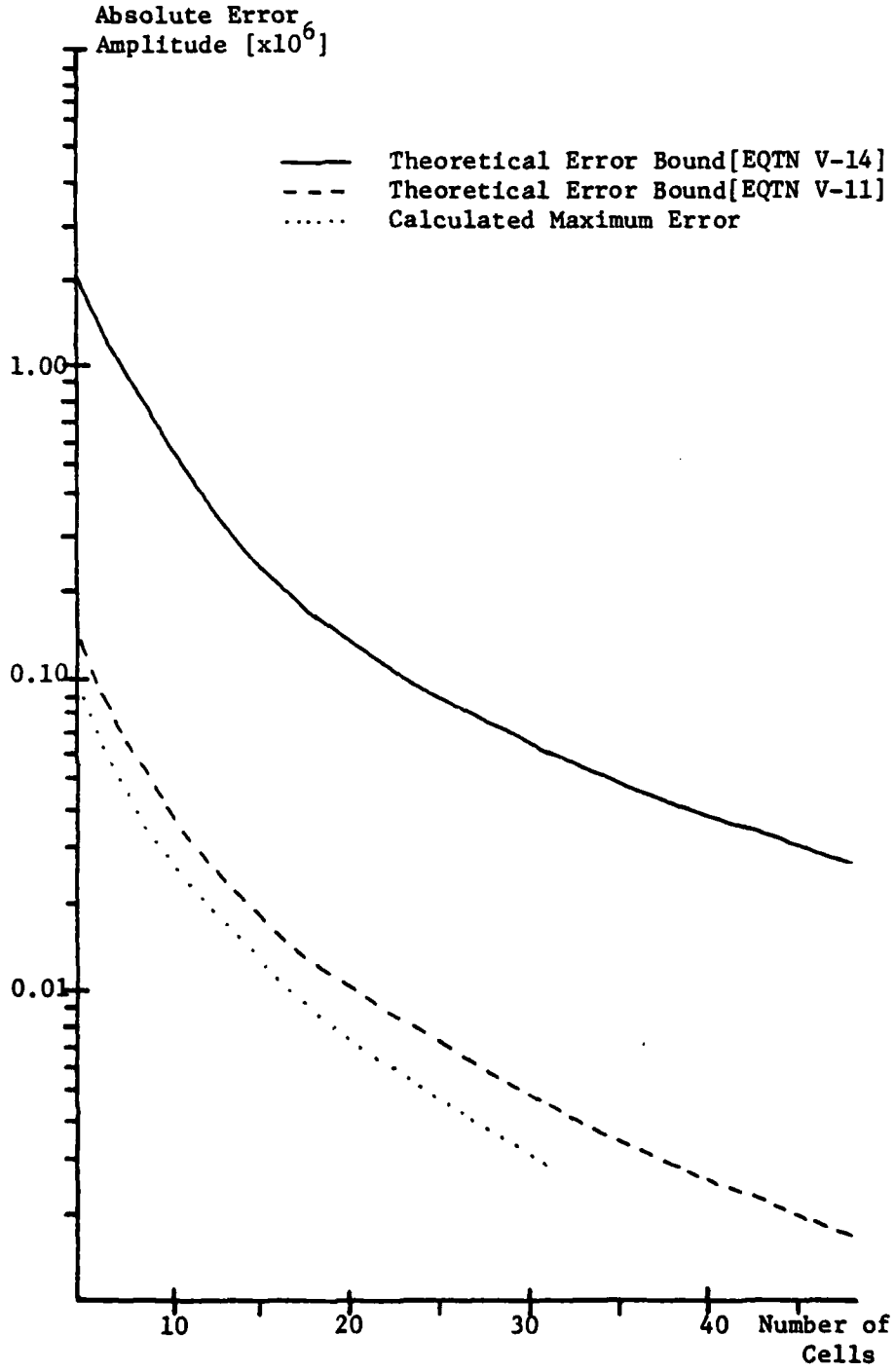

Figure 20 - Theoretical Error Bound and Maximum Calculated Errors as a Function of the Number of Elemental Cells Used to Model a Pulse with Sinusoidal AM and FM

VI. EXTRAPOLATION

A. DEVELOPMENT

The concept of extrapolation to the limit (Richardson/Romberg extrapolation) is attractive from the computational point of view since a relatively simplistic calculation uses two inexact solutions to generate a more exact solution. The technique involves some knowledge of the order of the error in the inexact solutions and some associated assumptions. The desire is to apply this type of technique to the elemental cell approach.

Consider the case of the unit amplitude pulse with arbitrary frequency modulation and elemental cells of uniform length. The maximum theoretical error bound for this case has been presented as:

$$E = \left| |P| - |\hat{P}| \right| \leq \frac{\pi M \tau_p^4}{12 n^2} \left(1 + \frac{2}{n}\right) \tag{VI-1}$$

where again τ_p is the pulsewidth, n is the number of elemental cells and M is the maximum value of the second derivative of the instantaneous frequency function over the pulse. Thus the approximate spectrum approaches the exact spectrum roughly as the inverse of the number of cells squared.

Let $|\hat{P}_1|$ be the approximate spectrum produced when n_1 cells are used to model a given pulse, then

$$|P(f) - \hat{P}_1(f)| \leq \frac{\pi M \hat{\tau}_p^4}{12 n_1^2} \left(1 + \frac{2}{n_1}\right) = e_1 \tag{VI-2}$$

(VI-3) $$|P(f) - \hat{P}_1(f)| \leq e_1$$

The inequality can be removed by writing:

(VI-4) $$\left| |P(f)| - |\hat{P}_1(f)| \right| = \gamma_1 e_1 \qquad 0 \leq \gamma_1 \leq 1$$

or by removing the absolute value signs:

(VI-5) $$|P(f)| - |\hat{P}_1(f)| = \alpha_1 e_1 \qquad 0 \leq \alpha_1 \leq 1$$

where α_1 and α_{12} are unknown and are, in general, functions of n and frequency.

Similarly let $|\hat{P}_2|$ be the approximate spectrum produced when n_2 cells are used, then

(VI-6) $$|P(f)| - |\hat{P}_2(f)| = \alpha_2 e_2 \qquad 0 \leq \alpha_2 \leq 1$$

Equations (VI-5) and (VI-6) are actually two equations in three unknowns: P, α_1 and α_2 . To attach some physical significance to α_1 and α_2 they can be thought as of the normalized errors for the two cases (n_1 and n_2) discussed above (normalized by the maximum error bound for a specified number of cells). If these normalized errors (or errors normalized to the maximum bound) are assumed to be equal, equations (VI-5) and (VI-6) form two equations in two unknowns. The equating of these two normalized errors in fact is an implicit assumption that for any given frequency component for n_1 and n_2 the convergence of the approximated spectrum to the exact spectrum parallels the convergence profile established

by the maximum theoretical error bound. In consonance with the discussions of Section (III-C), it is expected that the validity of this assumption is increased as n becomes larger and larger. Solving then the set of simultaneous equations for $|P|$ yields:

$$|P| = \frac{e_2|\hat{P}_1| - e_1|\hat{P}_2|}{e_2 - e_1} \qquad \text{(VI-7)}$$

$$|P| = \frac{n_2^3(n_1+2)|\hat{P}_2| - n_1^3(n_2+2)|\hat{P}_1|}{n_2^3(n_1+2) - n_1^3(n_2+2)} \qquad \text{(VI-8)}$$

As is the case with extrapolation to the limit techniques, $|P|$ in equation (VI-8) is not truly an exact value since in reality α_3 is not equal to α_2.

B. ILLUSTRATION AND ASSESSMENT

In this section two detailed illustrations of the extrapolation technique are presented along with a detailed analysis of the technique performance. For the purposes of demonstration, a unit pulse with sinusoidal frequency modulation (see Section II-B) is modeled.

Consider the case in which four (4) and then eight (8) elemental cells are used to model the pulse. The two approximated spectra that result using the techniques of Section II are shown in figures 21 and 22. If the results of these two modeling efforts (n_1=4;n_2=8) are applied to equation (VI-8), the extrapolated spectrum shown in figure 23 is

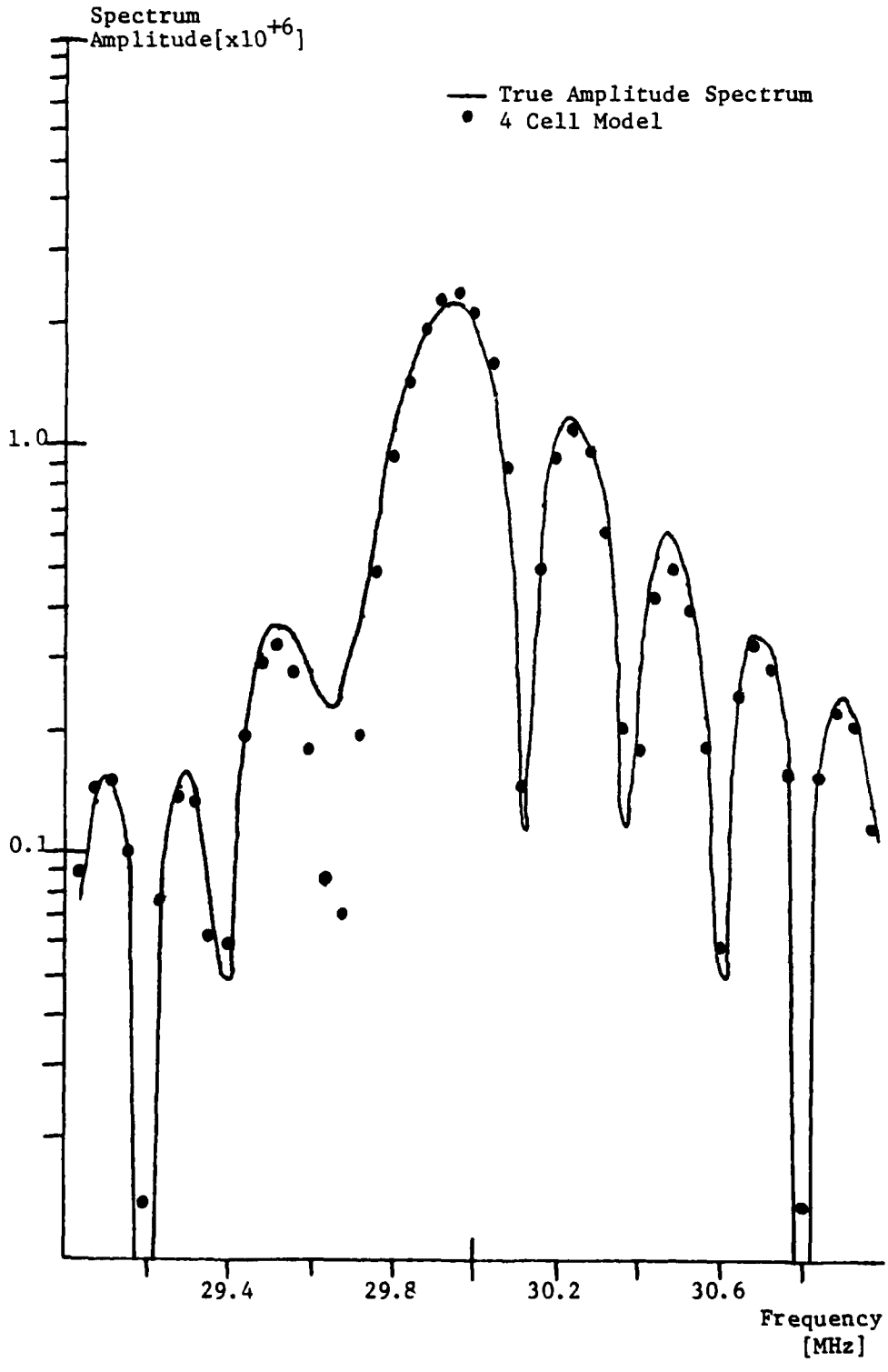

Figure 21 - Amplitude Spectrum for a Unit Pulse with Sinusoidal Frequency Modulation and Approximated Spectrum Using Four(4) Cells

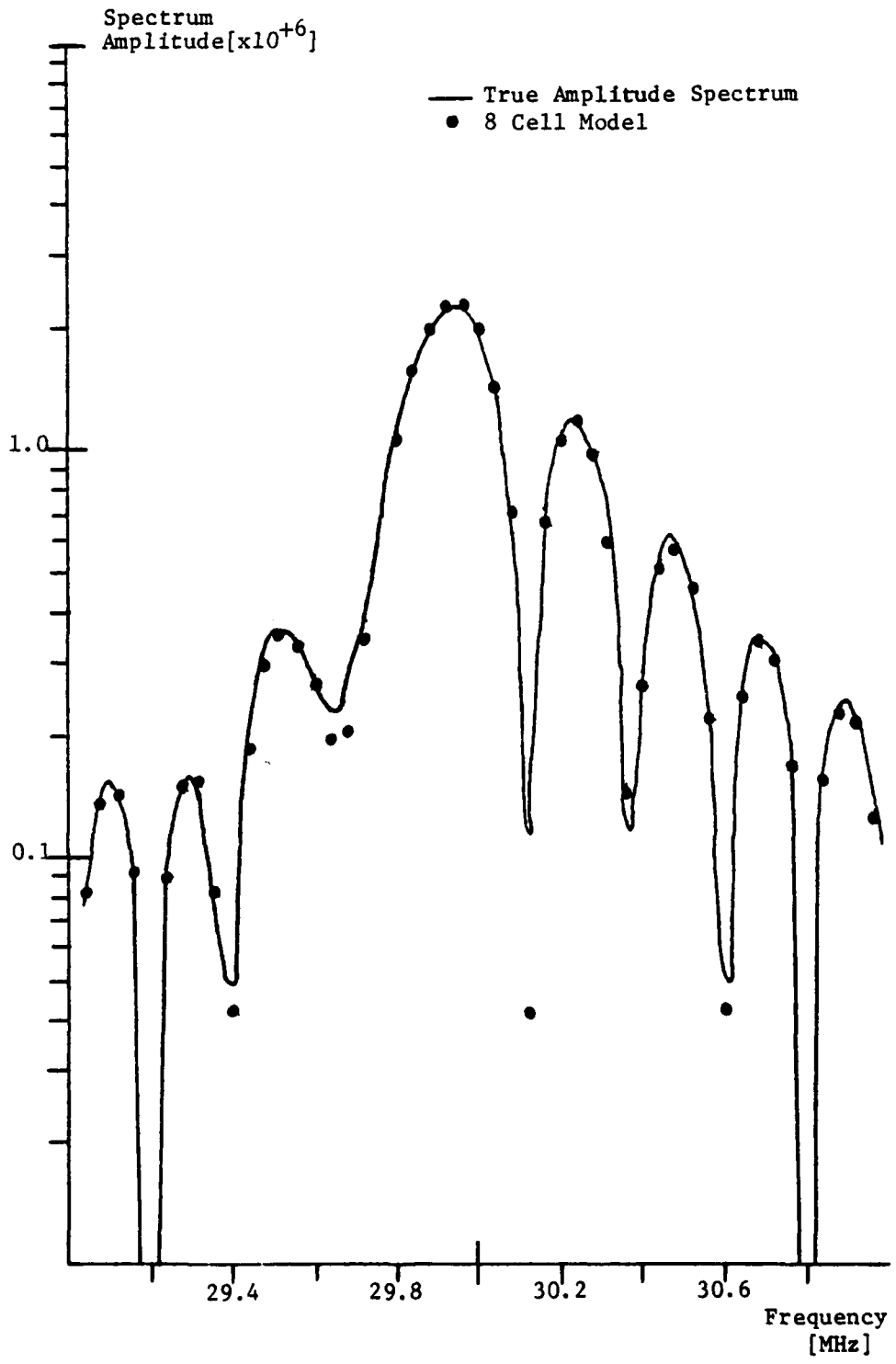

Figure 22 - Amplitude Spectrum for a Unit Pulse with Sinusoidal Frequency Modulation and Approximated Spectrum Using Eight(8) Cells

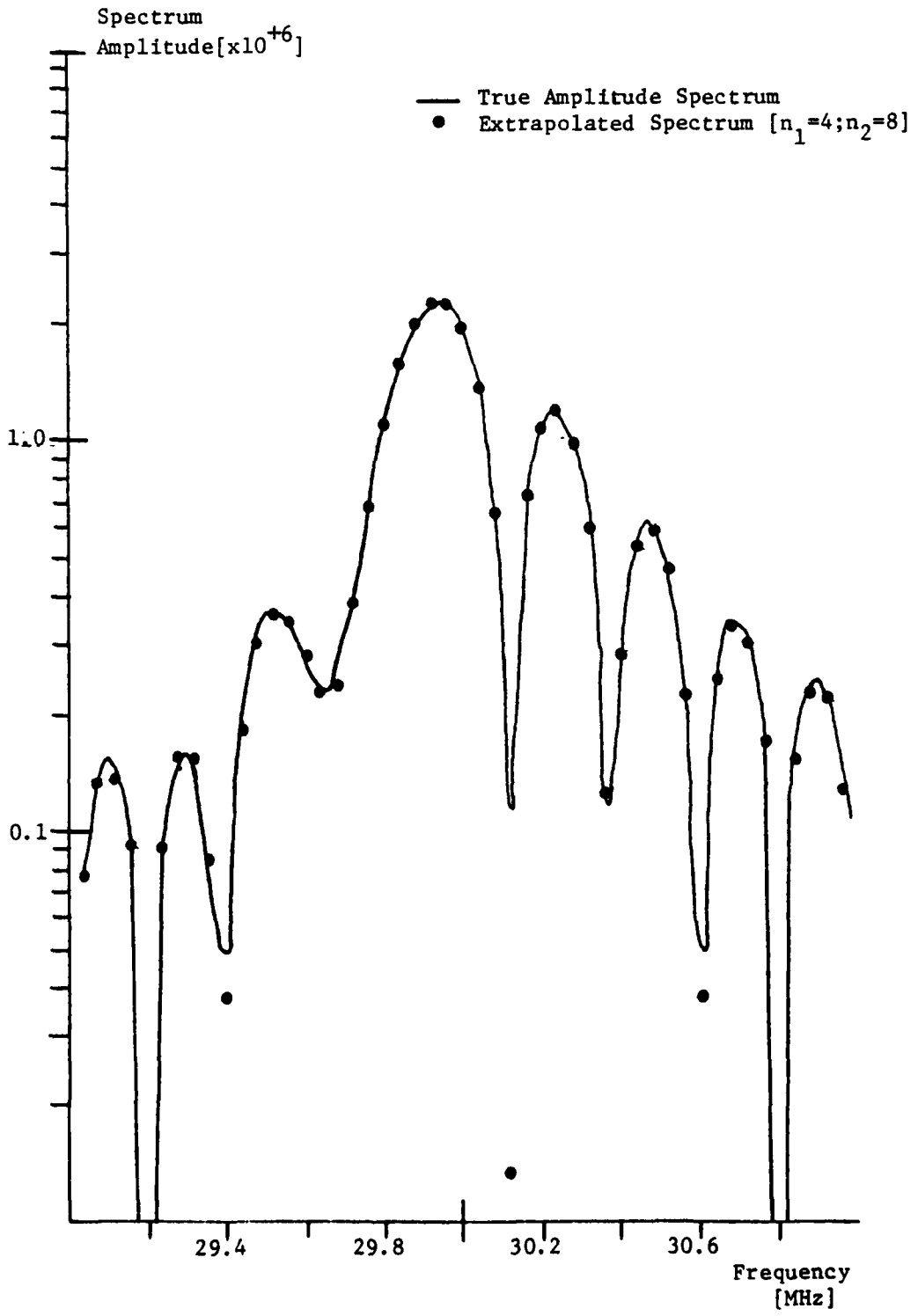

Figure 23 - Amplitude Spectrum for a Unit Pulse with Sinusoidal Frequency Modulation and Approximated Spectrum Using the Extrapolation Technique

produced. While a net improvement in the extrapolated spectrum can be seen in the first lower sidelobe, certain null values such as the amplitude associated with f=30.12 MHz show deterioration. To gain a better insight into the extrapolation technique performance, figure 24 illustrates the amplitude spectrum error associated with the four and eight cell models and that associated with the extrapolated spectrum. In general, across the central region of the spectrum (f=29.4 MHz to f=30.6 MHz), the error associated with the eight cell model is a factor of four less than the corresponding error associated with the four cell model. Additionally, in this central region, as the number of cells is increased from four to eight, the convergence to the exact spectrum is essentially at a uniform rate (i.e., the normalized errors α_1 and α_2 are approximately equal). The error associated with the extrapolated spectrum in this region lacks the uniformity seen in the two modeled spectra, but in general provides a reduction in the spectrum error by about a factor of four over the eight elemental cell model. On either side of this central region, the performance of the extrapolation technique is relatively poor. In the range from 29.0 MHz to 29.4 MHz, the inferior performance is the result of the fact that the eight cell and four cell models do not converge to the true spectrum at a uniform rate. In the range from 30.6 MHz to 31.0 MHz the same problem exists; however, its cause is more graphically evident in the misalignment of the spectrum error sidelobes of the four cell and eight cell models.

Before assessing the performance of the extrapolation technique further, consider a second example in which eight cells (n_1) and sixteen cells (n_2) are used to generate an extrapolated spectrum. The approximated spectra generated by the eight cell and the sixteen cell

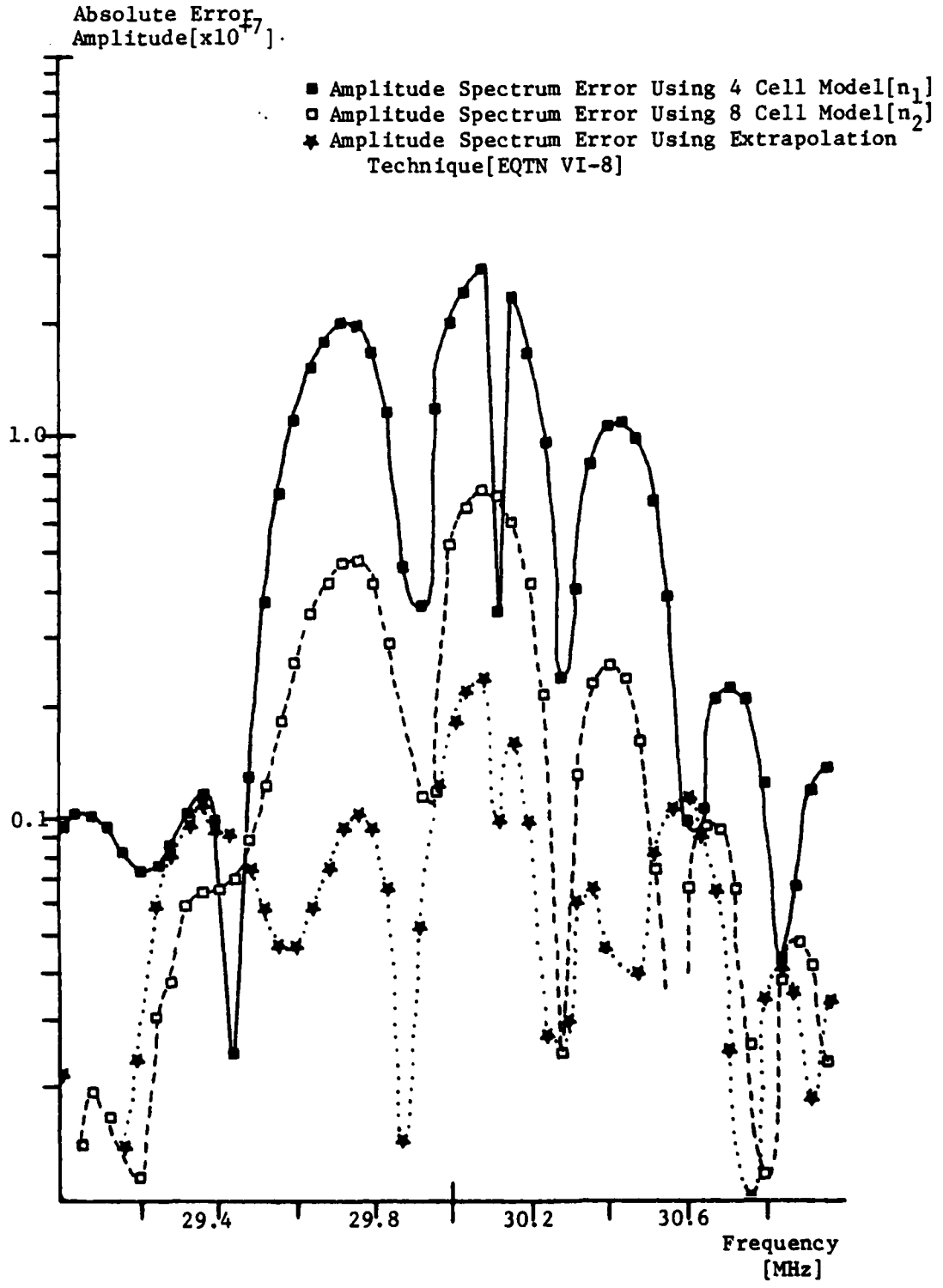

Figure 24 - Amplitude Spectrum Error for a Unit Pulse with Sinusoidal Frequency Modulation for Elemen al Cell Modeling with Four Cells and Eight Cells and for the Extrapolation Technique

models appear in figures 22 and 25 respectively. The resultant extrapolated spectrum is not shown in a presentation comparable to figure 23 since the difference between the extrapolated spectrum and that produced by the sixteen cell model is basically lost in the resolution of the graphical presentation. Instead, the spectrum errors associated with an eight cell model, a sixteen cell model, and the extrapolated spectrum (n_1=8;n_2=16) are shown in figure 26. Generally, across the spectrum, the convergence of the sixteen cell model parallels that of the eight cell model and exhibits the characteristic ($1/n^2$) convergence. The extrapolated spectrum parallels the convergence of the elemental cell models and further reduces the spectrum error by about a factor of six or seven. In this second example, the use of an increased number of elemental cells has reduced or eliminated some of the problems addressed in the previous example (figure 24). In the frequency range 30.6 MHz to 31.0 MHz, the alignment of the spectrum error sidelobes for the eight and the sixteen cell models has been greatly improved resulting in significantly more accurate extrapolated spectrum values. In the frequency range below 29.4 MHz, convergence of the two elemental cell models is much more consistent and anomalous results occur only between 29 MHz and 29.2 MHz.

In those cases when the assumption of Section VI-A (i.e. $\alpha_1 \approx \alpha_2$) holds, the extrapolated spectrum produced by using equation (VI-8) provides a substantial increase in the accuracy of the approximated spectrum. In the case of the first example (n_1=4;n_2=8), this is seen in the factor of four reduction in the spectrum error; in the second example (n_1=8;n_2=16), a factor of six reduction in the spectrum error. The key point is that these significant enhancements in spectrum accuracy are achieved by

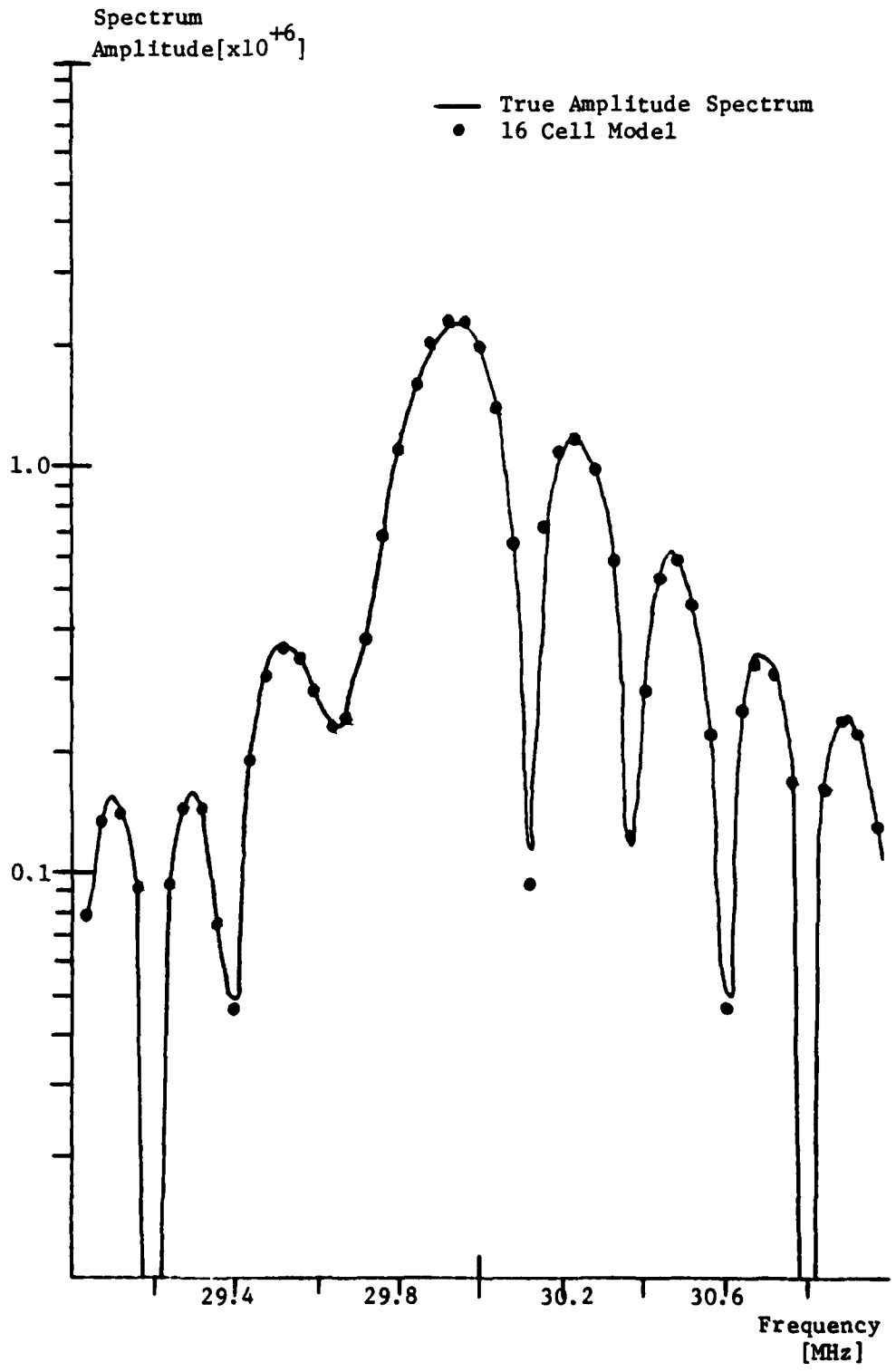

Figure 25 - Amplitude Spectrum for a Unit Pulse with Sinusoidal Frequency Modulation and Approximated Spectrum Using Sixteen(16) Cells

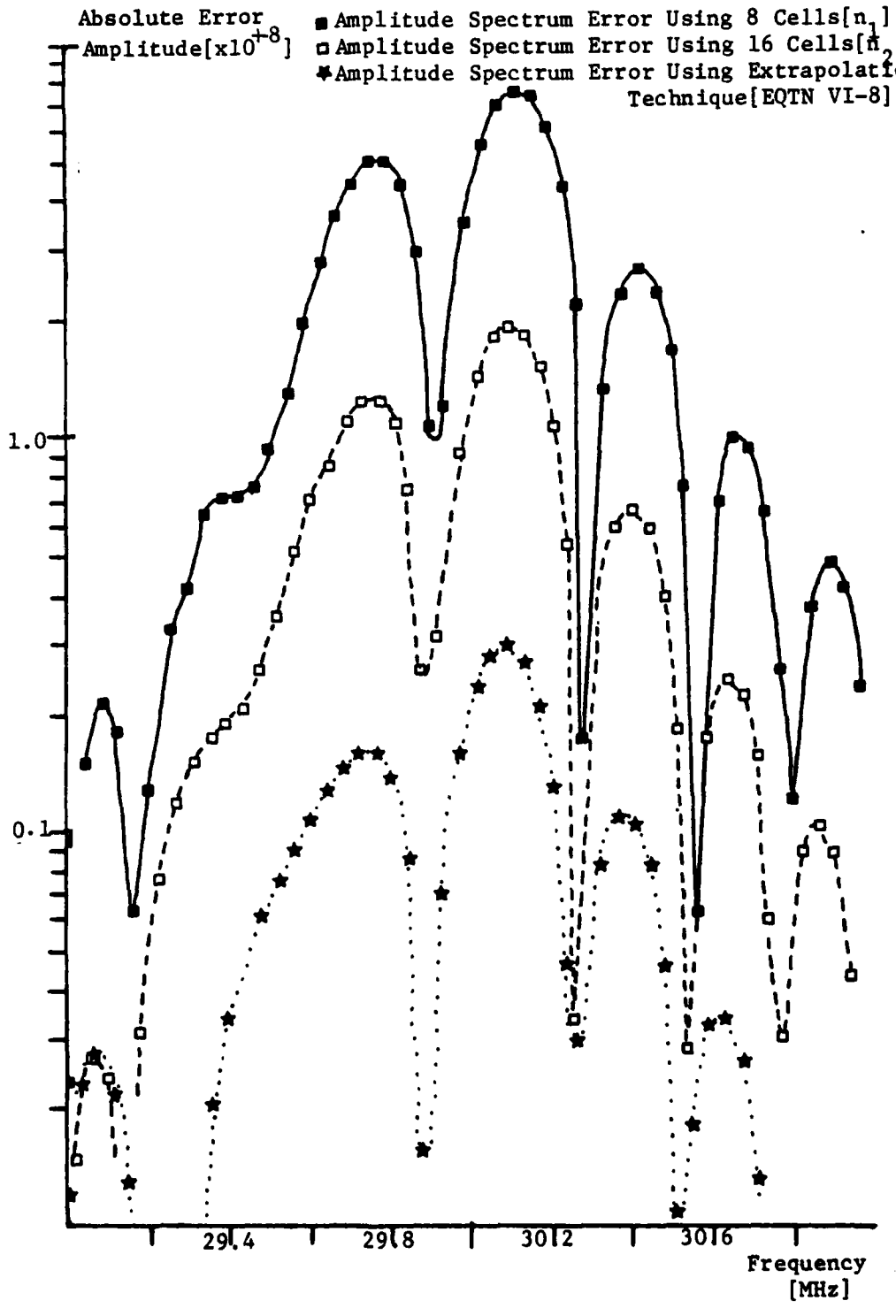

Figure 26 - Amplitude Spectrum Error of a Unit Pulse with Sinusoidal Frequency Modulation for Elemental Cell Modeling with Eight Cells and Sixteen Cells and for the Extrapolation Technique

virtue of a trivial calculation. To form a basis for comparison and to illustrate the power of these techniques, figure 27 presents an overlay of the extrapolated spectrum error (n_1=8;n_2=16) discussed above and the error associated with generating the spectrum with a 4K Discrete Fourier Transform (DFT). While the nature of the error is different, there are few cases in which the DFT spectrum provides better accuracy.

The potential power of the extrapolation technique is evident from the discussions above. The existence of anomalies addressed in discussing figures 24 and 26, however, needs further examination. Returning to the first example of this section (n_1=4;n_2=8), of the 100 frequency components between 29 MHz and 31 MHz examined, there are 32 cases in which the extrapolated spectrum values are less accurate than the corresponding spectrum values generated using the eight cell model. These 32 cases fall into three distinct categories which shall be referred to as Type(1), Type(2), and Type(3) errors:

(a) Type(1) Error. In six instances the spectrum values generated using the eight cell model are less accurate than the corresponding values generated using the four cell model. Obviously, if $|P_2|$ is less exact than $|P_1|$, the extrapolated value will, by equation (VI-8), be less exact than $|P_2|$.

(b) Type(2) Error. In 18 instances, the spectrum errors associated with $|P_1|$ and $|P_2|$ are oppositely signed. In the extrapolation process, this results in the extrapolated value being driven away from vice towards the true spectrum value. This type of error results from the nature of the

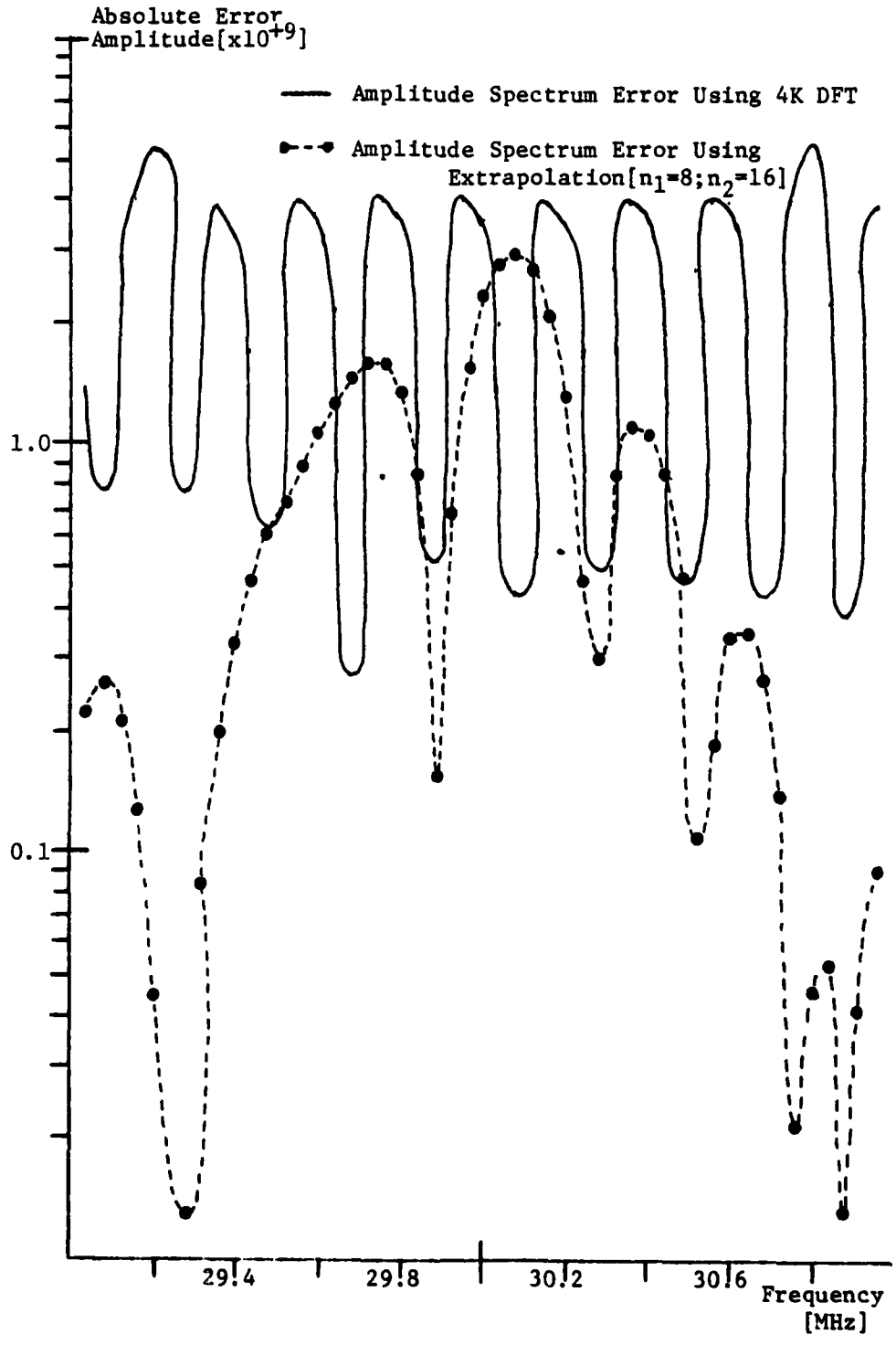

Figure 27 - Comparison of Amplitude Spectrum Error Associated with a 4K DFT and the Extrapolated [n_1=8;n_2=16] Elemental Cell Model

spectrum convergence which will be discussed below.

(c) Type(3) Error. In eight instances, a poor extrapolated value results because of the difference in the rate of convergence of the two approximated spectra to the true spectrum. Specifically, the value of $|P_1|$ is considerably different than $|P|$, while the value of $|P_2|$ is a much better approximation to $|P|$. While $|P_1|$ and $|P_2|$ are not oppositely signed, the relatively large difference between the two causes, in essence, an "over-extrapolation" to a less exact value.

Figure 28 presents a graphic illustration of how the three error types are actually generated.

To gain an insight into the behavior of the three types of error identified, a large number of cases are examined for various values of n_1 and n_2. As a general comment, it can be stated that the characteristics identified in the two examples presented at the beginning of this section hold. When $\alpha_1 \simeq \alpha_2$, the extrapolation technique results in a significant improvement in the accuracy of the approximated spectrum and when problems occur or anomalies exist, they are generally limited to the higher ordered sidelobes or local spectrum minima.

Table 1 is a matrix of the error types encountered for various values of n_1 and n_2 in exercising the extrapolation technique against the unit pulse with sinusoidal frequency modulation. Each block of the matrix is associated with a specific value of n_1 and n_2 and is divided into quadrants which represent the number of Type(1) errors, Type(2) errors and Type(3) errors as well as the total number of errors encountered. The legend in the figure provides a key for identifying the various error

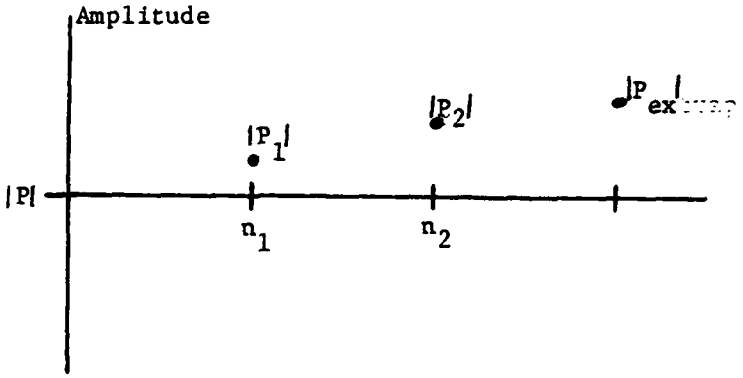

(a) Type (1) Error

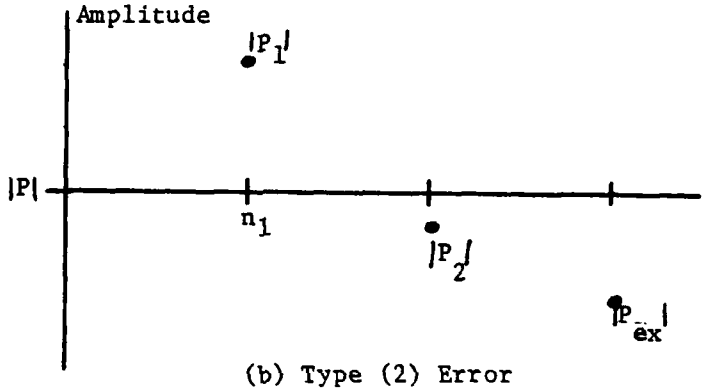

(b) Type (2) Error

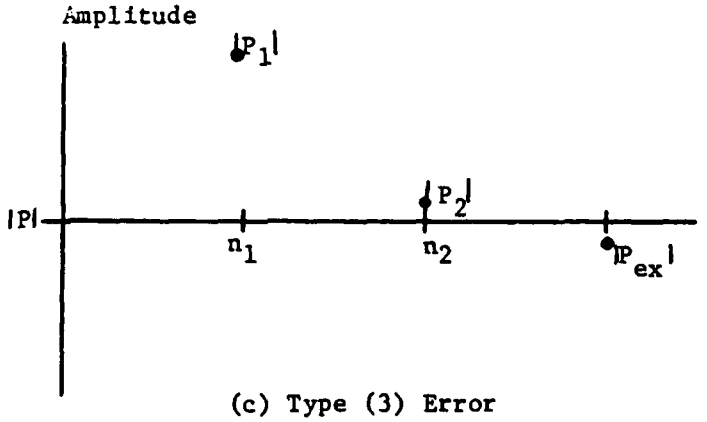

(c) Type (3) Error

Figure 28 - Illustration of the Three Basic Types of Errors Associated with the Extrapolation Technique

n_1 \ n_2	4	5	6	7	8	9	10	16	20	32
3	22 18 10 50	21 4 7 32	14 10 6 30	10 13 3 26	5 16 4 25	4 17 4 25	3 18 3 24	2 18 3 23	0 17 4 21	
4		28 11 5 44	23 8 6 37	8 17 6 31	6 18 8 32	5 20 7 32	5 20 9 34	1 22 10 34	1 22 11 34	0 22 11 33
5			21 8 15 44	7 11 11 29	3 12 11 26	3 13 9 25	2 13 7 22	0 14 8 22	0 14 6 20	
6				5 3 17 25	3 3 29 35	2 4 17 25	1 4 16 21	0 5 13 18	0 5 13 18	0 5 12 17
7					7 0 8 15	4 1 7 12	2 2 9 13	1 2 10 13	1 2 10 13	0 3 9 12
8						1 1 7 9	1 1 7 9	1 1 6 8	0 1 5 6	0 1 6 7
10	1 2 3 ALL							0 0 1 1	0 0 1 1	0 0 1 1

Legend of Error Types

Table 1 - Matrix of Error Types for Various Values of n_1 and n_2

types. For example, in the case discussed above (n_1=4;n_2=8), the appropriate block of the matrix identifies six Type(1) errors, 18 Type(2) errors, 8 Type(3) errors, and 32 total errors. Examination of the matrix yields some insights into the different types of errors and their behavioral characteristics. By examining the Type(1) errors, it can be seen that for a given n_1, as n_2 increases, the number of Type(1) errors goes to zero. This occurs since as n_2 increases all values of $P_2(f)$ will ultimately be more accurate than the corresponding value of $P_1(f)$, thus eliminating the source of the Type(1) error. It should be noted, however, that as n_2 increases and the Type(1) errors diminish that they may reappear as Type(2) or Type(3) errors. It is evident from the matrix that the number of Type(2) errors is determined by the selection of n_1. To some extent this is also true for Type(3) errors, but there also tends to be a slight decrease in the number of Type(3) errors as n_2 increases for a fixed n_1. This effect results from the fact that the extrapolated spectrum is the weighted sum of the two approximate spectra, $|P_1(f)|$ and $|P_2(f)|$, with the weights being determined by the selection of n_1 and n_2. As n_2 increases, the weight associated with $|P_2(f)|$ [the more exact of the two approximate spectra] increases and tends to dominate the weighted sum, diminishing the effect of $|P_1(f)|$ on the extrapolation process. In actual applications, the relationship between n_1 and n_2 is critically important. If these two values are too close together, the weighted sum is biased towards $|P_1(f)|$, typically the less accurate of the two approximate spectra. On the other hand, if n_2 is very much larger than n_1, $|P_2(f)|$ may be so heavily weighted that the feasibility of using an extrapolation approach becomes questionable. Figure 29 provides a quantitative insight into this problem by presenting the relative weighting

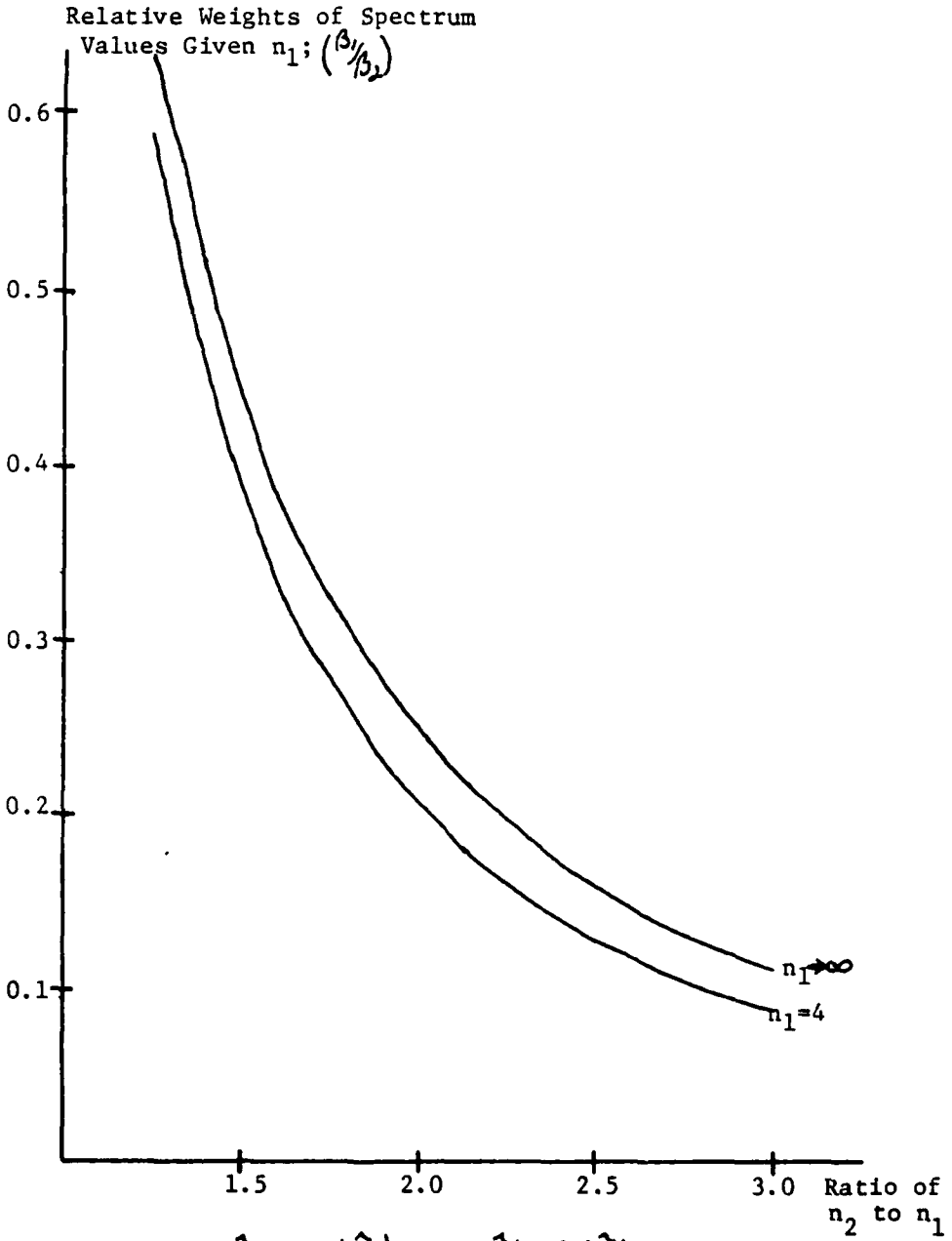

$$|P| = \frac{e_2|\hat{P}_1| - e_1|\hat{P}_2|}{e_2 - e_1} = \beta_1|\hat{P}_1| - \beta_2|\hat{P}_2|$$

Figure 29 - Illustration of the Impact that the Selection of n_1 and n_2 Has on the Weighting of the Two Approximated Spectrum Values in the Extrapolation Technique

AD-A086 567 NAVAL POSTGRADUATE SCHOOL MONTEREY CA F/G 9/4
MODELING OF PULSES HAVING ARBITRARY AMPLITUDE AND FREQUENCY MOD--ETC(U)
MAR 80 F M LUNNEY

UNCLASSIFIED NL

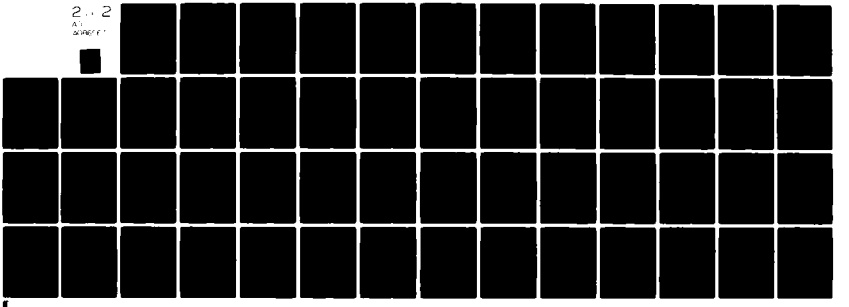

END
DATE FILMED
8-80
DTIC

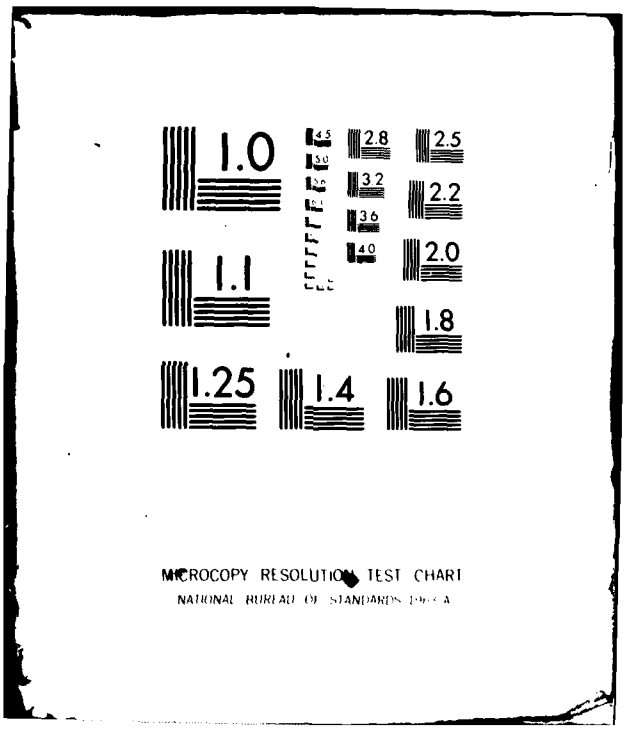
1.0
1.1
1.25
1.4
1.6
1.8
2.0
2.2
2.5
2.8
3.2
3.6
4.0
MICROCOPY RESOLUTION TEST CHART
NATIONAL BUREAU OF STANDARDS 1963-A

of the spectra $|P_1(f)|$ and $|P_2(f)|$ as a function of the ratio of n_2 to n_1.

The most important outcome of examining the matrix in Table 1 is the realization that to a large extent the successful application of the extrapolation technique rests very heavily on the proper selection of a value for n_1. The selection of this value and the ultimate effect that it has on the extrapolation process is driven by the manner in which the approximate spectra converge to the true spectrum as the number of elemental cells is varied. To gain an insight into the nature of this convergence problem, figures 30 thru 33 present the convergence profiles of various frequency components. The relative spectrum amplitude $[|P_n(f)| / |P(f)|]$ is plotted as a function of n, the number of elemental cells used to generate the approximate spectrum, $|P_n(f)|$, for specific frequency components. Figure 30 represents a well-behaved frequency component that converges nicely to the exact spectrum value. Figures 31 thru 33, however, display convergence profiles that may cause problems in applying the extrapolation technique. Figure 31 illustrates how a Type(1) error could occur with n_1=4 and n_2=8. In figure 32, it is easy to see how a Type(2) error could be generated if n_1 were less than eight. Figure 33 presents a case in which a Type(3) error could result if n_1 were four and n_2 were eight. In general all frequency components converge nicely to the exact spectrum value if the number of elemental cells is large enough. The problem in dealing with the extrapolation technique is to select n_1 and n_2 such that the initial transients in the convergence profiles do not impact on the extrapolation technique. Figures 30 thru 33 represent three different types of convergence profiles encountered in examining the unit pulse with sinusoidal frequency modulation. In

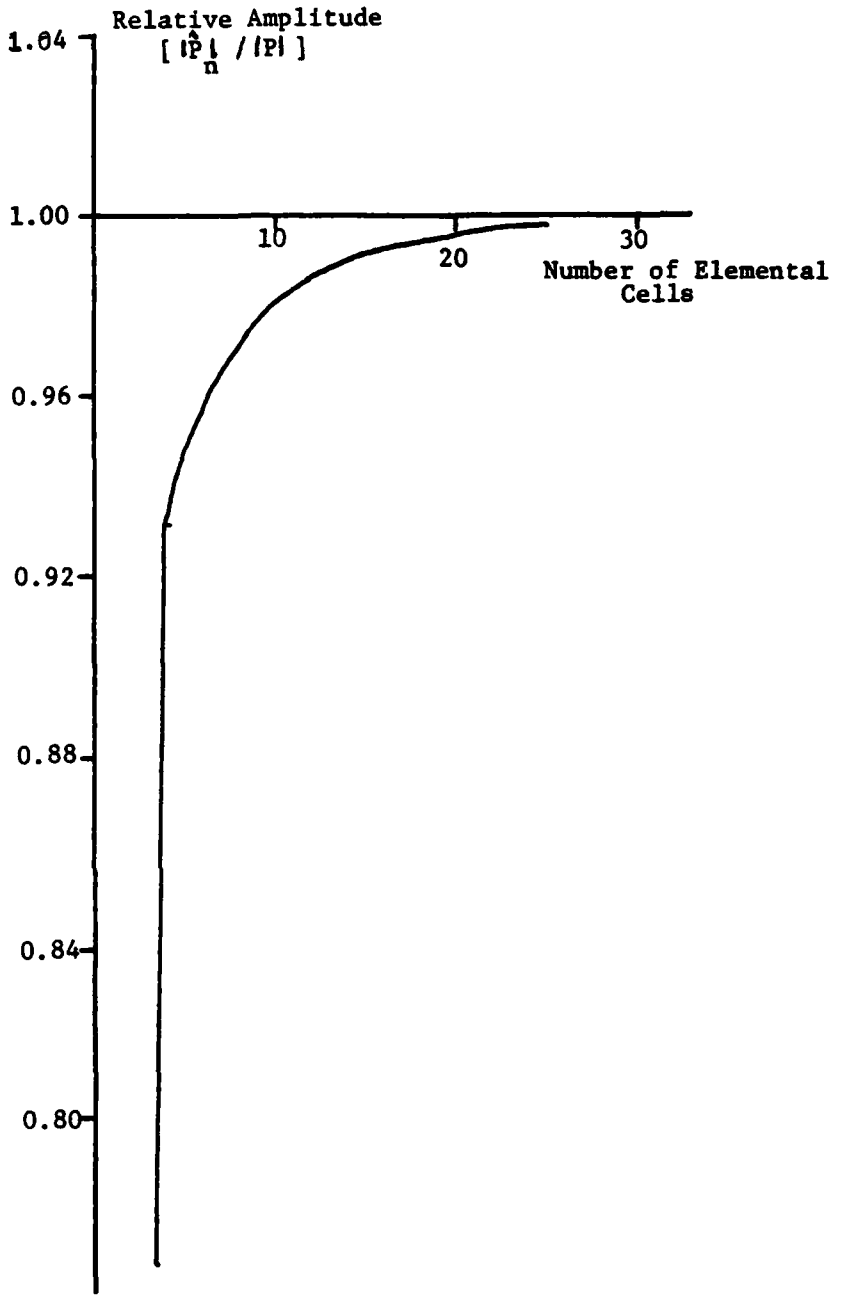

Figure 30 - Convergence Profile for f=29.5MHz

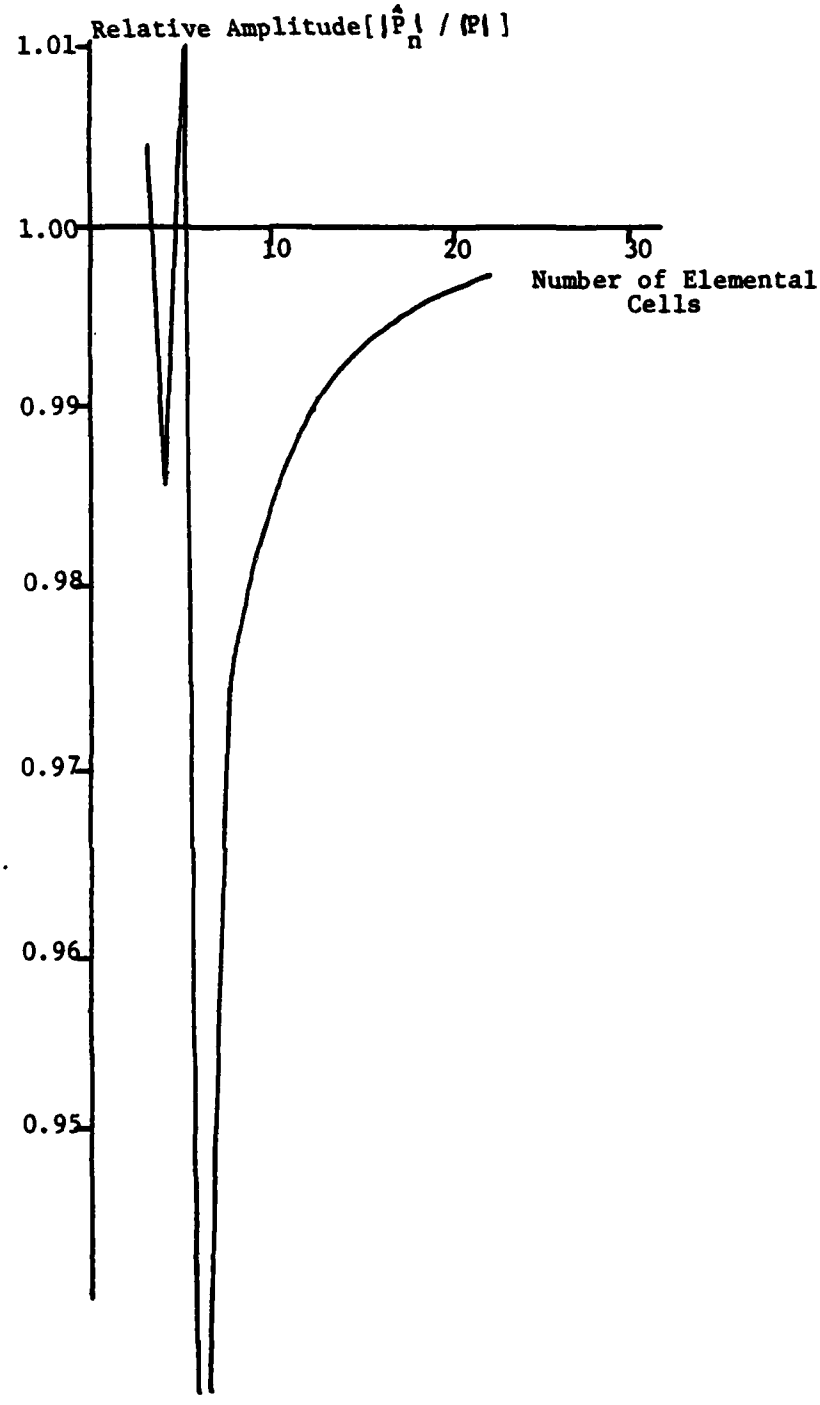

Figure 31 - Convergence Profile for f=30.84MHz

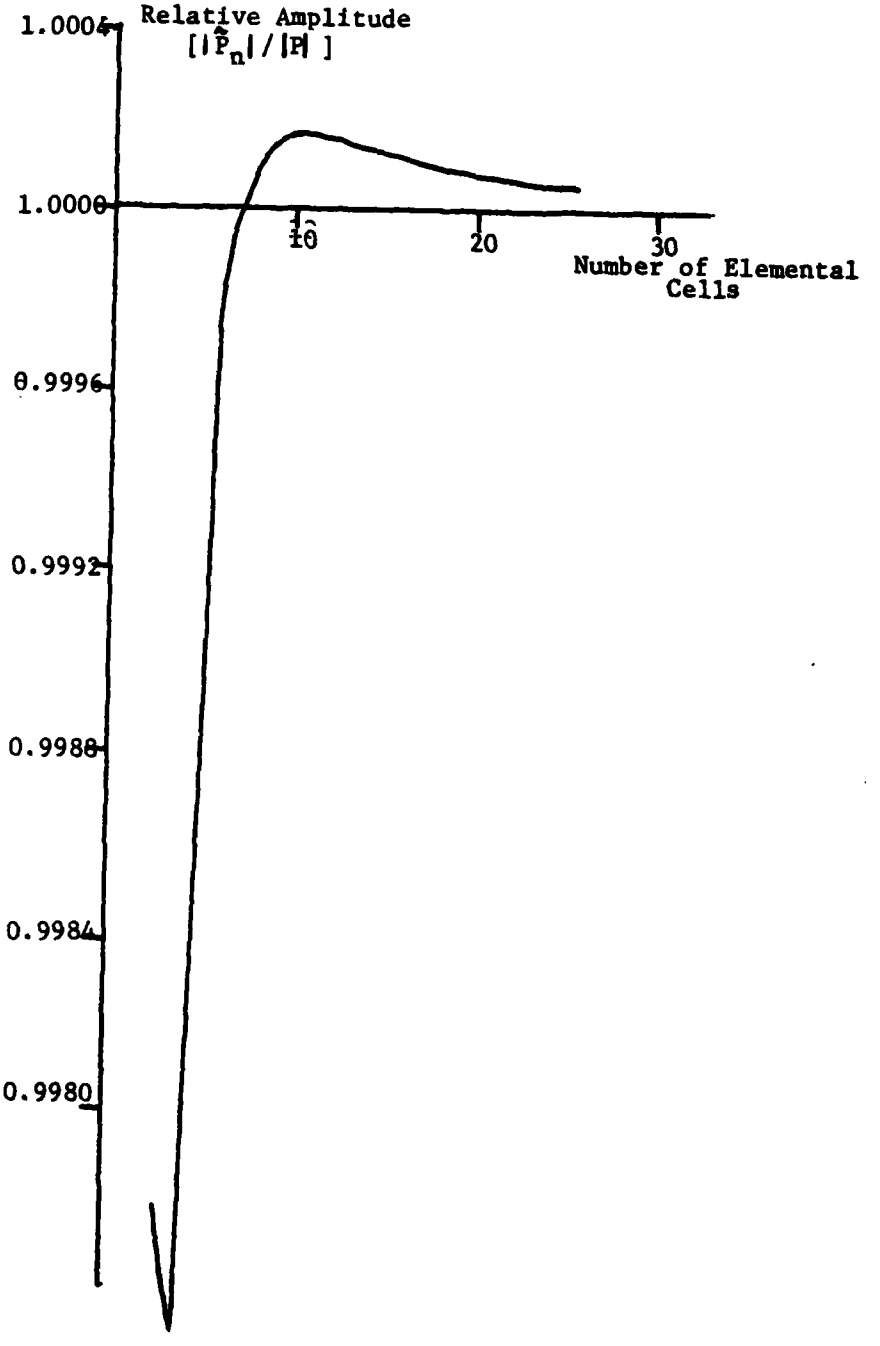

Figure 32 - Convergence Profile for f=29.9MHz

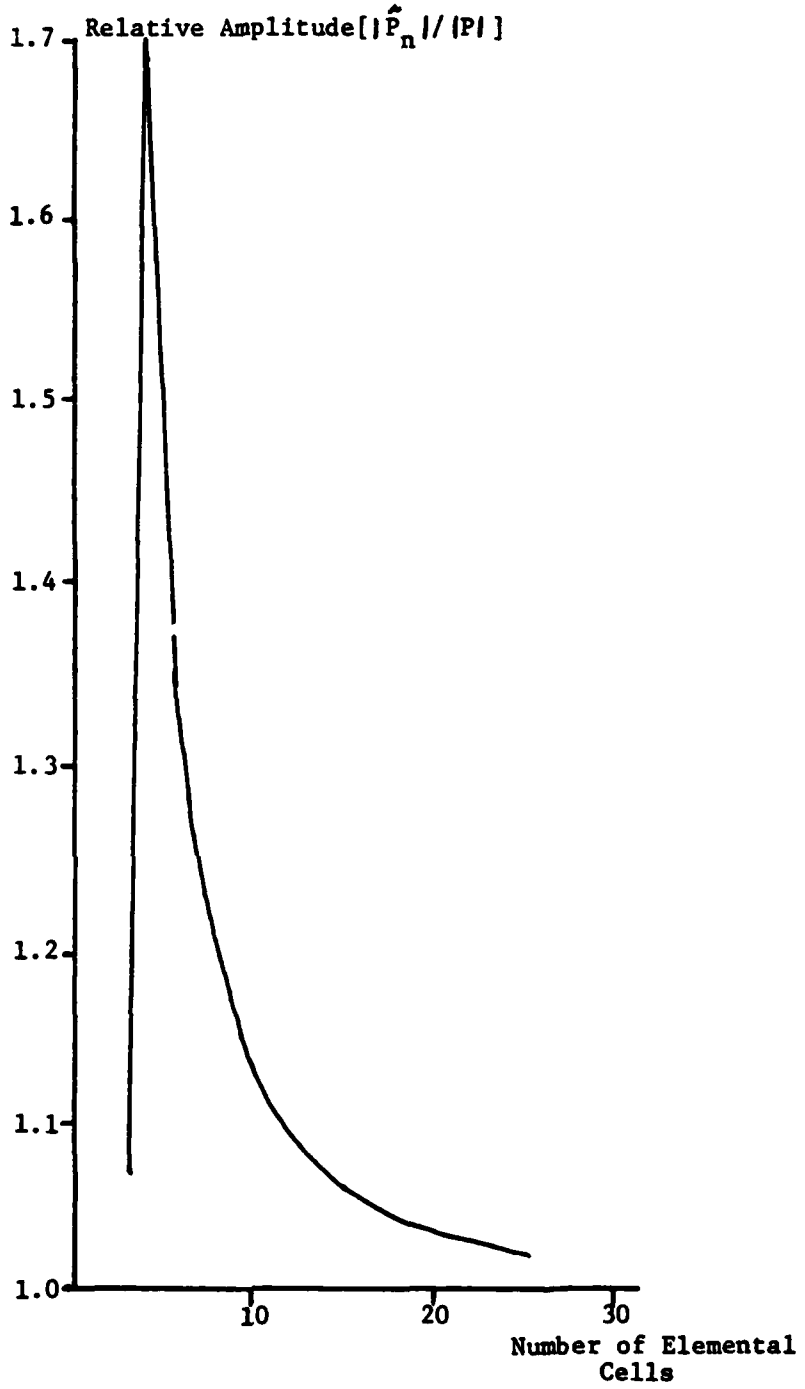

Figure 33 - Convergence Profile for f=30.36MHz

consonance with the discussions of the two examples presented at the beginning of this section, the convergence profile displayed in Figure 30 is representative of those frequency components within the mainlobe and major sidelobes. As frequency components farther above or below the mainlobe are examined, the convergence profile becomes more complex.

The extrapolation technique has been observed to provide significant increases in the accuracy of spectrum estimates at a minimal cost in computation. The use of this technique, however, requires a judicious selection of n_1.

VII. APPLICATION

The model developed in the previous sections can be a useful tool in the development and implementation of signal classification algorithms based on frequency domain analysis. The modulation that is present on pulsed signals may well be a useful discriminant in the classification process. This being the case the treatment of this discriminant in the frequency domain has the potential of being less susceptible to noise since the transformation is a smoothing process.

To address the discriminant selection in the frequency domain, consider the chirp radar pulse. As the chirp rate is increased or decreased for a given pulse duration, certain characteristic effects occur: (1) the spectrum is shifted in proportion to the chirp rate and (2) the sidelobe amplitudes change relative to the mainlobe as a function of chirp rate. Knowledge of the form of the spectrum provides an insight into the nature of the chirp pulse. In more general cases in which the frequency modulation may be more complex, does knowledge of the spectrum form provide useful information to the classification process?

To examine this question, let the discriminants that define the spectrum form do so in terms of the sidelobe structure relative to the mainlobe. This can be easily accomplished by choosing two types of discriminants: (1) the relative amplitudes of the sidelobe local maxima (relative to the maximum spectrum amplitude) and (2) the frequency differences between the sidelobe maxima and the center frequency of the mainlobe. The selection of these parameters establish the form of the spectrum.

To actually assess the feasibility of employing sidelobe structure in the classification process requires that the impact of the modulation

on the spectrum be understood. To gain an insight into this effect, consider a unit pulse with an instantaneous frequency function as shown in figure 34. Note that the initial portion of the pulse (0.2μs) is subject to a symmetrical triangular modulation of magnitude ΔFM. To investigate the impact of the modulation on the frequency domain, the values of the two discriminants (relative amplitude and relative frequency) are determined for the first three upper and lower sidelobes for a variety of pulses as ΔFM varies from zero to 5 MHz. Figure 35 displays the relative amplitudes of the upper sidelobe maxima as a function of ΔFM. For example, the first sidelobe has a relative maxima of 0.3 when the magnitude of the triangular modulation is ΔFM = 2.0 MHz. All three sidelobe maxima have the potential of functioning as discriminants since they are single valued and monotonically increasing. For example, the relative amplitude of the sidelobe for ΔFM = 2.0 MHz is easily distinguished from that for ΔFM = 2.5 MHz for all three sidelobes. Figure 36 is a similar presentation for the lower sidelobe maxima. For a pulse with initial triangular modulation, the lower sidelobes are inferior to the upper sidelobes as discriminants. This is due to the fact that the relative amplitudes extend over a much more confined range of values and that, in the case of the second sidelobe, points exist on the curve that are multi-valued. From figure 36 it appears that the first sidelobe disappears when ΔFM = 2.5 MHz. In fact, as the modulation magnitude increases past 2.0 MHz, the first and second sidelobes merge to form one and are arbitrarily associated with the second sidelobe. The inferior performance of the lower sidelobes in this example should not be cause to disregard them as discriminants, since by changing the polarity and location of the triangular modulation the relative merits of the upper and lower sidelobes

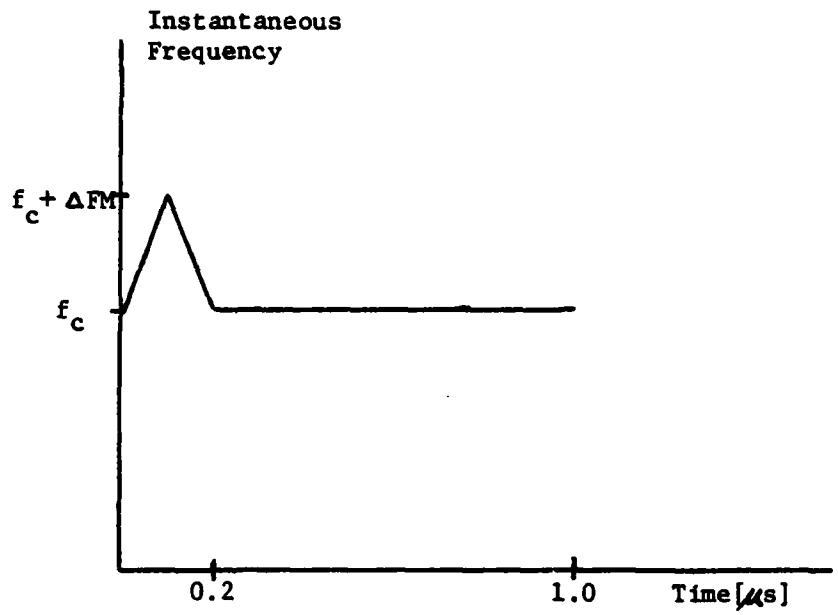

Figure 34 - Instantaneous Frequency Function with Triangular Modulation

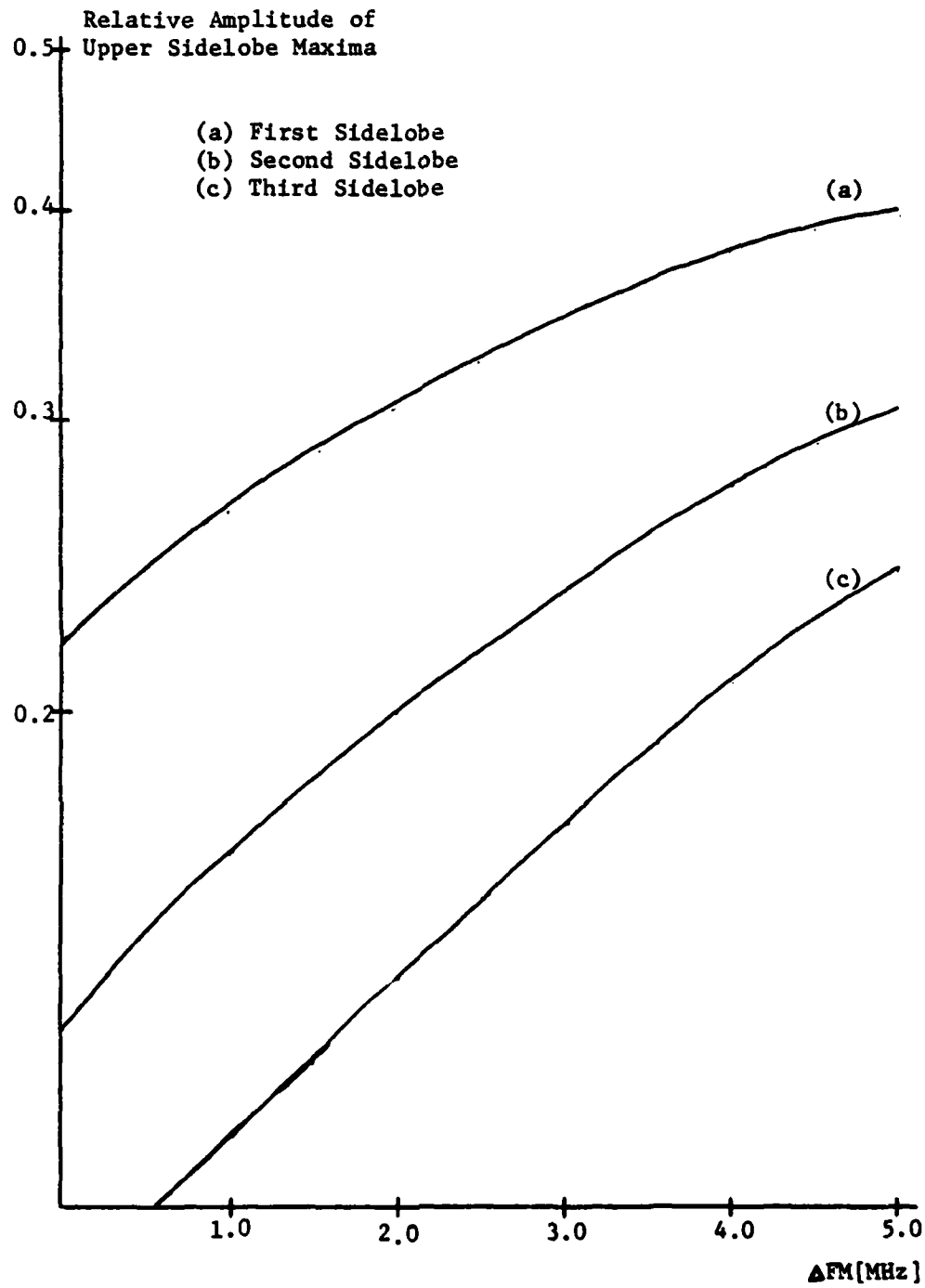

Figure 35 - Upper Sidelobe Relative Amplitude vs.

Frequency Modulation

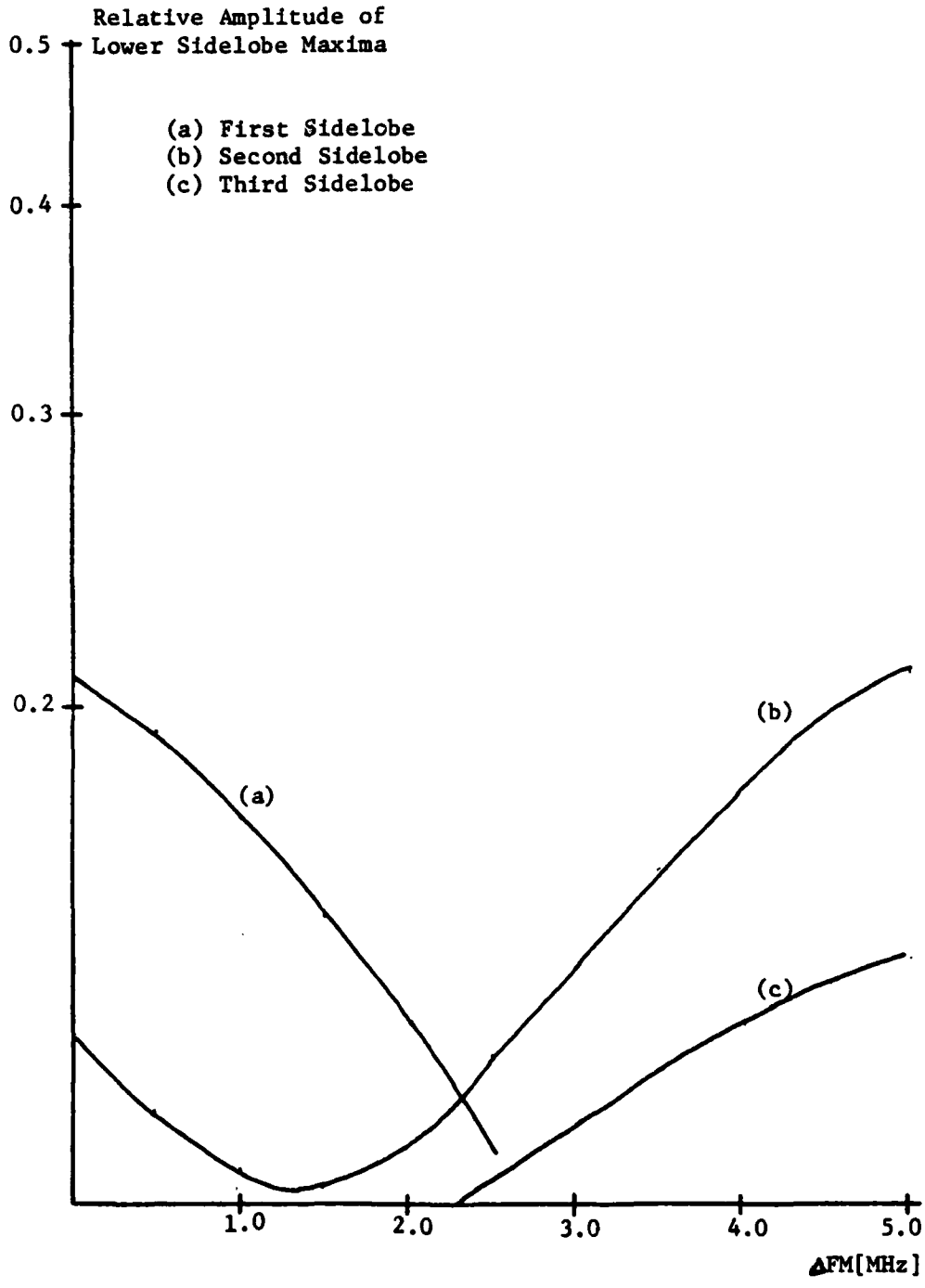

Figure 36 - Lower Sidelobe Relative Amplitude vs. Frequency Modulation

would be reversed. The relative amplitude of the sidelobe maxima display the characteristics desired of a discriminant for classification purposes.

Figure 37 displays the relative frequency of the upper sidelobe maxima as a function of ΔFM. In order to accomodate all three sidelobe profiles on the same scale, f_o is selected as the normalization factor. It represents the nominal frequency at which the sidelobe maxima would occur for the case of a constant frequency pulse. If τ is the pulse duration, the sin(x)/x spectrum will have local maxima at the following approximate spacings from the center of the mainlobe: $\pm 3/2\tau$, $\pm 5/2\tau$, $\pm 7/2\tau$, ... so that f_o, the location of the n^{th} sidelobe peak relative to the center frequency, is $\pm(n + 1/2)/\tau$. Thus as each of the three sidelobes is considered, the value of f_o changes. The range of values over which the relative frequencies extend is fairly small especially for ΔFM less than 2.0 MHz. Figure 38 presents the relative frequency of the lower sidelobe maxima. The first sidelobe provides no useful information. The second and third sidelobes however are quite robust due in large part to the fact that the first and second sidelobes merge at about ΔFM = 2.0 MHz. There appears some potential for relative frequency as a discriminant but its power does not appear comparable to that of relative amplitude.

To gain another feel for discriminant power consider a pulse as in figure 34 but with a triangular modulation that is not symmetrical. Such an instantaneous frequency profile is shown in figure 39. Again, the relative amplitude and relative frequency of the local sidelobe maxima can be examined. Figure 40 displays the relative amplitude for the upper sidelobe maxima. The results from figure 35 (symmetrical modulation) are

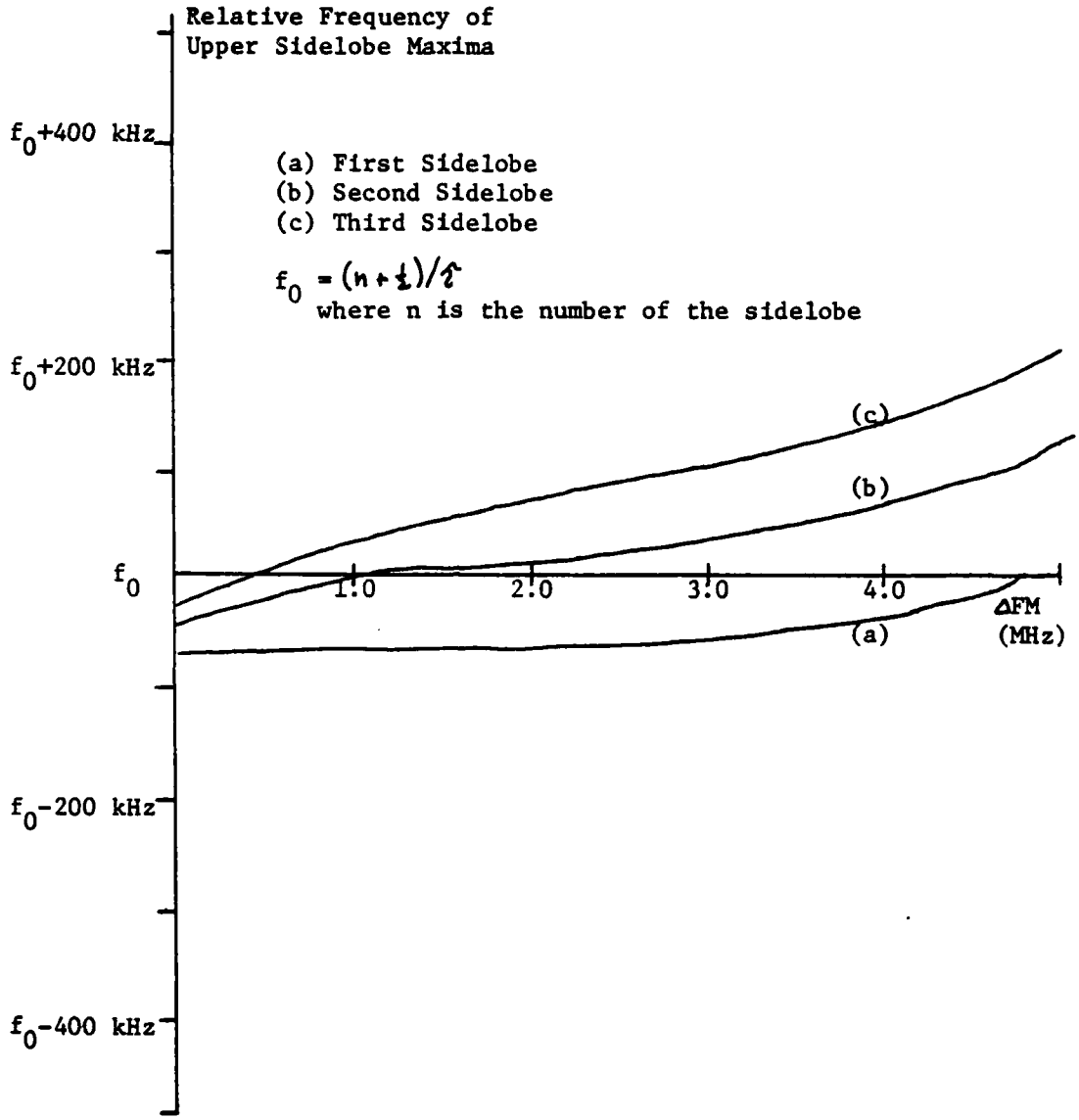

Figure 37 - Upper Sidelobe Relative Frequency vs.

Frequency Modulation

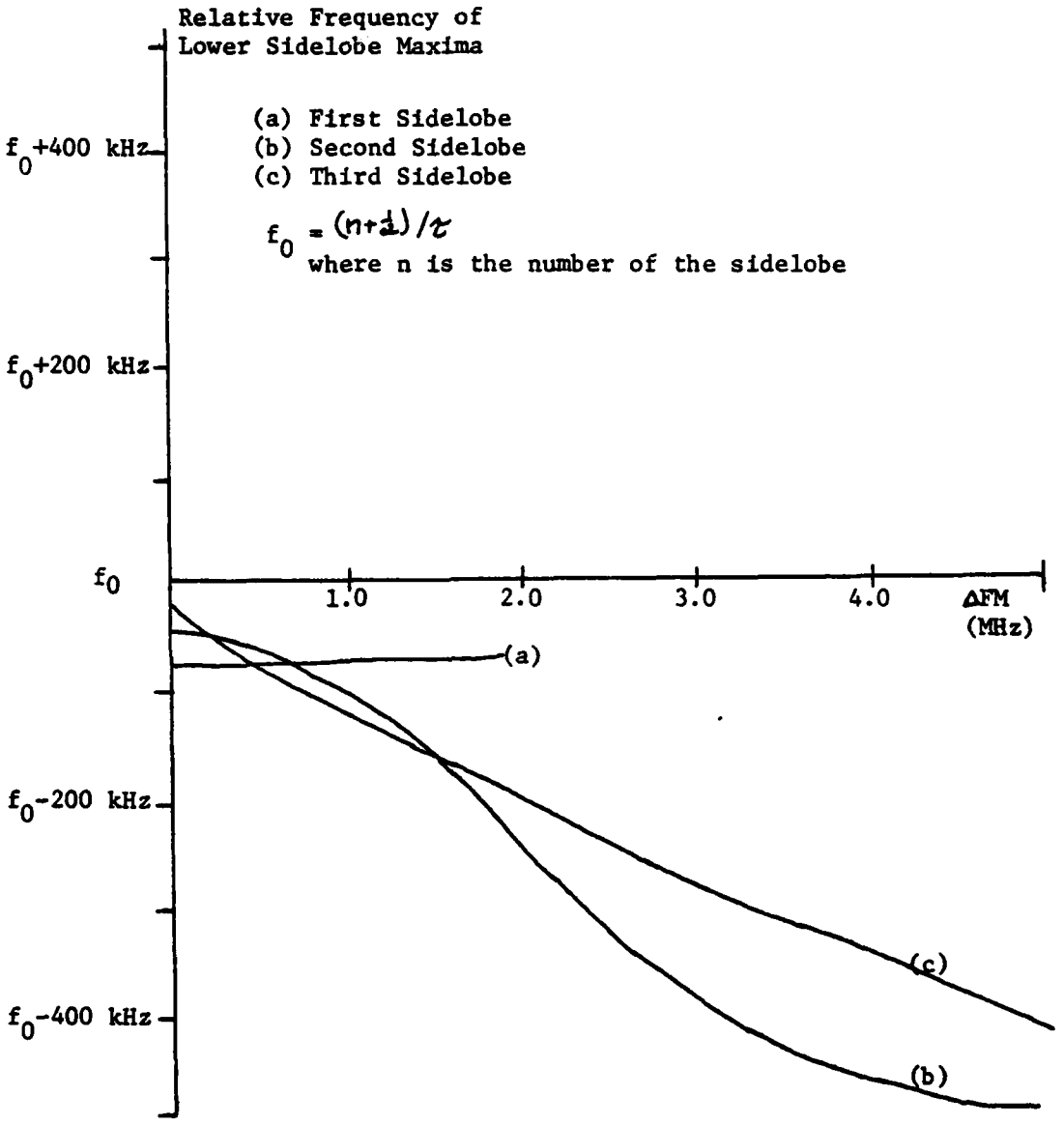

Figure 38 - Lower Sidelobe Relative Frequency vs. Frequency Modulation

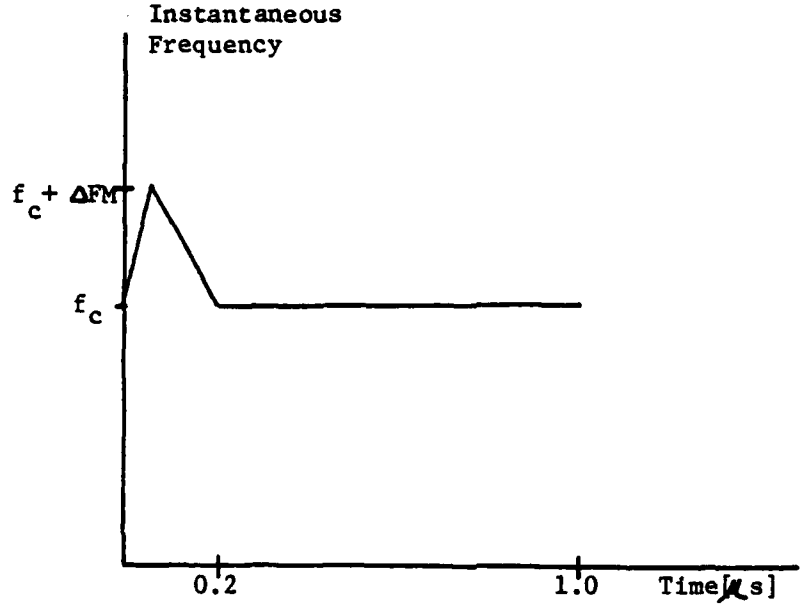

Figure 39 - Instantaneous Frequency Function with Triangular Modulation (asymmetrical)

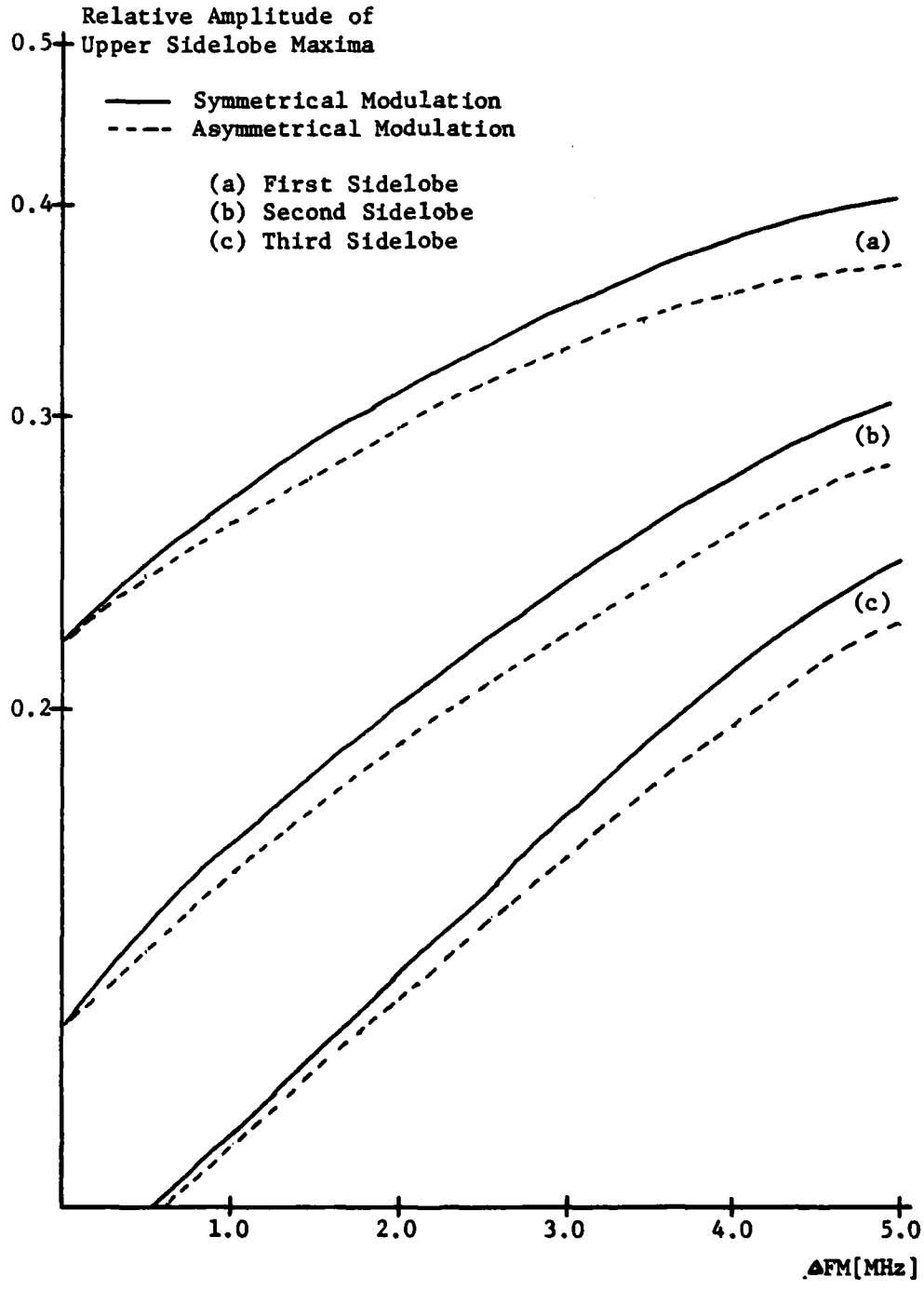

Figure 40 - Upper Sidelobe Relative Amplitude vs.

Frequency Modulation

plotted as solid lines for comparison. These discriminants appear to work well in distinguishing between these similar pulses especially for ΔFM greater than 2.5 MHz. A similar presentation for the lower sidelobe relative amplitudes appears in figure 41. The performance of the lower sidelobe discriminants parallels that of the upper sidelobes for these two similar pulses. Figures 42 and 43 present the relative frequency of the upper and lower sidelobes, respectively, as a function of ΔFM. Except for large values of ΔFM in the case of the second and third lower sidelobes, the overall performance of relative frequency in distinguishing between these two signals is marginal.

In summary, frequency domain techniques are reasonable for pulse classification purposes. The use of sidelobe structure in the form of relative amplitude and relative frequency as a classification discriminant is a valid approach to the problem with the former possessing the greater potential for success.

This type of analysis lends itself very well to the elemental cell model. Waveforms are easily constructed and implemented and local maxima can be readily identified to arbitrary precision.

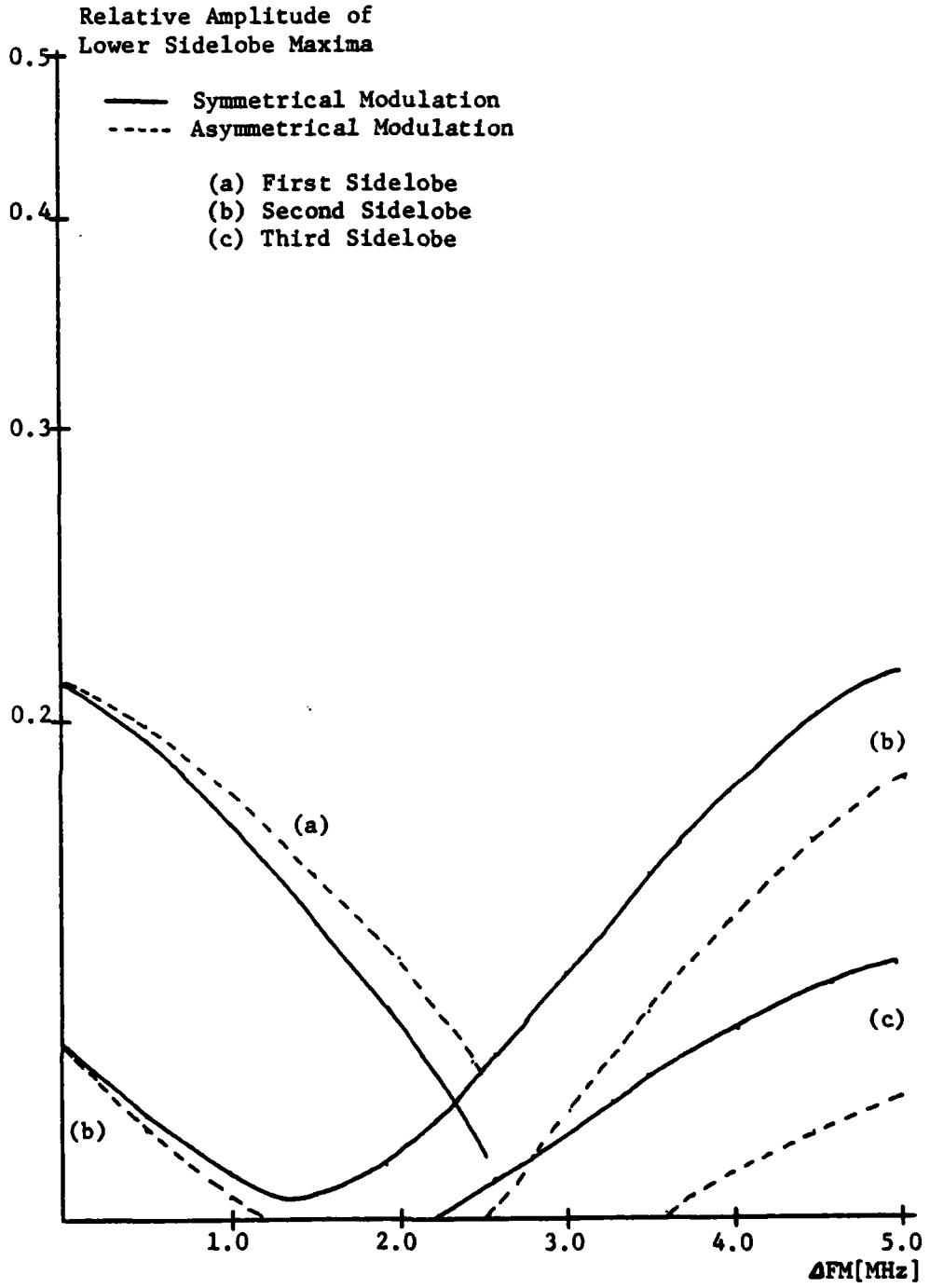

Figure 41 - Lower Sidelobe Relative Amplitude vs. Frequency Modulation

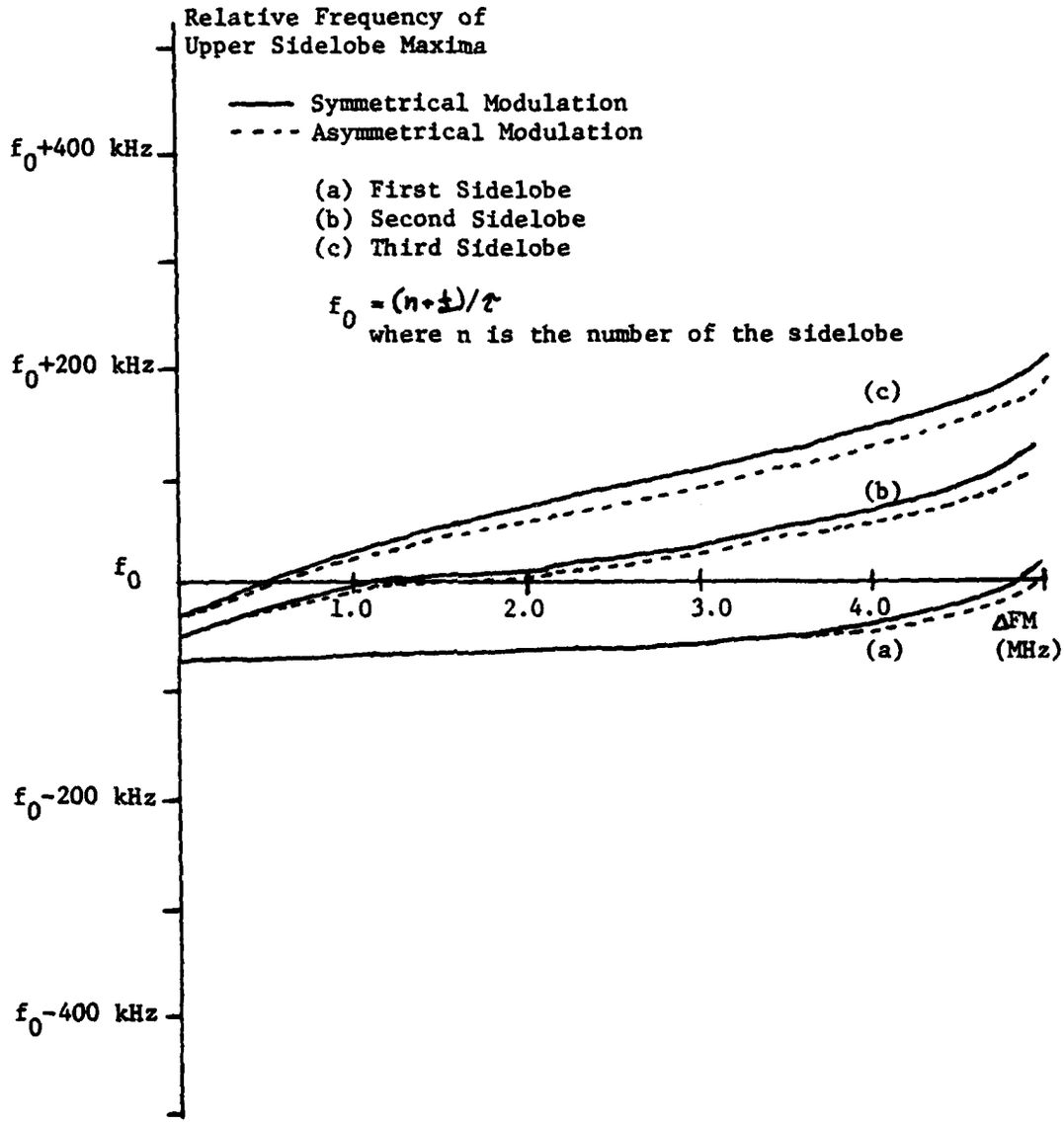

Figure 42 - Upper Sidelobe Relative Frequency vs.

Frequency Modulation

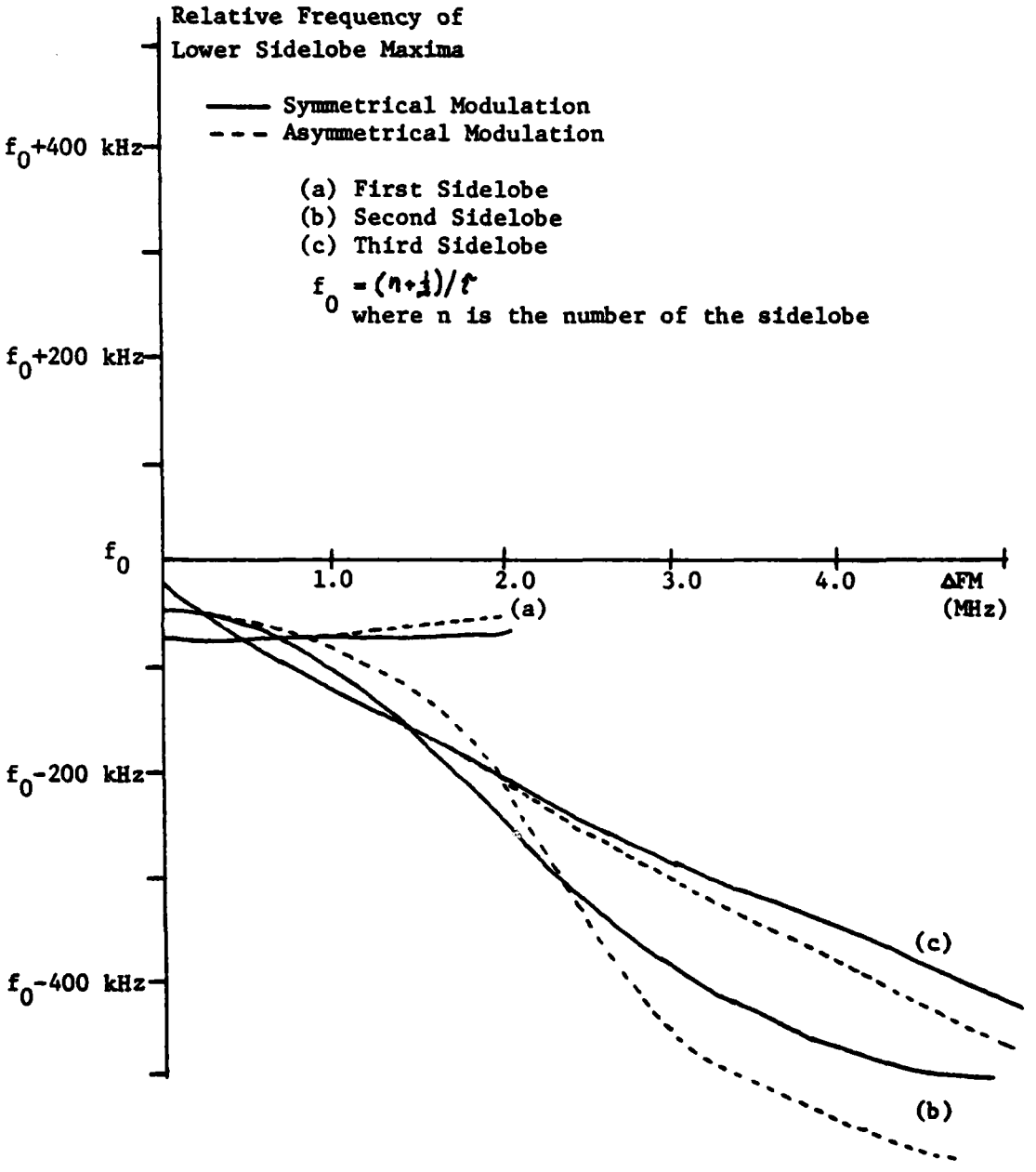

Figure 43 - Lower Sidelobe Relative Frequency vs.

Frequency Modulation

VIII. CONCLUSIONS AND RECOMMENDATIONS

A flexible, easy to use tool for modeling the spectra of pulse signals with arbitrary amplitude and frequency modulation has been developed along with the appropriate error bounds. When properly implemented, accuracy comparable to that of an FFT is achievable. The technique developed is not universally superior to the FFT; efficiency of one over the other is a function of specific applications. Computational speed can be an advantage in the elemental cell method in those cases where large FFT's are required relative to the product of the number of elemental cells (n) and the number of frequency components required (m).

The feasibility of using frequency domain discriminants in the signal classification process has been demonstrated.

There are a number of areas for further investigation and refinement. Appendix D addresses the comparison of the FFT and the elemental cell technique in terms of computational speed. Since most of the studies during this effort were focused on precision vice speed and since the execution time studies were conducted without modification to the basic subroutines (Appendix A), significant improvements can be made in the efficiency of the elemental cell subroutines. Several specific areas for improvement are:

(1) the conversion of double precision based routines to single precision. Preliminary investigation in this area has indicated that this can be accomplished with little degradation in model performance.

(2) the elimination of "left-hand" spectrum computations. The existing subroutines calculate both the "left-hand" and "right-hand" spectrum contributions to each frequency component. Under the proper conditions, the former can be eliminated without performance degradation.

(3) the streamlining of certain aspects of the overall computation. For example, the technique of James (5), discussed in Appendix C, for Fresnel integral evaluation should be assessed for use in place of the existing technique.

The time required to generate a spectrum using the elemental cell technique is a function of the number of cells used (n) and the number of frequency components required (m). The time required increases as the product of m and n. Since the calculation of each elemental cell spectra is independent of all other elemental cell spectra, individual elemental cell spectra can be calculated in parallel and then coherently summed. Investigation of the implementation of parallel processing arrays should be initiated. Under such an implementation, the computation time required for spectrum generation would be proportional to m vice m x n.

While the feasibility of using spectrum discriminants in signal classification has been established, further examination is required:

(1) the approach should be assessed against a noisy environment;

(2) the approach should be compared to other techniques on simulated and real data.

Further work might well be done in applying the elemental cell concept with different basis functions that lend themselves to certain classes of signals.

APPENDIX A

THE ELEMENTAL CELL MODEL

```
C
C                    ****************
C                    * MAIN PROGRAM *
C                    ****************
C
C
C  THIS PROGRAM GENERATES THE APPROXIMATE AMPLITUDE AND PHASE SPECTRA
C  OF A PULSE HAVING ARBITRARY AMPLITUDE AND FREQUENCY MODULATION.
C  THE INSTANTANEOUS FREQUENCY FUNCTION AND THE PULSE ENVELOPE
C  MUST BE APPROXIMATED BY LINEAR PIECEWISE CONTINUOUS FUNCTIONS.
C  THUS THE FUNCTIONS ARE PARTITIONED INTO "N" SEGMENTS, SO THAT THE
C  PULSE CAN BE THOUGHT OF AS BEING COMPOSED OF "N" ELEMENTAL CELLS.
C
C
C  THE INPUT PARAMETERS TO THE PROGRAM ARE:
C
C        (1) PHITO --- THE INITIAL CARRIER PHASE
C        (2) FSTART --- THE LOWEST FREQUENCY OF INTEREST
C        (3) RESLTN --- THE DESIRED FREQUENCY RESOLUTION
C        (4) NFREQ --- THE NUMBER OF FREQUENCY COMPONENTS OF INTEREST
C        (5) T(I) --- THE STARTING TIME OF THE ITH CELL
C        (6) F(I) --- THE INITIAL FREQUENCY OF THE ITH CELL
C        (7) A(I) --- THE INITIAL AMPLITUDE OF THE ITH CELL
C
C
C  SOME OF THE KEY PARAMETERS GENERATED BY THE PROGRAM ARE:
C
C        (1) RO --- THE CHIRP RATE OF THE ELEMENTAL CELL
C        (2) S --- AN INDICATOR OF POSITIVE (+1) AND NEGATIVE (-1)
C            CHIRP
C        (3) F1 --- THE INITIAL FREQUENCY OF THE ELEMENTAL CELL
C        (4) H --- THE SLOPE OF THE APPROXIMATED ENVELOPE OF THE
C            ELEMENTAL CELL
C        (5) AMPSRT --- THE INITIAL AMPLITUDE OF THE ITH CELL
C        (6) START --- THE LEFT ENDPOINT IN TIME OF THE CELL
```

```
C           (7) PW --- THE PULSE WIDTH OF THE ELEMENTAL CELL
C           (8) Z(I) --- THE ITH COMPLEX FREQUENCY COMPONENT
C
C
C
      DIMENSION Z(400), T(25), F(25), A(25)
      DIMENSION FREQ(400), AMP(400), PHASE(400)
      DIMENSION XAXIS(400)
      COMMON /SPEC1/ Z, FREQ, START, PW, AMPSRT, H, F1, RC, PHITC, S
      COMMON /SPEC2/ ZERO, PI, TWOPI, ZIP
      COMMON /SPEC3/ Z5, PIBY2, SQPIB2
      COMPLEX*16 Z, Z5, ZERO
      DOUBLE PRECISION FREQ, RO, F1, START,PW,AMPSRT,H,PHITO
      DOUBLE PRECISION PI, TWOPI, PIBY2, ZIP, HALF, T, F, A, FS
      DOUBLE PRECISION FSTART, RESLTN, SQPIB2
100   FORMAT(2E15.7,I5)
200   FORMAT(I5)
300   FORMAT(3E15.7)
900   FORMAT(10X,'   FREQUENCY   ',10X,'   AMPLITUDE   ',10X,'   PHASE
     1',//)
910   FORMAT(10X,2(E15.7,10X),F10.7)
920   FORMAT('1')
930   FORMAT(10X,'T(',I2,') = ',E14.7,8X,'F(',I2,') = ',E14.7,8X,'A(',I2
     1,' = ',E14.7)
940   FORMAT(10X,'NUMBER OF CELLS USED = ',I2,//)
950   FORMAT(10X,'RESOLUTION = ',E14.7,5X,'STARTING FREQUENCY = ',E14.7,
     15X,'NUMBER OF FREQUENCY COMPONENTS = ',I5,///)
C
C     DEFINE CONSTANTS
C
      PI=4.0*DATAN(1.0D+00)
      TWOPI=2.0*PI
      PIBY2=PI/2.0
      SQPIB2=DSQRT(PIBY2)
      ZIP=0.0D+00
      ZERO=DCMPLX(ZIP,ZIP)
      HALF=0.5D+00
      Z5=DCMPLX(ZIP,HALF)
C
C     READ IN PROGRAM PARAMETERS
C
      READ(5,300) PHITO
      READ(5,100) FSTART, RESLTN, NFREQ
      READ(5,200) NCELL
      NCELL1=NCELL+1
      WRITE(6,920)
      WRITE(6,940) NCELL
      WRITE(6,950) RESLTN, FSTART, NFREQ
```

```
      DO 10 I=1,NCELL1
      READ(5,300) T(I), F(I), A(I)
      WRITE(6,930) I, T(I), I, F(I),I, A(I)
10    CONTINUE
C
C     INITIALIZE VECTOR OF COMPLEX FREQUENCY COMPONENTS
C
      DO 20 I=1,NFREQ
      Z(I)=ZERO
20    CONTINUE
C
C     GENERATE THE FREQUENCIES OF INTEREST
C
      DO 30 I=1,NFREQ
      FREQ(I)=FSTART+(FLOAT(I-1)*RESLTN)
30    CONTINUE
C
C     CALCULATE THE FOURIER TRANSFORM FOR EACH CELL AND FORM
C     THE CUMULATIVE SUM OVER ALL CELLS
C
      DO 40 I=1,NCELL
C
C     GENERATE THE PARAMETERS WHICH DEFINE THE ITH CELL
C
      S=1.0
      AMPSRT=A(I)
      F1=F(I)
      FS=(F(I+1)-F1)/2.0
      START=T(I)
      PW=T(I+1)-T(I)
      IF(PW.EQ.0.0) GO TO 40
      M=(A(I+1)-A(I))/PW
      RO=2.0*FS/PW
C
C     IF THE SWEEP RATE IS LESS THAN THE THRESHOLD,
C     CONSIDER THE FREQUENCY TO BE CONSTANT AND CALL "CNST".
C     OTHERWISE SET THE PROPER FLAGS FOR NEGATIVE OR POSITIVE
C     SWEEP RATES AND CALL "CHIRP".
C
      IF(DABS(RO).GT.(1.0D-06)) GO TO 998
      CALL CNST(NFREQ)
      GO TO 40
998   IF(RO.GT.0.0) GO TO 999
      S=-1.0
      RO=DABS(RO)
999   CALL CHIRP(NFREQ)
40    CONTINUE
```

```
C
C    DEFINE A ZERO FOR PHASE CALCULATION PURPOSES
C
       ZNIL=(T(NCELL1)-T(1))*(1.0E-06)
C
C    FROM EACH COMPLEX FREQUENCY COMPONENT FIND THE AMPLITUDE AND PHASE
C
       DO 50 I=1,NFREQ
       AMP(I)=CDABS(Z(I))
       XREL=DREAL(Z(I))
       XIMAG=DIMAG(Z(I))
       IF(ABS(XREL).LT.ZNIL) XREL=0.0
       IF(ABS(XIMAG).LT.ZNIL) XIMAG=0.0
       RADIAN=100.0
       IF(XREL.EQ.0.0.AND.XIMAG.GT.0.0) RADIAN=PIBY2
       IF(XREL.EQ.0.0.AND.XIMAG.LT.0.0) RADIAN=-PIBY2
       IF(XREL.EQ.0.0.AND.XIMAG.EQ.0.0) RADIAN=0.0
       IF(RADIAN.NE.100.0) GO TO 997
       RADIAN=ATAN2(XIMAG,XREL)
997    PHASE(I)=RADIAN
50     CONTINUE
       WRITE(6,920)
       WRITE(6,900)
       DO 80 I=1,NFREQ
       WRITE(6,910) FREQ(I), AMP(I), PHASE(I)
       XAXIS(I)=FREQ(I)-FSTART
80     CONTINUE
       WRITE(6,920)
       CALL PLOTP(XAXIS,AMP,NFREQ,0)
       CALL PLOTP(XAXIS,PHASE,NFREQ,0)
       STOP
       END
```

```
C
C
C
C                                  **********************
C                                  * SUBROUTINE CHIRP *
C                                  **********************
C
C
C
C     SUBROUTINE CHIRP GENERATES THE COMPLEX FREQUENCY COMPONENTS OF AN
C     ELEMENTAL CELL WITH LINEARLY SWEPT FREQUENCY AND EITHER CONSTANT
C     OR LINEARLY VARYING AMPLITUDE MODULATION
C
C
        SUBROUTINE CHIRP(NFREQ)
        DIMENSION Z(400), FREQ(400)
        COMMON /SPEC1/ Z, FREQ, START, PW, AMPSRT, F, F1, RO, PHITO, S
        COMMON /SPEC2/ ZERO, PI, TWOPI, ZIP
        COMMON /SPEC3/ Z5, PIBY2, SQPI82
        COMPLEX*16 FINT1, FINT2, Z, BETAX1, BETAX2, ZERO
        COMPLEX*16 Z1, Z2, Z3, Z4, Z5, Z6, Z7, AM1, AM2
        DOUBLE PRECISION FREQ, RO, F1, START, PW, AMPSRT, F, PHITO, TSHIFT
        DOUBLE PRECISION PI, TWOPI, ZIP, A, B1, B2, FACTOR, BETA1, BETA2
        DOUBLE PRECISION C1L, C1H, C2L, C2H, S1L, S1H, S2L, S2H
        DOUBLE PRECISION FRESR1, FRESI1, FRESR2, FRESI2, TH
        DOUBLE PRECISION ZLO1, ZLO2, ZHI1, ZHI2, XLO1, XHI1, XLO2, XHI2
        DOUBLE PRECISION PIBYRO, PIBYA, T1, T2, T3, PIBY2, SQPI82
C
C     DEFINE CONSTANTS
C
        A=DSQRT(RO*PI)
        FACTOR=DSQRT(TWOPI)/(4.0*A)
        PIBYRO=PI/RO
        PIBYA=PI/A
C
C     GENERATE THE COMPLEX FREQUENCY COMPONENTS OF THE ELEMENTAL CELL
C     FOR THE FREQUENCIES OF INTEREST.
C
        DO 10 I=1,NFREQ
        AM1=ZERO
        AM2=AM1
        TSHIFT=TWOPI*FREQ(I)*START
        B1=PIBYA*(F1-FREQ(I))
        B2=PIBYA*(F1+FREQ(I))
        BETA1=-TSHIFT+PHITO-S*B1**2
        BETA2=TSHIFT+PHITO-S*B2**2
        BETA1=DMOD(BETA1,TWOPI)
        BETA2=DMOD(BETA2,TWOPI)
```

```
      BETAX1=DCMPLX(ZIP,BETA1)
      BETAX2=DCMPLX(ZIP,BETA2)
C
CC    ESTABLISH THE LIMITS OF INTEGRATION FOR THE FRESNEL INTEGRALS
C
      THI=A*PW
      ZLO1=S*B1
      ZHI1=THI+ZLO1
      ZLO2=S*B2
      ZHI2=THI+ZLO2
      XLO1=ZLO1**2
      XHI1=ZHI1**2
      XLO2=ZLO2**2
      XHI2=ZHI2**2
C
CC    EVALUATE THE FRESNEL INTEGRALS
C
      CALL CS(C1L,S1L,XLO1)
      IF(ZLO1.GE.0.0) GO TO 600
      C1L=-C1L
      S1L=-S1L
600   CALL CS(C1H,S1H,XHI1)
      IF(ZHI1.GE.0.0) GO TO 610
      C1H=-C1H
      S1H=-S1H
610   CALL CS(C2L,S2L,XLO2)
      IF(ZLO2.GE.0.0) GO TO 620
      C2L=-C2L
      S2L=-S2L
620   CALL CS(C2H,S2H,XHI2)
      IF(ZHI2.GE.0.0) GO TO 630
      C2H=-C2H
      S2H=-S2H
630   FRESR1=C1H-C1L
      FRESI1=S*(S1H-S1L)
      FRESR2=C2H-C2L
      FRESI2=S*(S2L-S2H)
      FINT1=DCMPLX(FRESR1,FRESI1)
      FINT2=DCMPLX(FRESR2,FRESI2)
C
C     IF THE CELL AMPLITUDE MODULATION IS LINEAR, TAKE THIS INTO
C     ACCOUNT BY ADDING THE REQUIRED TERMS
C
      IF(DABS(H).LT.(1.0E-05)) GO TO 666
      Z1=DCMPLX(ZIP,XLO1)
      IF(S.EQ.-1.0) Z1=DCONJG(Z1)
      Z2=DCMPLX(ZIP,XHI1)
      IF(S.EQ.-1.0) Z2=DCONJG(Z2)
```

```
      Z3=DCMPLX(ZIP,XLO2)
      IF(S.EQ.-1.C) Z3=DCONJG(Z3)
      Z4=DCMPLX(ZIP,XHI2)
      IF(S.EQ.-1.C) Z4=DCONJG(Z4)
      T1=(2.0*FACTOR*H)/PIBY2
      T2=SQPIB2*B1
      T3=SQPIB2*B2
      AM1=T1*((Z5*(CDEXP(Z1)-CDEXP(Z2)))-(T2*FINT1))*S
      AM2=T1*((Z5*(CDEXP(Z4)-CDEXP(Z3)))-(T3*FINT2))*S
666   Z6=(AMPSRT*FINT1)+AM1
      Z7=(AMPSRT*FINT2)+AM2
      Z(I)=Z(I)+FACTOR*(Z6*CDEXP(BETAX1)+Z7*CDEXP(-BETAX2))
10    CONTINUE
C
C     CALCULATE THE PHASE AT THE END OF THE CURRENT CELL
C     THIS WILL BE THE INITIAL PHASE OF THE NEXT CELL
C
      PHITO=PHITO+TWOPI*F1*PW+PI*RO*(PW**2)*S
      RETURN
      END
```

```
C
C
C
C                       *****************
C                       * SUBROUTINE CS *
C                       *****************
C
C
C
C     SUBROUTINE CS EVALUATES THE SINE (CS) AND THE COSINE (CC)
C     FORMS OF THE FRESNEL INTEGRAL FOR AN UPPER LIMIT OF X
C
C
C
      SUBROUTINE CS(DC,DS,X)
      DOUBLE PRECISION Z, CA, DB, DC, CC, DS, X
      Z=DABS(X)
      IF(Z-4.) 1,1,2
    1 DC=DSQRT(Z)
      DS=Z*DC
      Z=(4.0-Z)*(4.0+Z)
      CC=DC*((((((5.100785E-11*Z+5.244297E-9)*Z+5.541182E-7)*Z
     1+3.273308E-5)*Z+1.020418E-3)*Z+1.102544E-2)*Z+1.840965E-1)
      CS=CS*(((((6.677681E-10*Z+5.883158E-8)*Z+5.051141E-6)*Z
     1+2.441816E-4)*Z+6.121320E-3)*Z+8.026490E-02)
      RETURN
    2 DC=DCOS(Z)
      DS=DSIN(Z)
      Z=4./Z
      DA=((((((((8.768258E-4*Z-4.169289E-3)*Z+7.970943E-3)*Z-6.792801E-3)
     1*Z-3.095341E-4)*Z+5.972151E-3)*Z-1.606428E-5)*Z-2.493322E-2)*Z
     2-4.444091E-9
      DB=((((((-6.633926E-4*Z+3.401409E-3)*Z-7.271690E-3)*Z+7.428246E-3
     1)*Z-4.027145E-4)*Z-9.314910E-3)*Z-1.207998E-6)*Z+1.994711E-1
      Z=DSQRT(Z)
      DC=0.5+Z*(DC*DA+DS*DB)
      CS=0.5+Z*(DS*CA-CC*DB)
      RETURN
      END
```

```
C
C
C                              ********************
C                              * SUBROUTINE CNST  *
C                              ********************
C
C
C
C     SUBROUTINE CNST GENERATES THE COMPLEX FREQUENCY COMPONENTS OF AN
C     ELEMENTAL CELL WITH A CONSTANT CARRIER FREQUENCY AND EITHER
C     CONSTANT OR LINEARLY VARYING AMPLITUDE MODULATION
C
C
      SUBROUTINE CNST(NFREQ)
      DIMENSION Z(400), FREQ(400)
      COMMON /SPEC1/ Z, FREQ, START, PW, AMPSRT, F, F1, RC, PHITO, S
      COMMON /SPEC2/ ZERO, PI, TWOPI, ZIP
      COMPLEX*16 Z1, Z2, Z3, Z4, Z5, Z6, Z7, Z8, Z9, Z10, Z11, Z, ZERO
      DOUBLE PRECISION FREQ, RO, F1, START, PW, AMPSRT, F, PHITO, TSHIFT
      DOUBLE PRECISION PI, TWOPI, ZIP, WC, W, WS, WD, WS1, WD1, W1, W2
      DOUBLE PRECISION TSUM, TDIFF
      Z1=DCMPLX(ZIP,PHITO)
      Z2=DCONJG(Z1)
      WC=TWOPI*F1
C
CC    GENERATE THE COMPLEX FREQUENCY COMPONENTS OF THE ELEMENTAL CELL
CC    FOR THE FREQUENCIES OF INTEREST
C
      DO 10 I=1,NFREQ
      Z10=ZERO
      Z11=Z10
      W=TWOPI*FREQ(I)
      TSHIFT=-W*START
      Z3=DCMPLX(ZIP,TSHIFT)
      WS=WC+W
      WS1=-1.0/(2.0*WS)
      WD=WC-W
      IF(CABS(WD).GT.(1.0E-10)) GO TO 998
      Z8=AMPSRT*(PW/2.0)*CDEXP(Z1)
      GO TO 999
998   WD1=1.0/(2.0*WD)
      Z4=DCMPLX(ZIP,WD1)
999   W1=WD*PW
      W2=-WS*PW
      Z5=DCMPLX(ZIP,W1)
      Z6=DCMPLX(ZIP,WS1)
```

```
      Z7=DCMPLX(ZIP,W2)
      IF(DABS(WD).LT.(1.0E-10)) GO TO 997
      Z8=AMPSRT*Z4*CDEXP(Z1)*(1.0-CDEXP(Z5))
997   Z9=AMPSRT*Z6*CDEXP(Z2)*(1.0-CDEXP(Z7))
C
C     IF THE CELL AMPLITUDE IS NOT CONSTANT, TAKE THIS INTO ACCOUNT
C     BY ADDING THE REQUIRED TERMS
C
      IF(CABS(H).LE.(1.0E-05)) GO TO 996
      TSUM=-H/(2.0*(WS**2))
      IF(DABS(WD).GT.(1.0D-10)) GO TO 995
      Z10=(PW**2)*(H/4.0)*CDEXP(Z1)
      GO TO 994
995   TDIFF=-H/(2.0*(WD**2))
994   IF(DABS(WD).LT.(1.0D-10)) GO TO 993
      Z10=TDIFF*CDEXP(Z1)*(1.0-((1.0-Z5)*CDEXP(Z5)))
993   Z11=TSUM*CDEXP(Z2)*(1.00-((1.0-Z7)*CDEXP(Z7)))
996   Z(I)=Z(I)+(CDEXP(Z3)*(Z8+Z9+Z10+Z11))
10    CONTINUE
C
C     CALCULATE THE PHASE AT THE END OF THE CURRENT CELL
C     THIS WILL BE THE INITIAL PHASE OF TH NEXT CELL
C
      PHITO=PHITO+WC*PW
      RETURN
      END
```

APPENDIX B

SPECTRA OF SINUSOIDALLY MODULATED PULSES

Consider a pulse, s(t), which may be both amplitude and frequency modulated so that over the duration of the pulse:

$$s(t) = v(t)\cos[\phi(t)] \tag{B-1}$$

where v(t) represents the amplitude modulation and $\phi(t)$, the instantaneous phase, accounts for the frequency modulation. An expression for the frequency spectra of two specific cases of equation (B-1) is developed. In CASE A, the pulse envelope is simply represented by a unit pulse (i.e., v(t)=1 over the pulse width). In CASE B, the pulse envelope is allowed to vary sinusoidally. In both CASES A and B, however, the carrier frequency experiences a sinusoidal frequency modulation.

Consider a sinusoidal instantaneous frequency function as shown in figure (B-1) with f_c being the carrier frequency; f_m, the modulating frequency and k_f, the modulation index. The instantaneous frequency function, $f_i(t)$, is represented by:

$$f_i(t) = f_c + k_f f_m \cos[\omega_m t] \tag{B-2}$$

The instantaneous phase can then be written as:

$$\phi(t) = \omega_c t + k_f \sin[\omega_m t] + \phi(0) \tag{B-3}$$

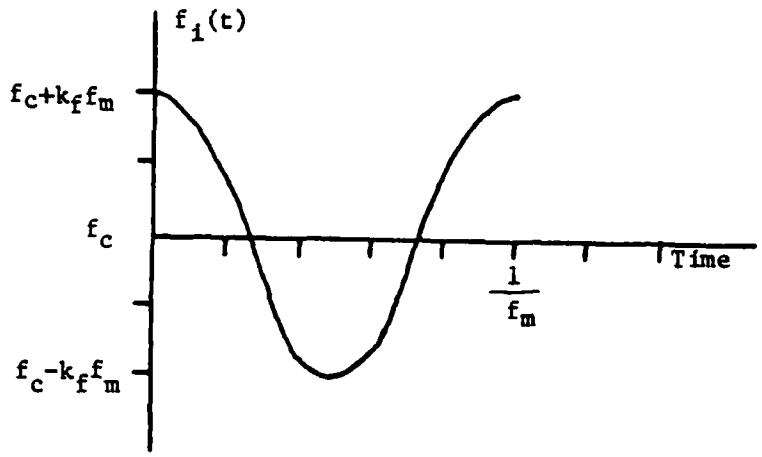

Figure B-1 - Instantaneous Frequency of a Sinusoidally Modulated Pulse

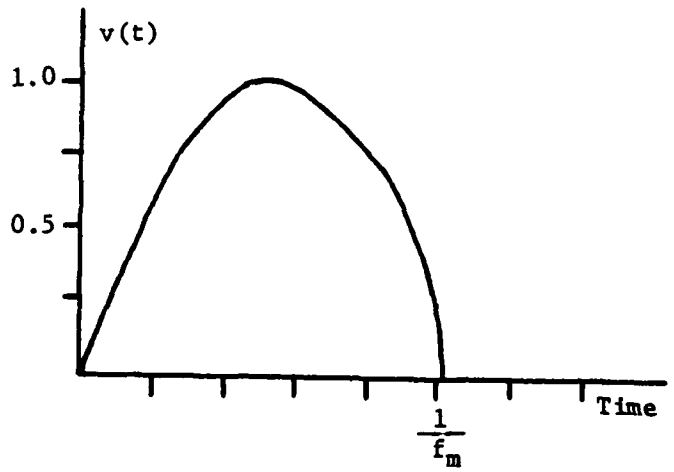

Figure B-2 - Envelope of a Sinusoidally Shaped Pulse

where $\Phi(o)$ is the initial carrier phase at time zero. For the purposes of this analysis, the interest is in the cosine of the phase function $\Phi(t)$

$$\cos[\Phi(t)] = \cos[\omega_c t + k_f \sin(\omega_m t) + \Phi(0)] \tag{B-4}$$

The right hand side of equation (B-4) can be expanded as an infinite series of sinusoidal functions weighted by Bessel functions (6).

$$\cos[\Phi(t)] = J_0(k_f)\cos[\omega_c t + \Phi(0)] + \sum_{i=1}^{\infty} (-1)^i J_i(k_f)\left\{\cos[(\omega_c - i\omega_m)t + \Phi(0)] + (-1)^i \cos[(\omega_c + i\omega_m)t + \Phi(0)]\right\} \tag{B-5}$$

This expression represents the sinusoidal FM associated with the pulse for which spectra are to be generated for CASES A and B below.

CASE A: SINUSOIDAL FM

The frequency spectrum for the unit pulse of duration τ with sinusoidal FM can be expressed as:

$$Z(f) = \int_0^{\tau} \cos[\Phi(t)] e^{-j\omega t} dt \tag{B-6}$$

Using the results of equation (B-5) and integrating, produces:

$$
\begin{aligned}
(B\text{-}7)\quad Z(f) = {} & -j\frac{J_0(k_f)}{2}\left\{\frac{e^{j\phi(0)}}{\omega_c-\omega}\left[e^{j(\omega_c-\omega)\hat{\tau}}-1\right]-\frac{e^{-j\phi(0)}}{\omega_c+\omega}\left[e^{-j(\omega_c+\omega)\hat{\tau}}-1\right]\right\} \\
& -j\sum_{i=1}^{\infty}\frac{(-1)^i J_i(k_f)}{2}\left\{\frac{e^{j\phi(0)}}{\omega_c-i\omega_m-\omega}\left[e^{-j(\omega_c-i\omega_m-\omega)\hat{\tau}}-1\right]\right. \\
& \qquad -\frac{e^{-j\phi(0)}}{\omega_c-i\omega_m+\omega}\left[e^{-j(\omega_c-i\omega_m+\omega)\hat{\tau}}-1\right] \\
& \qquad +\frac{(-1)^{i+1}e^{-j\phi(0)}}{\omega_c+i\omega_m+\omega}\left[e^{j(\omega_c+i\omega_m+\omega)\hat{\tau}}-1\right] \\
& \qquad \left.+\frac{(-1)^i e^{j\phi(0)}}{\omega_c+i\omega_m-\omega}\left[e^{j(\omega_c+i\omega_m-\omega)\hat{\tau}}-1\right]\right\}
\end{aligned}
$$

This frequency representation is essentially the convolution of the spectrum of a sinusoidally modulated carrier with the spectrum of a unit pulse. That is a sine(x)/x spectrum convolved with an infinite sequence of delta functions weighted by the Bessel functions, $J_i(k_f)$. Thus the spectrum is a function of the modulation index k_f. If k_f is small, the first few delta functions account for most of the power in the carrier(6). For example, if k_f=1, then J_0, J_1, and J_2 account for 98% of the signal power. In using equation (B-7) to generate a spectrum for CASE A, the first twenty terms of the series are evaluated. A program listing which evaluates equation (B-7) appears at the rear of the Appendix and is titled "SUBROUTINE SINE".

B. CASE B: SINUSOIDAL AM AND FM

Consider now CASE B in which the amplitude modulation is allowed to assume a sinusoidal form as shown in figure B-2. The frequency modulation is unchanged and generates the cos $\phi(t)$ term listed in equation (B-5). Allow the amplitude modulation to be expressed as:

$$V(t) = \sin[2\pi f_a t] \tag{B-8}$$

where $f_a = 1/2\tau$. Thus the pulse waveform equation can now be written:

$$s(t) = \sin[\omega_a t]\cos[\phi(t)] \tag{B-9}$$

With the aid of equation (B-4) and trigonometric identities, the pulse equation can be expressed as:

$$\begin{aligned} s(t) = {} & \frac{J_0(k_f)}{2}\left\{\sin[(\omega_c+\omega_a)t] - \sin[(\omega_c-\omega_a)t]\right\} \\ & + \sum_{i=1}^{\infty}(-1)^i \frac{J_i(k_f)}{2}\left\{\sin[(\omega_c - i\omega_m + \omega_a)t]\right. \\ & \quad -\sin[(\omega_c - i\omega_m - \omega_a)t] \\ & \quad +(-1)^i \sin[(\omega_c + i\omega_m + \omega_a)t] \\ & \quad \left.+(-1)^{i+1}\sin[(\omega_c + i\omega_m - \omega_a)t]\right\} \end{aligned} \tag{B-10}$$

By taking the Fourier transform of the pulse, the frequency spectrum

for CASE B can be expressed as:

$$
\begin{aligned}
(B\text{-}11)\quad Z(f) = \frac{J_0(k_f)}{2}\Bigg\{ & \sum_{K=1}^{\infty}(-1)^{K+1}\left(\frac{e^{j[\omega_c+(-1)^K\omega_a-\omega]\tau}-1}{\omega_c+(-1)^K\omega_a-\omega}\right)+(-1)^{K+1}\left(\frac{e^{-j[\omega_c+(-1)^K\omega_a+\omega]\tau}-1}{\omega_c+(-1)^K\omega_a+\omega}\right)\Bigg\} \\
& + \sum_{i=1}^{\infty}\frac{(-1)^i J_i(k_f)}{4}\Bigg\{\sum_{K=1}^{\infty}\Bigg[(-1)^{K+1}\left(\frac{e^{j[\omega_c-i\omega_m+(-1)^K\omega_a-\omega]\tau}-1}{\omega_c-i\omega_m+(-1)^K\omega_a-\omega}\right) \\
& \quad +(-1)^{K+1}\left(\frac{e^{-j[\omega_c-i\omega_m+(-1)^K\omega_a+\omega]\tau}-1}{\omega_c-i\omega_m+(-1)^K\omega_a+\omega}\right) \\
& \quad +(-1)^{K+i+1}\left(\frac{e^{j[\omega_c+i\omega_m+(-1)^K\omega_a-\omega]\tau}-1}{\omega_c+i\omega_m+(-1)^K\omega_a-\omega}\right) \\
& \quad +(-1)^{K+i+1}\left(\frac{e^{j[\omega_c+i\omega_m+(-1)^K\omega_a+\omega]\tau}-1}{\omega_c+i\omega_m+(-1)^K\omega_a+\omega}\right)\Bigg]\Bigg\}
\end{aligned}
$$

Again as with CASE A, the first twenty terms of the series are evaluated in establishing a reference. A program listing for CASE B appears at the rear of the appendix and is titled "SUBROUTINE ASINE".

```
C
C
C                    ********************
C                    * SUBROUTINE SINE *
C                    ********************
C
C
C     SUBROUTINE SINE GENERATES THE COMPLEX FREQUENCY COMPONENTS OF A UNIT
C     PULSE IN WHICH THE CARRIER FREQUENCY IS SINUSOIDALLY MODULATED.
C
C
      SUBROUTINE SINE(NFREQ)
      DIMENSION Z(400), FREQ(400)
      COMMON /SPEC1/ Z, FREQ, START, PW, AMPSRT, H, F1, RO, PHITO, S
      COMMON /SPEC2/ PI, TWOPI, ZIP, ZERO
      COMPLEX*16 XP1, XP2, XP3, XP4, Z, TERM1, TERM2, TERM3, TERM4, BJO
      COMPLEX*16 ZERO
      DOUBLE PRECISION FREQ, RO, F1, START, PW, AMPSRT, H, PHITO
      DOUBLE PRECISION PI, TWOPI, ZIP, FM, FC, BJO
      DOUBLE PRECISION W, W1, W2, W3, W4, WT1, WT2, WT3, WT4, WC, WM
800   FORMAT(10X,'$$$$$BESJ ERROR CODE =',I3,' FOR J =',I3,///)
      D=1.0E-05
C
C     SET THE PULSE PARAMETERS: MODULATION INDEX, CARRIER
C     FREQUENCY (FC) AND CARRIER MODULATING FREQUENCY (FM)
C
      BTX=1.0
      FM=200.0E+03
      FC=30.0E+06
      WC=TWOPI*FC
      WM=TWOPI*FM
C
C     GENERATE THE FREQUENCY COMPONENTS OF INTEREST
C
      DO 10 I=1,NFREQ
      W=TWOPI*FREQ(I)
C
C     CALCULATE THE FIRST TWENTY TERMS OF THE BESSEL SERIES EXPANSION
C     AND FORM THE CUMULATIVE SUM
C
      DO 20 K=1,20
      J=K-1
      W1=WC-FLOAT(J)*WM-W
      W2=WC-FLOAT(J)*WM+W
      W3=WC+FLOAT(J)*WM-W
```

```
      W4=WC+FLOAT(J)*WM+W
      WT1=W1*PW
      WT2=-W2*PW
      WT3=W3*PW
      WT4=-W4*PW
      W1=DMOD(WT1,TWOPI)
      W2=DMOD(WT2,TWOPI)
      W3=DMOD(WT3,TWOPI)
      W4=DMOD(WT4,TWOPI)
      XP1=DCMPLX(ZIP,WT1)
      XP2=DCMPLX(ZIP,WT2)
      XP3=DCMPLX(ZIP,WT3)
      XP4=DCMPLX(ZIP,WT4)
      TERM1=(0.0D+00,1.0D+00)*PW
      TERM2=(0.0D+00,-1.0D+00)*PW
      TERM3=(0.0D+00,1.0D+00)*PW
      TERM4=(0.0D+00,-1.0D+00)*PW
      IF(W1.NE.0.0D+00) TERM1=(CDEXP(XP1)-1.0)/W1
      IF(W2.NE.0.0D+00) TERM2=(CDEXP(XP2)-1.0)/W2
      IF(W3.NE.0.0D+00) TERM3=(CDEXP(XP3)-1.0)/W3
      IF(W4.NE.0.0D+00) TERM4=(CDEXP(XP4)-1.0)/W4
C
CC    CALCULATE THE BESSEL FUNCTION TO BE USED IN THE WEIGHTED SUM
C
      CALL BESJ(BTX,J,BJ,D,IERB)
      IF(IERB.NE.0) WRITE(6,800) IERB, J
      BJD=BJ
      BJC=DCMPLX(ZIP,BJD)
      Z(I)=Z(I)+((-1.0)**(J+1))*(BJC/2.0)*(TERM1-TERM2+((-1.0)**J)*TERM3
     1+((-1.0)**(J+1))*TERM4)
      IF(J.EQ.0) Z(I)=Z(I)/2.0
20    CONTINUE
10    CONTINUE
      RETURN
      END
```

```
C
C
C                    ********************
C                    * SUBROUTINE ASINE *
C                    ********************
C
C
C     SUBROUTINE ASINE GENERATES THE COMPLEX FREQUENCY COMPONENTS FOR A
C     SINUSOIDALLY SHAPED PULSE WHICH HAS A CARRIER FREQUENCY THAT IS
C     SINUSOIDALLY MODULATED
C
C
      SUBROUTINE ASINE(NFREQ)
      DIMENSION Z(400), FREQ(400)
      COMMON /SPEC1/ Z, FREQ, START, PW, AMPSRT, H, F1, RO, PHITC, S
      COMMON /SPEC2/ PI, TWOPI, ZIP, ZERC
      COMPLEX*16 Z, ZERO, XP1, XP2, XP3, XP4, XP5, XP6, XP7, XP8
      COMPLEX*16 T1, T2, T3, T4, T5, T6, T7, T8
      DOUBLE PRECISION FREQ, RO, F1, START, PW, AMPSRT, H, PHITO
      DOUBLE PRECISION PI, TWOPI, ZIP, FM, FC, FA, WM, WC, WA, W, BJD
      DOUBLE PRECISION W1, W2, W3, W4, W5, W6, W7, W8
      DOUBLE PRECISION WT1, WT2, WT3, WT4, WT5, WT6, WT7, WT8
800   FORMAT(10X,'$$$$$BESJ ERROR CODE =',I3,' FOR J =',I3,///)
      D=1.0E-05
C
C     SET THE PULSE PARAMETERS: MODULATION INDEX, CARRIER
C     FREQUENCY (FC) AND CARRIER MODULATING FREQUENCY (FM)
C     AND AMPLITUDE MODULATING FREQUENCY (FA)
C
      BTX=1.0
      FC=30.0E+06
      FA=100.0E+03
      FM=200.0E+03
      WC=TWOPI*FC
      WA=TWOPI*FA
      WM=TWOPI*FM
C
C     GENERATE THE FREQUENCY COMPONENTS OF INTEREST
C
C
C     CALCULATE THE FIRST TWENTY TERMS OF THE BESSEL SERIES EXPANSION
C     AND FORM THE CUMULATIVE SUM
C
      DO 10 I=1,NFREQ
      W=TWOPI*FREQ(I)
```

```
      DO 20 K=1,20
      J=K-1
      W1=WC-FLOAT(J)*WM+WA-W
      W2=WC-FLOAT(J)*WM+WA+W
      W3=WC-FLOAT(J)*WM-WA-W
      W4=WC-FLOAT(J)*WM-WA+W
      W5=WC+FLOAT(J)*WM+WA-W
      W6=WC+FLOAT(J)*WM+WA+W
      W7=WC+FLOAT(J)*WM-WA-W
      W8=WC+FLOAT(J)*WM-WA+W
      WT1=W1*PW
      WT2=-W2*PW
      WT3=W3*PW
      WT4=-W4*PW
      WT5=W5*PW
      WT6=-W6*PW
      WT7=W7*PW
      WT8=-W8*PW
      WT1=DMOD(WT1,TWOPI)
      WT2=DMOD(WT2,TWOPI)
      WT3=DMOD(WT3,TWOPI)
      WT4=DMOD(WT4,TWOPI)
      WT5=DMOD(WT5,TWOPI)
      WT6=DMOD(WT6,TWOPI)
      WT7=DMOD(WT7,TWOPI)
      WT8=DMOD(WT8,TWOPI)
      XP1=DCMPLX(ZIP,WT1)
      XP2=DCMPLX(ZIP,WT2)
      XP3=DCMPLX(ZIP,WT3)
      XP4=DCMPLX(ZIP,WT4)
      XP5=DCMPLX(ZIP,WT5)
      XP6=DCMPLX(ZIP,WT6)
      XP7=DCMPLX(ZIP,WT7)
      XP8=DCMPLX(ZIP,WT8)
      T1=DCMPLX(ZIP,PW)
      T2=DCMPLX(ZIP,-PW)
      T3=DCMPLX(ZIP,PW)
      T4=DCMPLX(ZIP,-PW)
      T5=DCMPLX(ZIP,PW)
      T6=DCMPLX(ZIP,-PW)
      T7=DCMPLX(ZIP,PW)
      T8=DCMPLX(ZIP,-PW)
      IF(W1.NE.0.0D+00)  T1=(CDEXP(XP1)-1.0)/W1
      IF(W2.NE.0.0D+00)  T2=(CDEXP(XP2)-1.0)/W2
      IF(W3.NE.0.0D+00)  T3=(CDEXP(XP3)-1.0)/W3
      IF(W4.NE.0.0D+00)  T4=(CDEXP(XP4)-1.0)/W4
      IF(W5.NE.0.0D+00)  T5=(CDEXP(XP5)-1.0)/W5
      IF(W6.NE.0.0D+00)  T6=(CDEXP(XP6)-1.0)/W6
```

```
      IF(W7.NE.0.0D+00) T7=(CDEXP(XP7)-1.0)/W7
      IF(W8.NE.0.0D+00) T8=(CDEXP(XP8)-1.0)/W8
C
CC    CALCULATE THE BESSEL FUNCTION TO BE USED IN THE WEIGHTED SUM
C
      CALL BESJ(BTX,J,BJ,D,IERB)
      IF(IERB.NE.0) WRITE(6,800) IERB, J
      BJD=BJ
      S1=(-1.0)**(J+1)
      S2=(-1.0)**(J)
      Z(I)=Z(I)+S2*(BJD/4.0)*(-T1-T2+T3+T4+S1*T5+S1*T6+S2*T7+S2*T8)
      IF(J.EQ.0) Z(I)=Z(I)/2.0
20    CONTINUE
10    CONTINUE
      RETURN
      END
```

APPENDIX C

FRESNEL INTEGRALS

The Fresnel integral, important in the theory of diffraction, can be written as:

$$C(x) - jS(x) = \int_0^x e^{-j(\pi/2)v^2} dv \qquad \text{(C-1)}$$

Plotting this integral in the complex plane yields a curve known as Cornu's spiral (figure C-1). The positive values of x appear in the first quadrant and the negative values in the third. A vector drawn from the origin to any point on the curve represents in both phase and magnitude the value of the integral in equation (C-1). (The phase of the vector is the negative of the phase of the integral.) Note from the Cornu spiral that as x goes to infinity, C(x) and S(x) both converge to one half.(7)

The integral in equation (C-1) can be expressed in terms of a series expansion as:

$$C(x) = \sum_{n=0}^{\infty} \frac{(-1)^n (\pi/2)^{2n}}{(2n)!(4n+1)} x^{4n+1} \qquad \text{(C-2a)}$$

$$S(x) = \sum_{n=0}^{\infty} \frac{(-1)^n (\pi/2)^{2n+1}}{(2n+1)!(4n+3)} x^{4n+3} \qquad \text{(C-2b)}$$

The fact that the Fresnel integral is not expressible in closdd form means that in application approximations to equation (C-1) must be employed. One such approach has been developed by Boersma(2) in which equation (C-1) is written with a change of variable ($w=\frac{\pi}{2}v^2$)

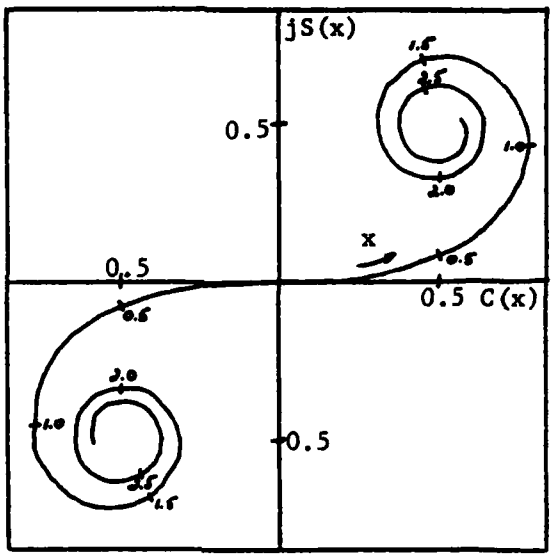

Figure C-1 - Cornu Spiral

so that:

$$(C\text{-}3) \qquad C(z) - jS(z) = \int_0^z \frac{e^{-jw}}{\sqrt{2\pi w}}\, dw$$

Boersma's technique makes use of the following approximations:

$$(C\text{-}4a) \qquad C(z) - jS(z) = e^{-jz}\sqrt{\frac{z}{4}}\sum_{n=0}^{11}(a_n + jb_n)\left(\frac{z}{4}\right)^n \qquad 0 \le z \le 4$$

$$(C\text{-}4b) \qquad C(z) - jS(z) = \frac{1-j}{2} + e^{-jz}\sqrt{\frac{4}{z}}\sum_{n=0}^{11}(c_n + jd_n)\left(\frac{4}{z}\right)^n \qquad z \ge 4$$

where the coefficients a_n, b_n, c_n and d_n are derived by the τ-method of Lanczos and are provided in (2). The maximum error associated with this approach is 1.6×10^{-9}. This technique of evaluating the Fresnel integrals has been employed in the subroutine CS listed in Appendix A.

Other techniques and approximations are also available to evaluate the Fresnel integrals; one of the more recent being presented by James(5). James' approach is unique in that it employs one concise approximate expression for all real values of the argument. The technique is implementable on a pocket calculator and provides a maximum amplitude error of eight per cent.

APPENDIX D

COMPARISON OF FFT AND ELEMENTAL CELL EFFICIENCY

Given a sequence x(n) where n = 1,2,.....(N-1), the Fourier coefficients associated with the sequence can be represented by the discrete Fourier transform (DFT):

$$X(k) = \sum_{n=0}^{N-1} x(n) W_N^{kn} \qquad 0 \le k \le N-1 \tag{D-1}$$

where $W_n = e^{-j\left(\frac{2\pi}{N}\right)}$. A straightforward calculation using equation (D-1) would require N^2 operations where the term "operation" is taken to mean a complex multiplication followed by a complex addition. More efficient methods are available for evaluating equation (D-1) which require considerably fewer than N^2 operations. Cooley and Tukey(8) developed a technique which has lead to a class of algorithms known as Fast Fourier Transforms (FFT's) which provided for the evaluation of equation (D-1) in less than $2N\log_2 N$ operations.

While the number of operations required is frequently used in DFT and FFT analysis as a measure of computational complexity or efficiency, it cannot easily be applied to the elemental cell model to establish a common base for comparison. The actual time required for an FFT or elemental cell calculation can be compared.

Using the subroutine HARM (IBM Scientific Subroutine Library), which is based on the algorithm of Cooley and Tukey(8), the Fourier transforms of 50 signals were generated to determine the average execution time of an N-point transform where N = 512, 1024, etc. for each set of 50 signals.

In similar fashion, the elemental cell spectra were generated for each of the four classes of elemental cells using one hundred frequency components. Table (D-1) lists the results of this analysis. In the case of the FFT, as the size of the transform is doubled, the time required for computation increases by approximately a factor of two. This is in keeping with what would be predicted by the measure of complexity discussed above. In the case of the elemental cell model, the time required for computation increases with the sophistication of the class of elemental cell.

In application, the time required to implement an FFT is a function of the transform size(N), which is in turn a function of the problem being addressed. The time required to implement the elemental cell model, on the other hand, is not only a function of the problem being addressed but also the nature of the elemental cells employed, the number of cells used and the number of frequency components to be generated. For example, the average execution time for an elemental cell model composed of ten constant amplitude cells with linear FM for which twenty spectral components are desired is (10 x 20 x 6.10msec =) 1.22 seconds.

A graphical comparison of the execution times of the two techniques appears in figure (D-1), in which execution time is plotted as a function of the product of the number of elemental cells (n) and the number of frequency components required (m). Nothing can be said unequivocally about the computational efficiency of the elemental cell model vis-a-vis the FFT approach. Under certain circumstances, when the transform size is large (e.g. greater than 2K) and the product of m and n is small (e.g. less than 200)

AVERAGE TIME TO EVALUATE AN N-POINT FFT

N	TIME
512	0.22 sec
1024	0.47 sec
2048	0.88 sec
4096	1.81 sec
8192	4.01 sec

AVERAGE TIME TO EVALUATE AN ELEMENTAL CELL FOR ONE FREQUENCY

CLASS OF CELL	TIME
CONSTANT AM CONSTANT FM	3.72 msec
LINEAR AM CONSTANT FM	5.55 msec
CONSTANT AM LINEAR FM	6.10 msec
LINEAR AM LINEAR FM	8.85 msec

Table D-1 - Average Times for FFT and Elemental Cell Calculations

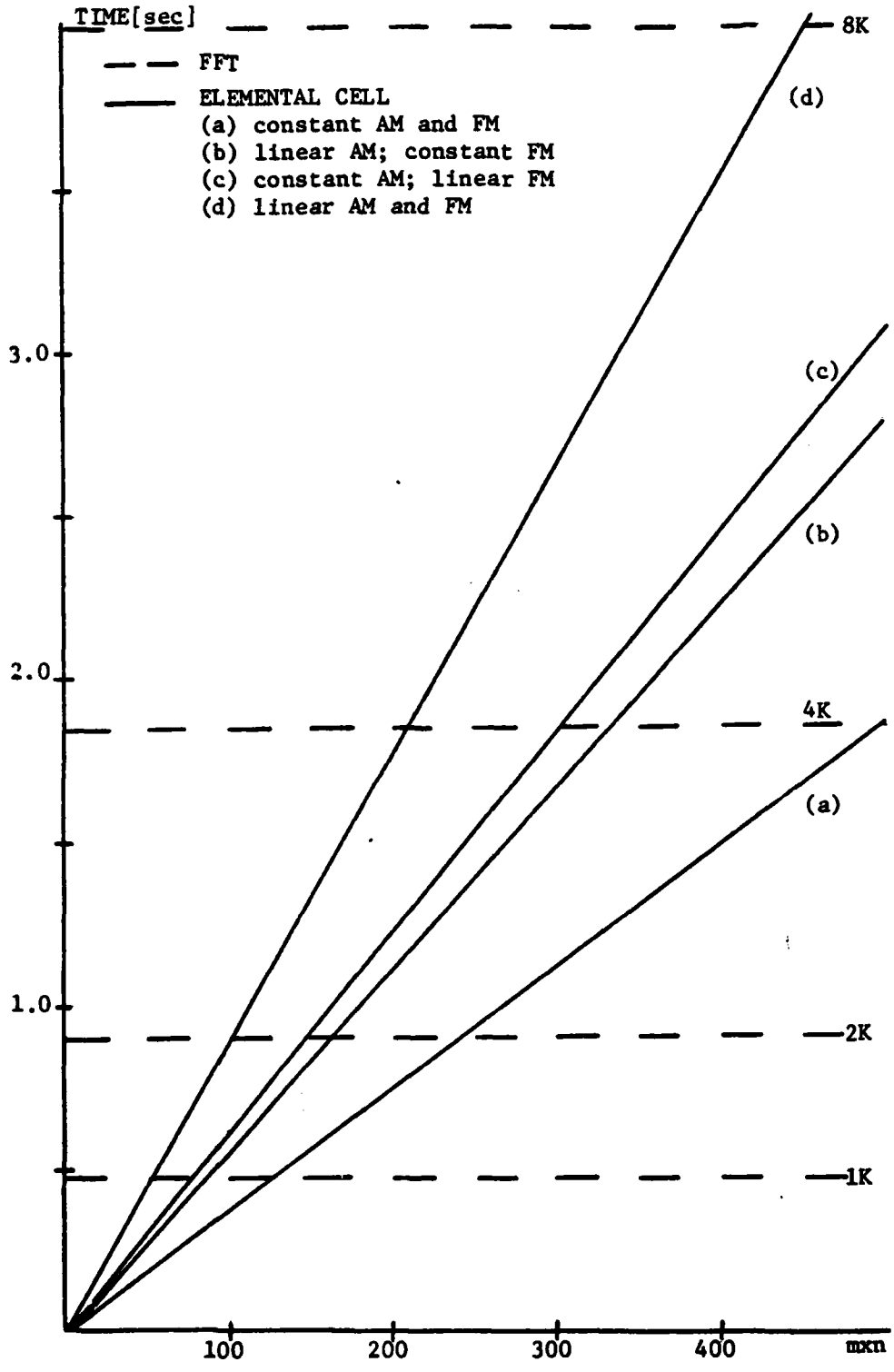

n = number of cells
m = number of frequency components desired

Figure D-1 - FFT and Elemental Cell Execution Times

speed can be obtained using the cell model at the cost of discriminating the signal of interest.

It should be noted that in this analysis the subroutines used to generate the elemental cell spectra are those listed in Appendix A and that no attempt at time optimization has been made. In fact, at the cost of efficiency, precision has been stressed. It is expected that by modifying the existing subroutines to handle only the "right hand" spectrum and to function in single vice double precision that the execution time could be reduced by nearly a factor of four.

BIBLIOGRAPHY

(1) Holway, L. H. and Mullen, J. A., "Exact and Approximate Spectra for Trapezoidal FM," Proceedings of the IEEE, v. 64, no. 3, p. 380-381, MAR 76.

(2) Boersma, J., "Computation of Fresnel Integrals," Mathematical Tables and Other Aids to Computation, v. 14, no. 72, 1960.

(3) Gerald, C. F., Applied Numerical Analysis, p. 43-44;60-64, Addison-Wesley, 1973.

(4) Schoenstadt, A. L., Private Correspondence.

(5) James, G. L., "An Approximation to Fresnel Integrals," Proceedings of the IEEE, v. 67, no. 4, p. 667-668, APR 79.

(6) Taub, H. and Schilling, D. L., Principles of Communications Systems, p. 118-125, McGraw, 1971.

(7) Jordan, E. C. and Balmain, K. G., Electromagnetic Waves and Radiating Systems, p. 500-502, 2nd ed., Prentice Hall, 1968.

(8) Cooley, J. W. and Tukey, J. W., "An Algorithm for the Machine Calculation of Complex Fourier Series," Mathematics of Computation, p. 297-301, APR 65.

INITIAL DISTRIBUTION LIST

		No. Copies
1.	Defense Documentation Center Cameron Station Alexandria, Virginia 22314	2
2.	Library, Code 0142 Naval Postgraduate School Monterey, California 93940	2
3.	Department Chairman, Code 62 Department of Electrical Engineering Naval Postgraduate School Monterey, California 93940	1
4.	Assoc. Professor C. A. Myers Code 62Mv Department of Electrical Engineering Naval Postgraduate School Monterey, California 93940	1
5.	Assoc. Professor A. L. Schoenstadt Code 53Sc Department of Mathematics Naval Postgraduate School Monterey, California 93940	1
6.	Assoc. Professor J. B. Knorr Code 62Ko Department of Electrical Engineering Naval Postgraduate School Monterey, California 93940	1
7.	Assoc. Professor A. R. Washburn Code 55Wa Department of Operations Research Naval Postgraduate School Monterey, California 93940	1
8.	Assoc. Professor S. Jauregui Code 62Ja Department of Electrical Engineering Naval Postgraduate School Monterey, California 93940	10
9.	Assoc Professor B. O. Shubert Code 55Sh Department of Operations Research Naval Postgraduate School Monterey, California 93940	1

	No. Copies
10. LCDR Francis Martin Lunney, USN 6143 Gatsby Green Columbia, Maryland 21045	1

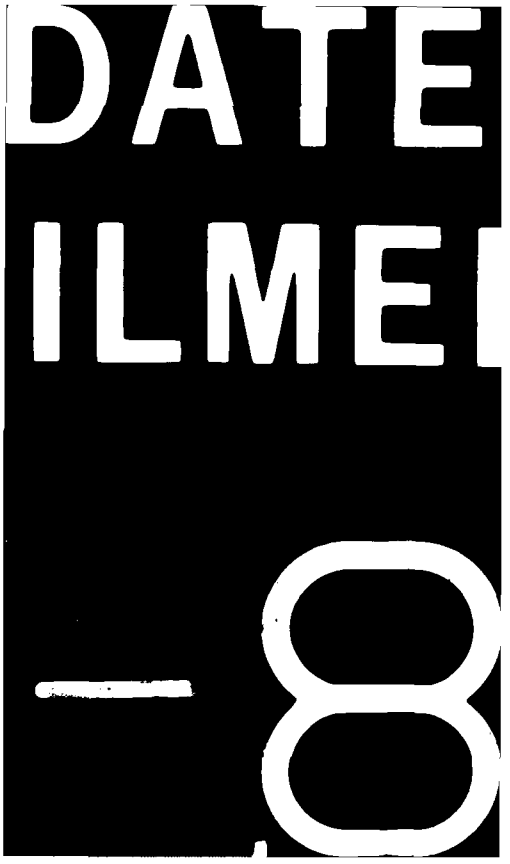
DATE
ILME
8